Energy Efficient Sensing and Networking: A Visible Light Perspective

YANG YANBING

School of Computer Science and Engineering

Nanyang Technological University

A thesis submitted to the Nanyang Technological University
in partial fulfilment of the requirement for the degree of
Doctor of Philosophy (Ph.D)

2018

To my family, for their unconditional love and endless support.

Acknowledgement

First and foremost I would like to thank my supervisor, Prof. Jun Luo, for his great support, guidance, and encouragement over the years. It has been a great pleasure working with him.

Special thanks to the Thesis Advisory Committee (TAC) members, Prof. Mo Li and Prof. Yuanjin Zheng, for their invaluable feedback and advices on my research. Many thanks to my co-authors, Prof. Sinno Jialin Pan, Dr. Jie Hao, Jiangtian, and Shuya for their suggestions and insightful discussions.

My deepest gratitude goes to my family, especially my wife Xiaodan Liu, for their unconditional love and support. I owe to them every step of my progress in my life.

I am greatly thankful for my friends and colleagues in CNCL and CeMNet, for the friendship and encouragement. I would always appreciate their lovely company during my Ph.D. study.

Finally, I thank the technicians, Ms. Chua, Mr. Roy and Mr. Toh, in my lab for their kind help and patience.

Abstract

While the traditional communication technique with radio frequency is getting its bottlenecks in terms of available spectrum and energy consumption, visible light has attracted a lot of research attentions as a promising supplement of communication medium, since it is ubiquitous and necessary in our daily lives. Known as a green technology, *Visible Light Communication* (VLC) piggybacking on existing lighting system has been considered as a promising access technique for next-generation wireless systems (5G). However, whereas major research efforts in the field of VLC are pursuing higher data rate, exploring the potential of VLC employing *Commercial Off-The-Shelf* (COTS) devices and providing seamless connectivity for mobile users seem to be ignored. To this end, in this thesis, we focus on developing a practical VLC system which can offer roaming support for users with commonly handy devices, e.g. smartphones.

In the first part, we design and implement CeilingTalk as an LED-Camera VLC broadcast system using COTS *Light Emitting Diode* (LED) luminaires as transmitters and smartphone cameras as receivers so that it can be fully hosted in a smartphone and is feasible for all possible indoor environments. CeilingTalk innovates in both encoding and decoding to achieve an adequate throughput for realistic applications. On one hand, it employs Raptor coding to allow multiple LED luminaires to transmit collaboratively so as to benefit both throughput and reliability. On the other hand, it presents a lightweight decoding scheme to handle the asynchrony (both spatial and temporal) in transmissions. Moreover, we analyze the impact of various parameters on the performance of CeilingTalk, in order to derive an analytical model for such VLC systems enabled by COTS devices and hence provide general guidance for future VLC deployments in larger scales. Finally, we conduct extensive field experiments to validate the effectiveness of our LED-Camera VLC model, as well as to demonstrate the promising performance of CeilingTalk: up to 1.0 kb/s at a distance of 5 meters.

During we develop CeilingTalk, we notice that the lack of feedback from receivers in LED-Camera VLC results in extremely difficult to offer seamless connectivity to mobile users. We hereby exploit the sensing ability of an LED luminaire to detect user presence so as to provide possible feedback for VLC. To evaluate the possibility using LEDs to sense occupants, we innovate CeilingSee, a dedicated occupancy inference system free of heavy infrastructure deployments and user involvements in the second part of this thesis. In realizing CeilingSee, we first re-design the LED driver to leverage LED's photoelectric effect so as to transform a light emitter to a light sensor. In order to produce accurate occupancy inference, we then engineer efficient learning algorithms to fuse sensing data gathered by multiple LED luminaires. We build a testbed covering a 30 m^2 office area; extensive experiments show that CeilingSee is able to achieve very high accuracy in occupancy inference.

Finally, we propose RoCLight integrating CeilingTalk with CeilingSee to provide seamless connectivity for mobile VLC users. We innovate in converting part of the LED luminaires (already used as the VLC transmitters) into light sensors to have a proper feedback channel for roaming support. By sensing the disturbance to the ambient diffuse reflection change caused by user presence and mobility, RoCLight is able to adaptively handoff its transmissions from one luminaire to another, so as to keep up with user mobility and hence to offer an adequate roaming support. We implement RoCLight as a small-scale testbed with five LED luminaires spanning a length of 7.5 meters, and conduct extensive evaluations on the roaming support capability of RoCLight based on this testbed; all our experiments strongly demonstrate its promising performance.

Keywords

Visible Light Communication, Visible Light Sensing, Rateless Code, Roaming.

Contents

List of Figures

List of Tables

Chapter 1

Introduction

With the development of communication techniques, the traditional *Radio-Frequency* (RF) communication encounters its bottleneck in terms of scarce bandwidth and energy consumption. Furthermore, the increasing of demands of data service and mobile traffic is appealing to new paradigms to revolutionize the conventional RF communication approaches. VLC, known as a spectrum-rich alternative to RF and 'green' communication method, is drawing the attention from both academic and industrial researchers. In this thesis, we are focusing on extending the conventional VLC system to enable handily practical applications driven by COTS devices, e.g. illumination LEDs and smartphones. Meanwhile, we deeply exploit the sensing ability of LED transmitters used in VLC. In particular, we leverage the photoelectric effect of an LED to realize a promising approach for user detection so as to drive forward both sensing and communication via visible light.

1.1 Background

As fourth-generation mobile communication systems are under large-scale deployment, 5th generation (5G) wireless systems are increasingly attracting attentions from both manufactures and the scientific community [1, 2]. It is commonly agreed with that the 5G and beyond systems will not only improve throughput, but also lower energy consumption [3]. To this end, VLC is gaining great concern as an access technique thanks to its higher system spectral efficiency, network capacity and low energy consumption [4]. Taking advantage of visible light spectrum as the communication media

has a long history that can be dated from 19 century, while using white LEDs for communications is starting at the end of 20 century [5, 6, 7], and VLC has been possessing the promise of extremely high data-rate and very low-cost for a few decades [8, 9]. Nevertheless, it is the boosting replacement of inefficient lighting by LEDs that has greatly expedited the development of VLC as a complement to current wireless communication. As energy efficient LEDs are turning into the ubiquitous lighting source for both indoor and outdoor environments such as shopping malls and street buildings, and they have a ready access to power/information networks, we now have a handy infrastructure for implementing VLC-enabled wireless systems. However, whereas major research efforts have been made to boost the capacity of VLC [10, 11] and enable indoor localization [12, 13, 14] in a small-scale experimental room, harnessing the potential of LED-VLC with COTS devices covering large indoor areas seems to be largely neglected. Therefore, in this thesis, we aim to extend the VLC to practical applications with roaming support for covering a larger space by only using COTS devices.

The first seminal work of [15], realizing a VLC receiver by only leveraging the rolling-shutter effect of a *Complementary Metal-Oxide-Semiconductor Transistor* (CMOS) camera on a smartphone, opens a new area of LED-Camera VLC using COTS devices [13, 16], which revolutionizes traditional VLC systems based on customized light sensors. However, the system built in [15] requires a plain surface for light reflecting, which substantially confines the practicality in terms of communication range and supporting mobile users. More generally, the individual LED luminaire in an LED-Camera VLC system has very limited communication range comparing to the cellular network scenario, thus roaming support is necessary to maintain wireless connectivity upon user mobility and cover large space. Although a practical VLC system may not need to support a full range roaming due to it is normally believed to be considered as a location-based service provider, it at least has to ensure the continuity in receiving messages when a user is wandering in a room-level area lit by multiple luminaires.

In [17], the authors proposed the concept of integrated VLC system combining scalable VLC networking and accurate sensing mobile users in the room. However, there is still no real implementation of such a system. All other existing LED-Camera VLC systems can only provide one-way communication, so it has made it nearly impossible to support roaming as a feedback channel is obligatory for relaying the message between adjacent luminaires [9]. With the help of mature RF communication techniques,

hybrid VLC-RF networks could rely on RF to offer a feedback channel for supporting seamless connectivity in a VLC system [18, 19], which in turn enables further energy-efficient optimization to be performed on the user-to-network association structure [20]. Nonetheless, a HetNet infrastructure incurs extra management and operation overhead, so it may substantially confine the applicability of COTS-enabled VLC systems that are meant to operate in a plug-and-play mode at places where RF may not be available.

1.2 Scope of Research

In this thesis, we aim to confront the aforementioned challenges in an LED-Camera VLC system so that it produces a practical LED-Camera VLC system with roaming support only relying on visible light as both communication and sensing medium. To this end, we first re-visit the issue of implementing VLC-based broadcast using LEDs as transmitters and smartphone cameras as receivers. We build an LED-Camera VLC system, namely *CeilingTalk*, to develop a communication model to characterize this LED-Camera VLC by extracting parameters from field experiments, and evaluate our proposals on employing rateless codes to improve both reliability and the network throughput through cooperative transmissions.

Subsequently, we exploit the sensing ability of LED luminaires to form a feedback channel for roaming support in VLC, since it is extremely difficult to get feedback from smartphone cameras to LED transmitters. As a result, we build our second testbed of *CeilingSee*, an innovative *Visible Light Sensing* (VLS) prototype based on LED sensing. We re-design the LED driver to convert an LED luminaire into a light sensor to detect the presence of users, so as to potentially enable VLC transmitters to automatically associate perceived users. Meanwhile, we make an attempt to develop CeilingSee as a complete system to monitor indoor occupancy only applying ceiling-mounted LED lighting systems.

To reach our final goal, we creatively integrate CeilingTalk with CeilingSee to generate *RoCLight* (**Ro**aming in **C**onnecting **Light**). In RoCLight, the system intelligently tracks user location with the ceiling-mounted LED lighting system, and relays a communication session among neighboring LED luminaires upon user mobility and trajectory. Our extensive field experiments show a high accuracy of user detection by LED sensing,

and strongly demonstrate its effectiveness to form a feedback channel for supporting roaming in an LED-Camera VLC system.

1.3 Contributions

In a nutshell, the following contributions have been made in this thesis:

- We develop and deploy a practical LED-Camera system, **CeilingTalk**, which works perfectly under normal indoor scenarios. CeilingTalk innovates in both encoding and decoding to achieve an adequate throughput for realistic applications. Moreover, we analyze the impact of various parameters on the performance of CeilingTalk, in order to derive a model for such VLC systems enabled by COTS devices and hence provide general guidance for future VLC deployments in larger scales. We also introduce rateless codes to LED-Camera VLC systems to allow multiple LED luminaires to transmit collaboratively so as to benefit both throughput and reliability.

- We propose the novel idea of applying ceiling-mounted LED transmitters for detecting user presence, and further invent **CeilingSee**, a dedicated occupancy inference system free of heavy infrastructure deployments and user involvements. In realizing CeilingSee, we first re-design the LED driver to leverage LEDs photoelectric effect so as to transform a light emitter to a light sensor. In order to produce accurate occupancy inference, we engineer efficient learning algorithms to fuse sensing information gathered by multiple LED luminaires.

- We design and implement **RoCLight** as a lightweight solution to provide roaming support to LED-Camera VLC systems. We innovate in converting part of the LED luminaires (already used as the VLC transmitters) into light sensors. By sensing the disturbance to the ambient diffuse reflection caused by user presence and mobility, RoCLight is able to adaptively handoff its transmissions from one luminaire to another, so as to keep up with user mobility and hence to offer an adequate roaming support.

Chapter 2

Literature Survey

In this chapter, we review the existing proposals involving the 'green' technology of using visible light as communication and sensing medium. We hereby survey the work in both two branches refer to visible light: VLC and VLS. In particular, we highlight researches about LED-Camera VLC systems which this thesis focuses on, and then introduce the latest research in VLS. Finally, we dive into studying the related literature about roaming support to VLC for mobile users.

2.1 Status of Visible Light Communication

We first introduce preliminary of a VLC system, and then survey the related work in low rate VLC as well as their typical applications in this section.

2.1.1 VLC System Overview

Similar to all other communication systems, a typical VLC system consists of an LED luminaire as transmitter and receivers. Especially, a complete LED luminaire contains an LED lamp (consisting of multiple LED chips or beads), a driver circuit and other components, e.g. ballast housing. As VLC systems are expected to piggyback on the existing lighting infratrcuture, VLC transmitters, i.e. LEDs, should satisfy the demand for white light illumination. There exist two ways to generate white light that is universally used indoor and outdoor illumination applications by far. The former one is producing white light by using a blue LED emitting blue light traversing through a yellow coating [21]. The latter produces white light by proper mixing of red, green

and blue light [22], yet it raises the cost and driving complexity of an LED luminaire containing three separately colored LED chips compared to the former. Thus the majority of commercial white LED luminaires are the blue LED with a phosphor for illumination applications including the settings in this thesis.

The receiver in VLC has two typical types: a light sensor (photodetector) and camera (image sensor). The light sensor converts the incident light into current directly so that it easily samples the received light with a frequency up to tens of MHz [23, 24]. However, due to its vulnerability to the interference and unavailability on COTS devices, light-sensor-based VLC systems are still not ready for realistic applications. Consequently CMOS cameras have been proposed to use for VLC [25, 26]. It is obvious that cameras can capture light with information since we use them to shoot pictures or record video in our daily lives. Nevertheless, limited by the frame rate of a camera sensor, typically no more than 40 fps (frame per second) for image sensor in a commercial smartphone, it is hard to directly use the camera sensor to receive information via modulated light. Very recently the rolling-shutter effect of the camera sensor, detailed in following Sec.3.2, has been exploited and used widely in VLC to boost data rate [14, 15, 27, 28]. Thus, in this thesis, we take our efforts on the novel and open area of camera-based VLC system and its applications.

2.1.2 Screen-Camera Communication

As an important branch of camera based VLC, *Screen-Camera Communication* mainly focuses on designing sophisticated coded images to boost data rate [29, 30, 31, 32, 33], or to enhance link reliability [34, 35, 36]. To improve data rate, SBVLCD [29] and COBRA [30] exploit advanced barcode design, PixNet [31] leverages efficient modulation mechanism, SoftLight [32] employs channel coding, and NLE/LE [33] utilizes channel equalization and nonbinary channel coding. Reliability is addressed in terms of either frame synchronization [36] or barcode detection under a prolonged communication distance and device diversity [34, 35]. Moreover, recent studies intend to enhance the viewing experience by hiding information in a given screen content without interfering communications. PiCode [37] integrates barcodes with existing images to reduce the visual artifacts, while HiLight [38] avoids modifications on RGB values by utilizing the alpha channel to encode bits into the pixel translucency changes. To enable Screen-Camera VLC on commonly commerical screens with low screen refresh rate,

Table 2.1: Summary of Screen-Camera VLC Systems.

	Capacity	Distance (m)	Modulation/Coding
SBVLC [29]	200 kb/s	0.17	Barcode
COBRA [30]	172 kb/s	0.25	Barcode
PixNet [31]	12 Mb/s	10	OFDM
SoftLight [32]	317.3 kb/s	0.20	Rateless codes
HiLight [38]	1.1 kb/s	0.27	BFSK
CSC [39]	16.67 kb/s	0.90	Spatial Visual Modulation

CSC [39] adopts a spatial visual modulation scheme and Gaussian-absed block design to deliver a reasonable throughput. In most cases, Screen-Camera VLC only offers a sub-meter transmission distance (unless a large screen is dedicated to serving as the transmitter [31]), as briefly summarized in Table 2.1, thus substantially confining its application domain.

2.1.3 LED-Camera Communication

LED-Camera Communication mostly exploits the rolling-shutter effect of a CMOS camera on the smartphone. Unlike the high rate VLC where similar LED transmitters are used, the bottleneck lies on the smartphone receiver, which is where innovations can be made. Recent research [15] achieves real data rates up to 148 b/s at 20 fps. However, it requires a second media, i.e. a plain surface, to reflect lights so as for the camera to capture the banded images, making its practicality questionable. Further research is made in [40], which employs the undersampled phase shift *ON-OFF Keying* (OOK) achieving a data rate of 150b/s for a range up to 12 m with a lens. As an important application of this type of VLC, *Visible Light Positioning* (VLP) [13, 14, 16] make use of light as the only communication media to transmit location identifiers, and this is further extended by RollingLight [27] to build a new LED-Camera VLC system. Dynalight [28] attempts to analyze the impact of communication distance on channel capacity and proposes a scheme which is able to maximize its channel capacity w.r.t. transmitter-receiver distance. *Color Shift Keying* (CSK) is employed in ColorBars [41] to improve the throughput by utilizing tri-RGB LED luminaires. In [42] a novel *Polarized Light Intensity Modulation* scheme is employed to largely extend the

Table 2.2: Summary of LED-Camera VLC Systems.

	Capacity	Distance (m)	Error Correction
Seminal [15]	148 b/s	0.09	N.A.
CamCom [40]	150 b/s	12.00	N.A.
Luxapose [14]	N.A.	6.00	N.A.
VLandmark [13]	1.25 B/s	6.50	Hamming codes
HybridVLC [16]	1.30 B/s	0.05	N.A.
RollingLight [27]	11.32 B/s	1.60	Parity
Dynalight [28]	N.A.	1.2	N.A.
ColorBars [41]	5.2 kb/s	0.03	Reed-Solomon codes
POLI [42]	34 B/s	5.00	N.A.
CeilingTalk	1.0 kb/s	5.00	Raptor codes

communication distance, but it achieves a very low data rate from their field experiments. Nevertheless, all these proposals require either complicated modulation or heavy decoding computations that may not be feasible for COTS devices to operate in a long distance and/or scale-up scenario, and they treat several transmissions independently rather than leveraging them for throughput/reliability enhancement. Our CeilingTalk and RoCLight proposed in this thesis are designed to fill these gaps so as to make VLC practical, and they significantly outperform the state-of-the-art RollingLight [27] and ColorBars [41] in either throughput or transmission distance. We also aim to develop a communication model to characterize this LED-Camera VLC system to offer universal guidelines on realistic deployments of LED-Camera VLC systems. We summarize these proposals in Table 2.2.

2.1.4 Visible Light Positioning

As an important branch of VLC, visible light positioning largely extends VLC's application and significantly improves the performance of VLC. Typically, VLP employs a light sending location IDs and a receiver obtaining the IDs to infer user's own position. Liqun Li and Pan Hu et al. [43] present a novel sub-meter localization system exploiting visible light communication, which encodes IDs via *Binary Frequency Shift Keying* (BFSK) and receives the encoding message through an extra light-sensor attached on

a smartphone. Further, Luxapose [14] improves visible light position by directly leveraging rolling-shutter camera on a smartphone to receive packets from LED luminaires without extra sensors, in this paper, they also proposed an image-processing based method to demodulate bits from banded images. A polarization-based modulation method was proposed in [44], which is flicker-free to enable a low pulse rate visible light communication. However, this polarization-based modulation not only needs to attached extra *Twisted Nematic* (TN) liquid crystals on both luminaires and receivers, but also suffers from very limited frequency due to crystals resulting very low data rate in real. Besides, other variations of localization works based on VLC include [45] leveraging both *Received Signal Strength* (RSS) and *Angle of Arrival* (AoA) and [46] employing multiple tilted receivers to improve localization accuracy. Kown as very high location accuracy and piggybacking on existing indoor illumination infrastructure, VLP is extremely extending the application of visible light communication, and acceleratively boosting techniques improvement of VLC.

2.2 Visible Light Sensing

Extending VLC to VLS is a growing interest in improving human-computer interaction, enhancing ubiquitous connectivity, and enabling human centralized VLC networking. In [17], authors propose a novel concept of iVLC (*integrated Visible Light Communication*) illustrated in Figure 2.1. In such an iVLC system, ceiling-mounted VLC transmitters emit modulated lights to illuminate a room and simultaneously transmit a message to smart devices held by users, consequently users' shadows cast on the floor. Therefore, it is feasible to detect and track users by simply sensing their shadows with floor-mounted light sensors. To this end, Lisense [47] is first proposed and implemented to monitor human's gestures by densely deploying light sensors on the floor. With the similar idea in [47], a human identification system is presented in [48] by further excavating users' shadow information which inherently implies users' body parameters, e.g. shoulder width and arm length. StarLight [49] largely decreases the number of required photosensors on the floor by optimizing sensor layout and data processing algorithms so as to make it more practical. Besides monitoring human, a VLS-based user-mobile interaction system, Okuli [50], is devised and realized by using a controlled LED and

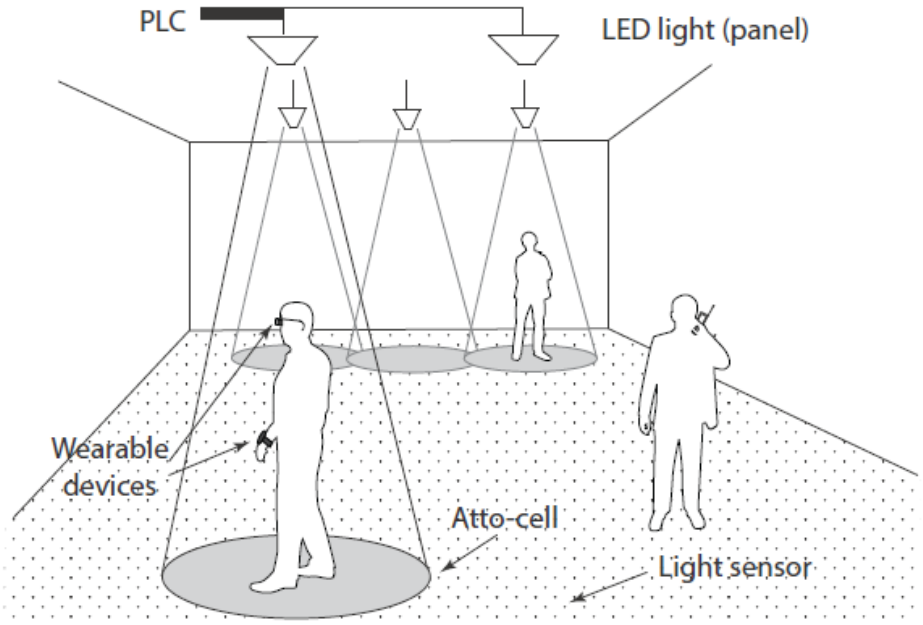

Figure 2.1: Concept of iVLC (*integrated Visible Light Communication*) [17]. LED luminaires on the ceiling are integrated with power line communication (PLC) and transmit message to smart devices carried by users. Light sensors on the floor capture the users' gesture and movement. Image from [17].

two photodiodes to track the reflection caused by a user's finger. Nevertheless, aforementioned systems need controllable luminaires to actively emit modulated light, which limits potential applications of VLS [51] due to the overwhelming majority of natural and artificial light sources are passive light sources, such as the sun and fluorescents.

Hence, many researchers are increasingly interested in exploiting benefits of passive visible light very recently. For example, PSync [52] and FLIGHT [53] use visible light for time synchronization for IoT devices. LocalLight [54] can localize the object by sensing distortion of ambient light caused by object's shadow on the floor. Passive light sensing is utilized for activity sensing in [55], where the authors co-locate light sensors with light sources to observe the reflection changes in light level caused by occupant's activity. Further research on recognizing hand gestures via ambient light is presented in [56] by employing a 3×3 array of photodiodes and advanced machine learning approaches. A passive localization system which could track a car via ambient light and passive VLC [57] is invented in [58], which drives conventional VLS/VLC with modulated light to a new area of leveraging widely uncontrolled light sources. However,

all existing researches require extra light sensor deployment, and ignore the important sensing ability of LED luminaires in both existing VLS and VLC. Therefore, we intend to realize a VLS system without special sensors but exploiting LED's perceiving ability of ambient light in this thesis so as to potentially extend both VLC and VLS.

2.3 Supporting Mobile Users in VLC

Maintaining seamless connectivity for both stationary and mobile users is essential for wireless networks. VLC (a.k.a. free space optical wireless communication) is very difficult to provide mobile communications due to lack of constant *Line-of-Sight* (LOS) communication channel between VLC transmitters and mobile terminals [59, 60]. Furthermore, a lighting cell in VLC has a far smaller coverage comparing to RF femtocells [61, 62]. Consequently, hybrid systems integrating RF and VLC access technologies have been proposed to achieving seamless connectivity for mobile users [63, 64]. Meanwhile, some proposals have started to apply coordinated broadcasting with several neighbor VLC transmitters to extend the network coverage beyond a couple of square meters under a single VLC transmitter [62, 65, 66]. Similar to traditional RF cellular communication, handover scheme is also theoretically studied in VLC upon user mobility to provide seamless connectivity when mobile users cross neighbor lighting cells and evaluated by only simulation results [62, 67].

Nevertheless, it is still an open issue that how a certain transmission is handed over from one transmitter to others upon user mobility. It is possible to serve user mobility by combining RF with VLC [18, 19, 64] to form feedback channels through an RF uplink. However, such a VLC-RF HetNet has two drawbacks: i) the complication incurred in managing and operating such a system is non-negligible, and 2) it compromises the inherent flexibility of COTS-VLC systems that should be deployable largely independent of infrastructure support. As a result, we aim to devise and realize a roaming supported VLC system solely upon a lighting infrastructure for both downlink VLC and uplink mobility awareness.

2.4 Summary

In this chapter, we first investigate the system overview of a VLC system and related literature on low rate camera-based VLC systems which this thesis focuses on. In the second section, we highlight existing works on sensing via both active and passive visible light, and obtain inspiration of innovating current VLS systems by LED sensing. Finally we survey existing works which challenge the roaming issue in VLC for mobile users. From those seminal works, we can see that either VLC or VLS systems are still open for researchers albeit both are extensively exploited by our pioneers. Therefore in this thesis, we attempt to make innovations in terms of both VLC and VLS to push forward with implementing practical VLC/VLS systems.

Chapter 3

CeilingTalk: Lightweight Indoor Broadcast Through LED-Camera Communication

In this chapter, we re-study the issue of realizing VLC-based broadcast using LEDs as transmitter and smartphone cameras as receivers. On one hand, we present CeilingTalk as a practical LED-Camera VLC system enabling LED-VLC using COTS devices. We innovate both coding and decoding mechanisms to cooperate transmission among multiple adjacent lights, so as to boost throughput and improve the link reliability. On the other hand, we build a model for such an LED-Camera VLC system to provide guidelines on future deployments of VLC systems. Based on the testbed of CeilingTalk, extensive experimental results demonstrate the effectiveness of our LED-Camera VLC model and the performance of CeilingTalk.

3.1 Introduction

Using visible light spectrum as the communication media has a long history that can be traced back to 19th century, and VLC has been holding the promise of extremely high data-rate and very low-cost for a few decades [8]. Nevertheless, it is the boosting market of LED that has drastically accelerated the development of VLC as a supplement to existing wireless standards (e.g., Wi-Fi). As LEDs are becoming the pervasive lighting source for indoor environments such as shopping malls and office/residence buildings,

and they have a ready access to power/information networks, we now have a handy infrastructure for implementing VLC-enabled wireless systems. However, whereas major research efforts have been made to boost the capacity of VLC [10, 11] and to enable indoor localization [12, 13, 14], harnessing the potential of LED-VLC using COTS devices seems to be largely neglected.

Following the seminal work of [15], implementing a receiver applying the rolling-shutter effect of a CMOS camera has become a de facto standard for LED-VLC using COTS devices [13, 16]: only a customized light sensor may serve as an alternative because light sensors in smartphones are optimized for dynamic range rather than response speed [43]. So it appears to be a common belief that enabling LED-VLC using COTS devices is an addressed problem. However, the system built in [15] requires a secondary medium, a plain surface (to avoid interference from textures), for light reflecting. While the *Signal Noise Ratio* (SNR) of such reflected VLC could be very low in a well-lit room, the difficulty in finding a satisfactory surface in an indoor space may substantially confine the practicality of such a system. Consequently, the validity of the derived models and insights also become questionable.

In fact, VLC has quite a few advantages over existing wireless infrastructures (e.g., Wi-Fi and BLE) even without its high data-rate promise. First, the communication infrastructure is virtually free due to the default lighting requirement of indoor spaces. Secondly, the energy consumption of LED transmission is negligibly low as it is incurred only by the control units. Last but not least, the location-bound communication ability of VLC meets perfectly the need from the long envisioned location-based service: coupons or advertisements can be delivered exactly according to the users' locations. Practical VLC implementations using COTS devices may immediately bring these benefits to us, while allowing for a better understanding of future VLC deployments from theoretical and modeling perspectives.

In this chapter, we re-visit the issue of realizing VLC-based broadcast using LEDs as transmitter and smartphone cameras as receiver. On one hand, we aim to build a practical system that works perfectly under normal lighting conditions. We design a coding mechanism that enables cooperative transmission among multiple close-by light sources, and we also innovate in an efficient decoding scheme to handle the transmission asynchrony. On the other hand, we intend to extract model parameters (e.g., which

factors affect the data rate) and hence provide guidelines on future deployments of VLC system. Our major contributions are:

- We build CeilingTalk as a practical wireless broadcast system, using common LEDs as transmitters and smartphone cameras as receivers, without relying on media other than the light itself.
- We are the first to employ rateless codes to enhance reliability and also to improve the network throughput through cooperative transmissions.
- We also innovate in a lightweight decoding scheme that avoids intensive image processing for tackling both spatial and temporal asynchrony in transmissions, making it amenable to a full smartphone-based implementation.
- We develop a communication model to characterize this LED-Camera VLC by extracting parameters from the experiments on CeilingTalk.
- We conduct extensive field experiments to validate the effectiveness of our LED-Camera VLC model, as well as to demonstrate the promising performance of CeilingTalk.

The rest of this chapter is organized as follows. We first introduce the important preliminary of CMOS camera's rolling-shutter effect in Sec. 3.2. Subsequently, we illustrate the system architecture of CeilingTalk in Sec. 3.3 and analyze the factors impacting system performance in Sec. 3.4. The extensive evaluations on CeilingTalk are reported in Sec. 3.5. Finally Sec. 3.6 quickly summarizes this chapter.

3.2 Rolling-Shutter Effect of a CMOS Camera

Since the rolling-shutter effect of a CMOS camera is an important building block of CeilingTalk, we briefly introduce its basics along with related terminologies before diving into our system design. Suppose we have an LED luminaire emitting modulated light (i.e., it turns ON and OFF according to a preset pattern) that is to be received by a CMOS camera. The rolling-shutter effect of a camera, instead of exposing the whole image at once, conducts the exposure in a column-by-column (or row-by-row) manner: a column is exposed for T_e before it is read out for T_r, and the next column

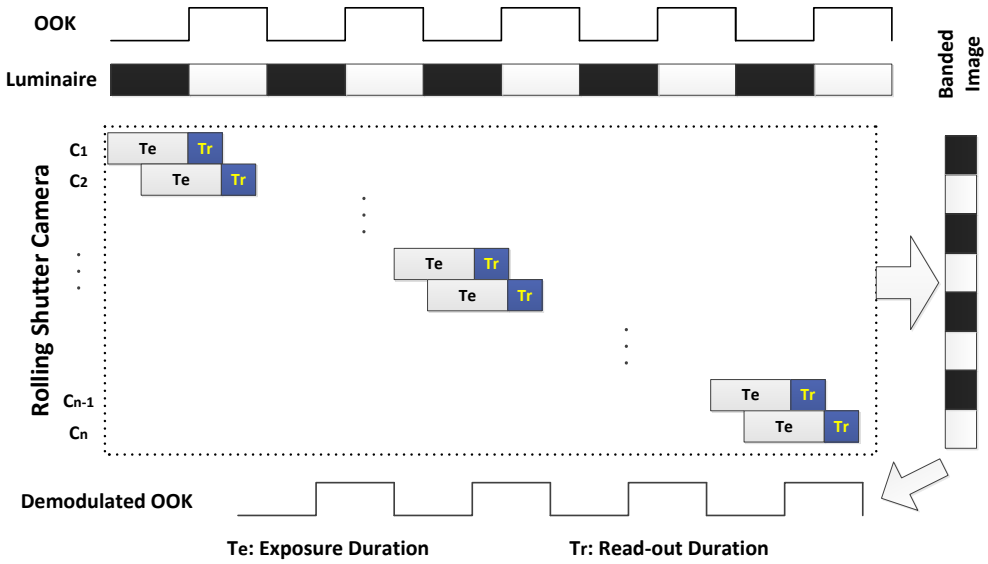

Figure 3.1: Rolling-shutter effect of a CMOS camera on a smartphone.

gets exposed T_r after the previous one. When the luminaire is ON and a column is exposed at the same time, the column is bright; otherwise it is dark. As a result, the camera is sampling the intensity modulated signals with an interval T_r and thus a sampling frequency $F_r = 1/T_r$, leading to a banded image that carries the information sent by the luminaire. Here F_r is known as *rolling-shutter frequency*; it actually bounds the modulation frequency from above: as F_r is often in the order of tens of kHz, the supported modulation frequency is up to several kHz according to Nyquist Sampling Theorem [68]. A graphical illustration is provided in Fig. 3.1. In reality, the camera may expose and read out multiple columns at the same time, resulting in another important parameter W_r, or *rolling-shutter width*. Consequently, in a banded image sampled by the camera, either the whole W_r columns are bright or they are dark; this further suggests that the width of each band should be a multiple of W_r. The detailed relations between these parameters and the throughput shall be explored in 3.4.2.

3.3 System Architecture

CeilingTalk consists of two main components: COTS LED luminaires as stationary transmitters to emit intensity modulated light and smartphones as receivers. A user holding a smartphone may freely wander in the indoor environment and receive location-

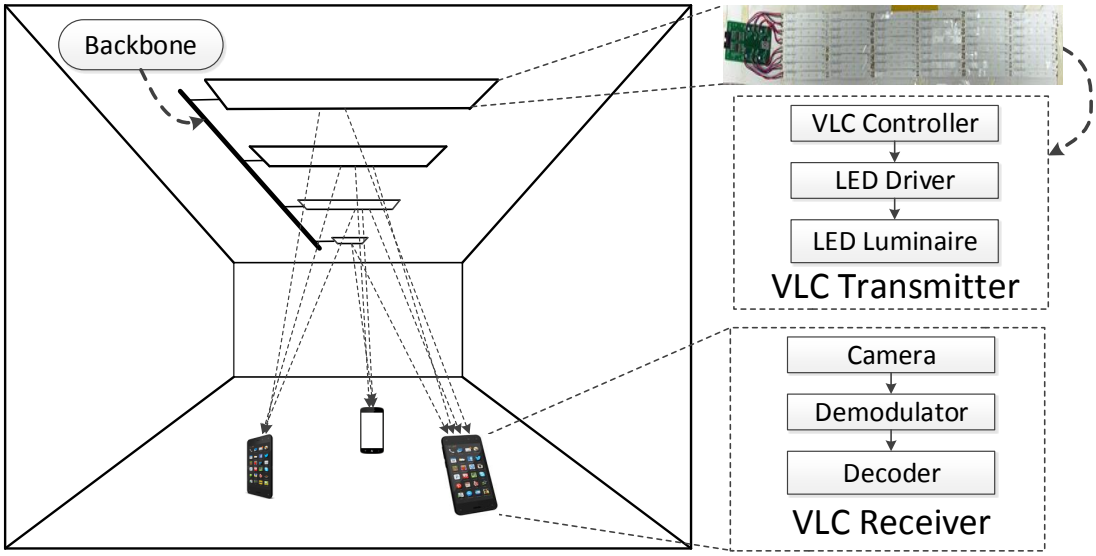

Figure 3.2: System architecture of CeilingTalk.

bound information from nearby LED luminaires, as illustrated in Fig. 3.2. In this section, we focus on presenting our innovations in designing the coding/decoding mechanisms. In particular, we explain how we may combine several transmissions from multiple luminaires to achieve higher throughput and reliability. And we also describe an efficient decoding scheme that avoids computation intensive image processing for handling both spatial and temporal asynchrony in transmissions.

3.3.1 A Hybrid OOK-PWM Modulation

CeilingTalk employs a hybrid modulation of *On-Off Keying* (OOK) and *Pulse-Width Modulation* (PWM) as shown in Fig. 3.3. As the simplest modulation method, OOK is universally employed on VLC, where the LED is switched ON or OFF to represent data bits "1" or "0", respectively. We further embed a high frequency PWM in each OOK bit for dimming control: it allows the light intensity of an LED luminaire to be adjusted without either causing flicker or interfering data transmission. We refer to Sec. 3.3.5 for more details. As the PWM is supposed to be undetectable by the rolling-shutter effect at the receiver, it runs at 80 kHz in CeilingTalk.

The packet structure in CeilingTalk is set according to Fig. 3.4. Each packet has a preamble of bit string "111110" and it always ends with a single bit "0". The *Packet Sequence Number* (PSN) comes after the preamble and it is followed by the payload.

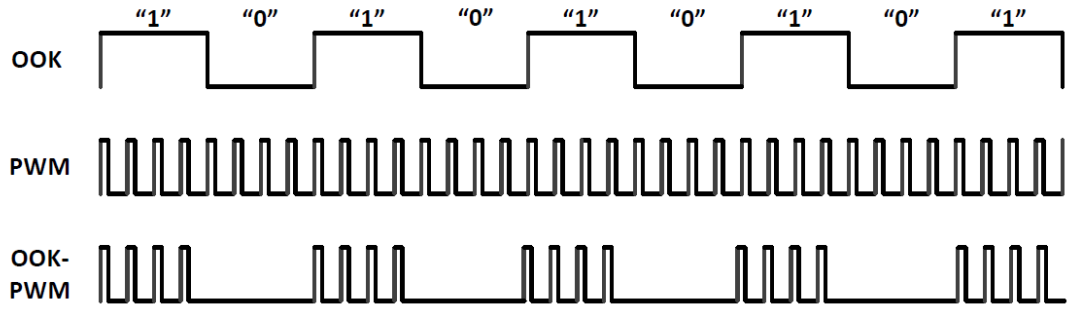

(a) OOK-PWM with duty cycle less than 50%

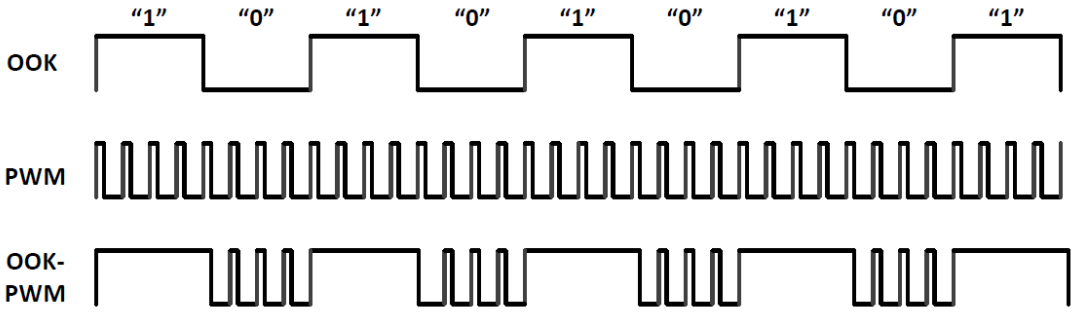

(b) OOK-PWM with duty cycle more than 50%

Figure 3.3: OOK-PWM modulation: the combination of OOK-PWM effectively avoids flicker and also allows for dimming control.

For bits in both the PSN and payload, CeilingTalk applies 4B6B *Run Length Limit* (RLL) line coding [8] for its simplicity and absent of DC component. As 4B6B coding guarantees no more than four adjacent "1" or "0" bits, the preamble generates the widest bright band in the image and is hence easy to be detected as the indication of the start of a packet. Note that the five adjacent "1" in the preamble would not cause flicker. Within the duration of one packet, there are only 5 continuous bright bands out

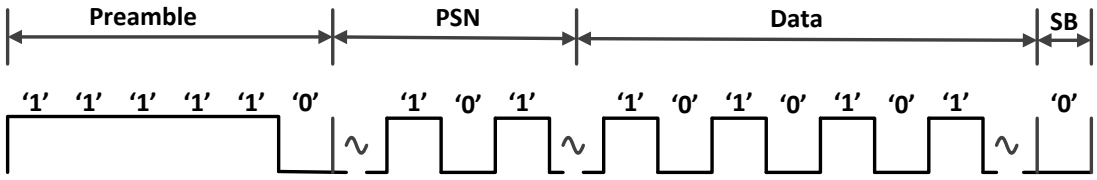

Figure 3.4: CeilingTalk packet structure: a packet consists of a preamble "111110", up to 8-bit PSN, 32-bit data payload, and a tailer "0".

of 67 bands in total. The flicker factor is thus too low to be discernable. Moreover, we can adjust the duty cycle of PWM for the continuous bands to further alleviate flicker.

3.3.2 Encoding and Code Assignment

As LED-Camera VLC is normally unidirectional, a transmitter has no knowledge about the reception status of a receiver. Therefore, a *Forward Error Correction* (FEC) scheme has to be in place to combat the packet loss. Moreover, simultaneous transmissions from multiple luminaires also call for an encoding mechanism that enables the transmitters to cooperatively improve the throughput and reliability. To this end, rateless codes appear to be an appealing choice, as it encodes k original packets into a potentially infinite number of packets so that the receiver can successfully recover the original packets by receiving any $m > k$ encoded packets.

Among all rateless codes, Raptor code [69] comes with linear time encoding and decoding, causing low computation complexity and decoding overhead. Therefore, CeilingTalk adopts Raptor code and its implementation [70]. As shown in Fig. 3.5, a set of intermediate packets are firstly derived from the original packets so that the intermediate packets can sufficiently reconstruct the original ones. Repair packets are then produced by applying LT encoding; each is derived by XORing a number of intermediate packets. The final encoded packets are the combination of the original and repair ones. As CeilingTalk has no acknowledgement from the camera for the transmitter to stop coding and sending, we regulate the transmitter to send out only $n = 1.25k$ encoded packets for every k original packets. Upon receiving slightly more k packets, a receiver uses Gaussian elimination to start recovering the original ones.

As CeilinTalk relies on the lighting system to transmit packets, it has the opportunity to leverage multiple close-by luminaires to perform cooperative transmissions for improving both throughput and reliability. Imagine a simple scenario that a smartphone receives messages from two luminaires. Suppose we let the luminaires to work independently, then either we waste the capacity of one luminaire if the message is sent by only one luminaire or individual packets loss may ruin both messages if two luminaires are transmitting. However, if we allow the two luminaires to cooperatively transmitting, then we may either reduce the transmission time or let the two transmissions complement each other using the Raptor coding. In fact, the reliability enhancement is particularly useful when a user is moving. Nonetheless, the challenge here is how we

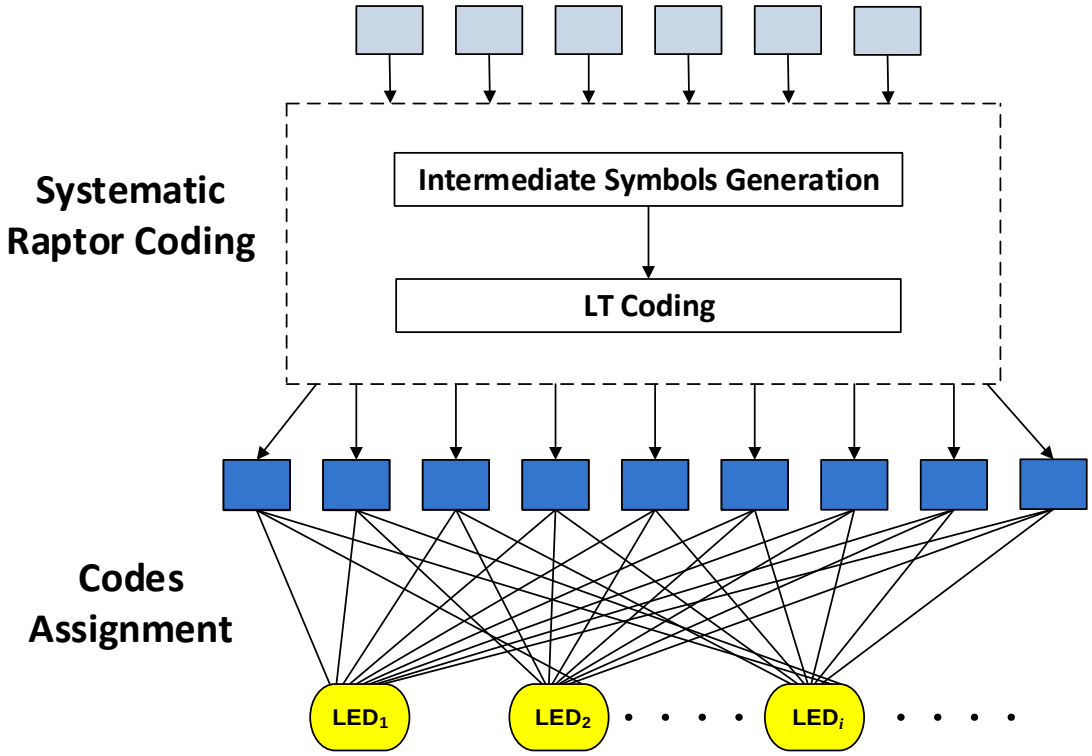

Figure 3.5: Raptor coding and codes assignment.

assign the encoded packets to individual luminaires, so that every received packet from any of luminaire can effectively contribute to decoding.

Suppose there are $N_L : N_L \ll n$ luminaires in a cooperative domain, and they are labeled as $\mathsf{LED}_0, \mathsf{LED}_1, \cdots, \mathsf{LED}_{N_L-1}$. CeilingTalk currently adopts a cyclic assignment scheme in which it assigns all the n encoded packets (codes) to each luminaire but in a circular shift manner, as illustrated in the lower part of Fig. 3.5. In particular, we set the offset of the i-th luminaire as $o_i = i\lceil n/N_L \rceil, 0 \leq i \leq N_L - 1$, then the sequence numbers of the codes assigned to this luminaire is $\{o_i, o_i+1, \cdots, n-1, 0, 1, \cdots, o_i-1\}$. Apparently, this assignment may increase the throughput by N_L times if the reception from each luminaire is perfect, and it certainly allows for quick compensations of lost packets. In a large indoor facility, there can be multiple cooperative domains, and our assignment scheme is applied individually to each of these domains. Since the luminaires are all connected to the same power grid, *Power Line Communication* (PLC) [71] can be used for scheduling transmissions.

3.3.3 Pre-Decoding: RoI Extraction

Given a frame captured by a camera, only the banded sections in it contain information to be decoded. Such an information-containing region is termed *Region of Interest* (RoI) [72]. Due to the **spatial asynchrony** inherent to the transmissions, the location of RoIs within a photo is not known in advance. Though it is visually straightforward to recognize these RoIs, extracting them automatically is far from trivial. Existing proposals [14, 27] resort to sophisticated *Computer Vision* (CV) techniques, introducing such a high computational overhead that the computations have to be offloaded to a cloudlet server [14].

Our innovative scheme makes use of the default function of the camera to produce RoI masks so that the intensive image processing can be largely avoided. During a continuous reception, the first frame of every p frames is exposed normally (e.g., 1/60s) as shown in Fig. 3.6(a) and the rest are quickly exposed (e.g., 1/7500s) to obtain Fig. 3.6(d). The first frame is then converted to a binary RoI mask for extracting the RoIs from the remaining $p-1$ frames. As a normal exposure would over-expose the luminaires, we convert the first frame to a binary one shown in Fig. 3.6(b) by setting pixels with Y value (the luma component of YCbCr color space) exceeding threshold Y_t to "1" and otherwise to "0"; here Y_t is normally set to 240 as the Y value for a luminaire under the normal exposure is almost always 255. Then the algorithm builds a rectangular contour for each cluster of "1" pixels to create the RoI mask shown in Fig. 3.6(c). Obviously, the information to be decoded from the remaining frames can only exist within these contours. As the frames are shot within a very short period of time, we assume there is no tilting/shifting between the mark and the remaining information frames. However, we are also on the way to design an gyroscope-assisted algorithm to compensate for hand motions.

To establish a baseline, we also propose a CV-based RoI extraction scheme. Basically, each frame first goes through a Gaussian blur, and then the aforementioned binary conversion (with a different threshold) and contour detection procedures are used to extract the RoIs. All these functions are carried out by using OpenCV for Android, and this scheme is already a much simplified version of those used in [14, 27]. Obviously, the Gaussian blur procedure is both time and energy consuming.

(a) Normally exposed frame

(b) Binary frame

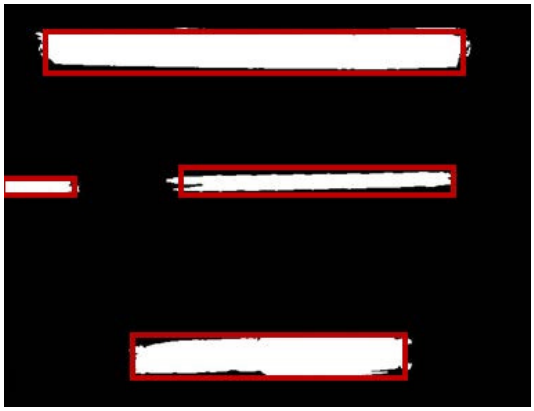

(c) Detected ROIs

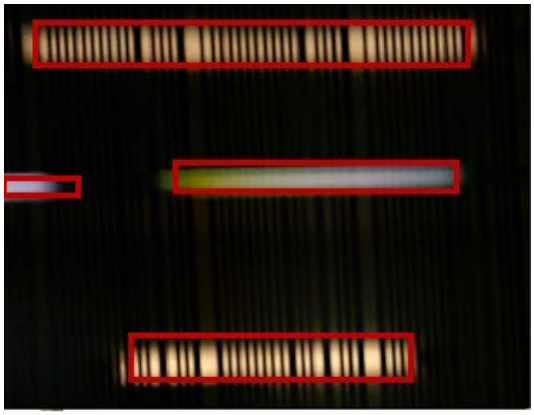

(d) ROIs for decoding

Figure 3.6: Lightweight RoI extraction: for each normally exposed frame (a), we convert it to a binary frame in (b) and detect contours in (c), so that RoIs in a quickly exposed frame (d) can be extracted.

3.3.4 Demodulation and Decoding

The traditional demodulation methods often pre-determine a set of sampling times and then compare the samples with a threshold (to distinguish bright and dark bands). Whereas earlier proposals suggest using polynomial regression [15] to determine the threshold due to low SNR, CeilingTalk (with a sufficient level of SNR) achieves a satisfactory detection accuracy by simply setting the threshold as the average of the maximum and minimum pixel illuminance values within a RoI. Nevertheless, the blooming effect of a camera (bleeding or smearing photons from saturated pixels to adjacent

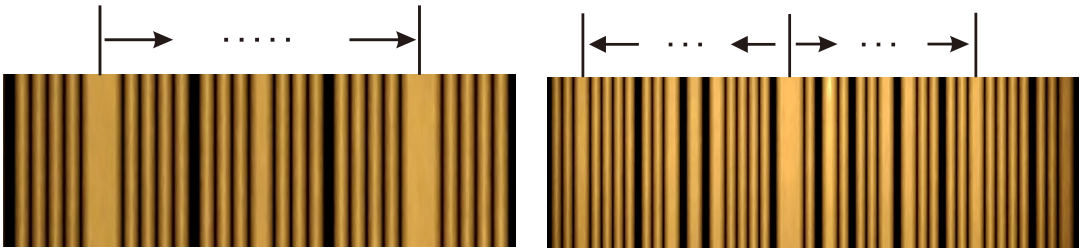

(a) Normal demodulation. (b) CeilingTalk demodulation

Figure 3.7: Compare CeilingTalk demodulation with the normal one. (a) Normal demodulation requires two preambles, and (b) CeilingTalk demodulates in for- and back-ward directions starting from the preamble.

pixels) brings difficulty in determining the sampling times. For CeilingTalk, we make demodulation decisions by reasoning on the widths of bright/dark bands. Given the packet structure described in Section 3.3.1, we can only have four widths for white bands and four for dark bands to be decoded after the preamble, namely $W_{1b}, ..., W_{4b}$ for bright bands and $W_{1d}, ..., W_{4d}$ for dark bands, whereas the preamble has a signature of W_{5b}, where W_{1b} represents the width of one bright band and likewise for other symbols. As the blooming effect diminishes with the number of consecutive bright bands, we derive 5 possible relations between the symbol width W the aforementioned quantities: i) $W_{2b} \leq 2W_{1b}, W_{2d} \geq 2W_{1d}$, ii) $W = W_{1b} + W_{1d}$, iii) $2W = W_{2b} + W_{2d}$, iv) W_{3b} or $W_{3d} \approx 1.5W$, and v) W_{4b} or $W_{4d} \approx 2W$, where $W = W_r F_r / F$ is determined by the camera parameters explained in Section 3.2: F_r is the rolling-shutter frequency, W_r is the rolling-shutter width, and F is the working frequency of an LED luminaire.

Following the aforementioned reasoning, the demodulation algorithm scans through the whole packet to recognize the widths of bands. A normal demodulation scheme identifies and scans a packet as the region between two widest bright bands of width W_{5b} (roughly equal to $2.5W$) as shown in Fig. 3.7(a). This would, however, sacrifice half of the RoI length (hence halving the throughput) in the worst case given the **temporal asynchrony** in transmissions: a packet could start anywhere within a RoI. Therefore, CeilingTalk employs a bidirectional demodulation process as shown in Fig. 3.7(b): it starts the scanning from a single widest bright band and collects all the bright and dark bands in both forward and backward directions. All bright/dark bands are clustered into 4 groups, namely $W_{1b}/W_{1d}, \cdots, W_{4b}/W_{4d}$. As there are at most several tens of bands, the clustering can be conducted efficiently. Finally, starting from the widest

band again, the bits are recognized in both directions until a predetermined number of bits are decoded. This demodulating flow is shown in Fig. 3.8. We also give a concrete example in Fig. 3.9 to demonstrate the demodulation procedure using a packet with 8 bits (12 RLL 4B6B bits) as an example. From the widest bright band, the bits obtained in backward direction are "0001101" and the bits forward are "0011100". As there are 12 RLL bits in total, we can combine the two sequences by removing the duplicate bit

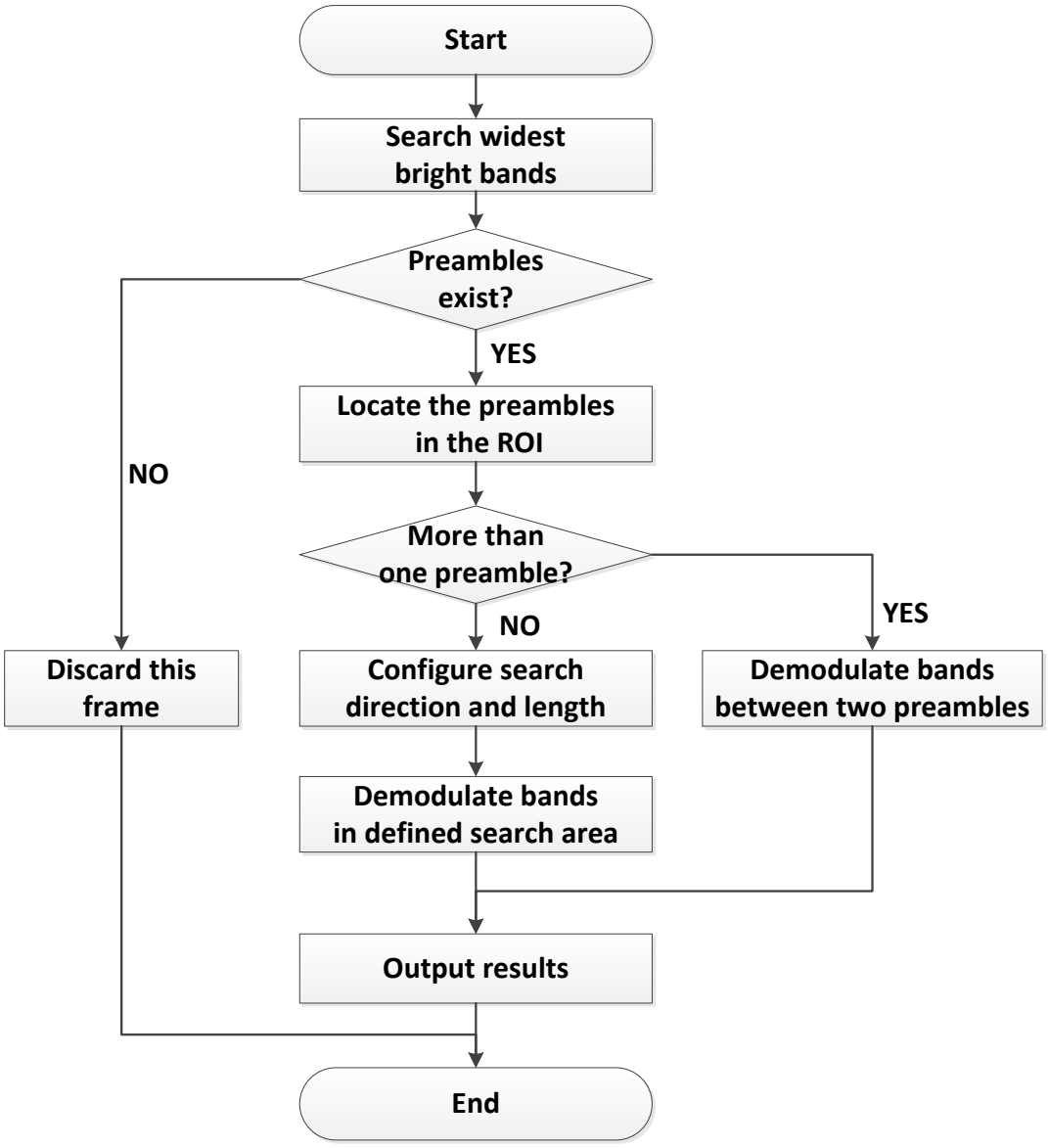

Figure 3.8: Demodulation procedure flowing chart.

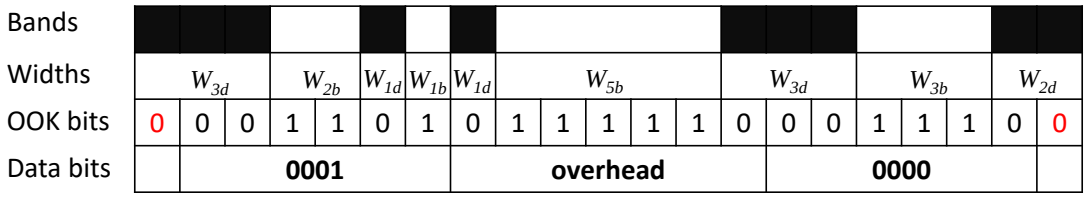

Figure 3.9: Demodulation procedure for an 8-bit packet.

"0" and obtain the complete packet as "001110001101" and then "00000001" after RLL 4B6B decoding.

After the demodulation, Raptor decoding procedure takes over with the knowledge of the size of a packet and the number of original packets k. Upon receiving $m = k(1+\epsilon)$ encoded packets ($\epsilon = 0.15$ is chosen to be the overhead of LT codes for CeilingTalk), Gaussian elimination is used for decoding. As one frame may capture multiple RoIs, the decoder waits for all RoIs to be demodulated and combines all received packets in one frame for decoding, so as to reduce the decoding latency dramatically. As mentioned in Sec. 3.3.2, this allows for almost immediate compensation of packet loss and a manyfold increase in throughput.

3.3.5 Dimming

Dimming is an important requirement posed by IEEE 802.15.7. As mentioned in 3.3.1, CeilingTalk can support wide range dimming duty cycle by its hybrid modulation. As the duty cycle of OOK D_{OOK} is fixed given the defined packet structure, we can tune that of PWM D_{PWM} to meet a certain dimming requirement. Specifically, we can tune the overall duty cycle D from 0 to D_{OOK} by embedding the PWM signal into OOK "1":

$$D = D_{\text{OOK}} \times D_{\text{PWM}}, \tag{3.1}$$

as shown in Fig. 3.3(a). To reach a full range of D, we can further embed the PWM signal into OOK "0" so that the value of D can go all the way up to 100%:

$$D = D_{\text{OOK}} + (1 - D_{\text{OOK}}) \times D_{\text{PWM}}, \tag{3.2}$$

as shown in Fig. 3.3(b). Obviously, making D too close to 0 or 100% can hurt the SNR and thus the throughput, so a preferable range of D for CeilingTalk is from 10% to 70%.

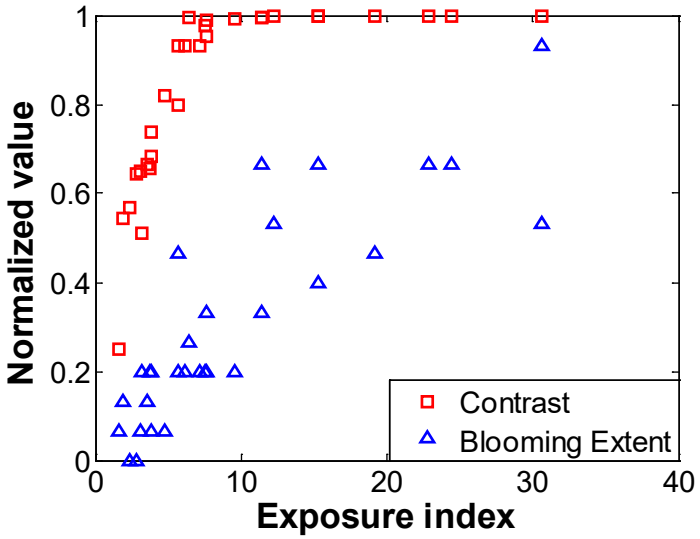

Figure 3.10: The image quality with varying exposure indices. A higher exposure index leads to a higher contrast but also a more severe blooming extent.

3.4 Performance Analysis

In this section, we analyze the performance-impacting factors and present the achievable performance of CeilingTalk under realistic constraints.

3.4.1 Receiver-Camera Configurations

The major issue hampers the performance of CeilingTalk is the inter-symbol interference caused by the blooming effect. Ideally, bright and dark bands should have the same width and the demodulation should be trivial. However, the blooming effect causes a bright band to leak into a neighboring dark band, resulting in irregular widths in bands. While reducing exposure index may suppress this effect, it affects SNR too. So we intend to verify the impacts of various combinations of LED illuminance and camera sensitivity settings on both the SNR (contrast in the case of CeilingTalk) and blooming effect.

We have three parameters at hand: illuminance, ISO and exposure time; they control output of each pixel (sensor) by adjusting the incident light intensity, sensor sensitivity, and time to receive photons, respectively. We vary the LED illuminance from 153lux to 301lux (corresponding to those obtained at 1.5m distance with the PWM duty cycle from 10% to 25%), the ISO sensitivity from 100 to 300, and exposure

time from 1/7500s to 1/5000s, and the exposure index is proportional to the product of illuminance, ISO and the reciprocal of exposure time. In order to unify contrast and blooming effect into the same perspective, we normalize them before plotting the results in Fig. 3.10. The normalized contract is computed as $(Y_b - Y_d)/Y_{\max}$, with Y_b, Y_d, and $Y_{\max}$ being the luminance values of the bright band, the dark band, and the camera specified maximum. We indicate the blooming effect by W_{1b} and compute its normalized value as $(W_{1b} - 0.5W)/(0.5W)$. Fig. 3.10 shows that, though the contract increases with the exposure index initially, it quickly gets saturated. At the same time, the blooming effect appears to grows linearly with the exposure index. In fact, when we reach the highest exposure index, W_{1b} reaches up to 32 pixels, almost occupying its neighboring dark band. Apparently, the optimal exposure index should be right before the saturation of the contrast, where the blooming effect is still well controlled. Considering that the bands can be even narrower if the LED frequency is further increased to enhance throughput, CeilingTalk could be more sensitive to the blooming effect. Therefore, given a normal indoor illuminance between 200 to 700lux by standard illumination requirement, we tune the PWM duty cycle to meet the requirement, while choosing ISO as 200 and exposure time as 1/7000s in the office environment where CeilingTalk is deployed and tested; more detailed justifications on these settings will be presented in Sec. 3.5.2.

3.4.2 System Model

We hereby explain how we set the packet length packet (in particular the payload length according to the structure specified in Sec. 3.3.2) and also derive the achievable bit rate given several design parameters.

We first set up the relations between key system parameters and the admissible packet length (thus bit rate), then we deduce their quantities based on the specific devices adopted by our current implementations. Let us assume i) the LED transmitter has length L long and works at frequency F, ii) the camera receiver has a focal length f_c, sensor width S_w, frame width I_w, column resolution P_c, rolling-shutter frequency F_r and its corresponding width W_r at given column resolution, and frame rate R, and iii) the communication distance is less than d and there are N_L transmitters within this range, we have:

- The projected RoI in a frame has the length of $L_{\text{RoI}} = \frac{\phi L}{d}\sin(a_v) \leq P_c$, where $\phi = f_c I_w / S_w$ and a_v is the view angle.
- The number of OOK bits an RoI can cover should satisfy $N \leq \left\lfloor \frac{L_{\text{RoI}} F}{W_r F_r} \right\rfloor \leq \frac{P_c F}{W_r F_r}$.
- To ensure that an RoI can cover at least one complete packet under asynchronous transmission, the packet size in data bits should satisfy $P_{\text{size}} \leq \lfloor \eta(N-7) \rfloor$, where η is the encoding efficiency of employed modulation scheme, e.g. $\eta = 4/6$ for 4B6B, and each packet has 7 bits of overhead.
- According to above analysis, we can bound the bit rate of the CeilingTalk as:

$$\begin{aligned} C = N_L R P_{\text{size}} &\leq N_L R\Big(\left\lfloor \eta \times (\frac{L_{\text{RoI}} F}{W_r F_r} - 7) \right\rfloor \Big) \\ &\leq N_L R\Big(\left\lfloor \eta \times (\frac{P_c F}{W_r F_r} - 7) \right\rfloor \Big) \end{aligned} \tag{3.3}$$

Now we can put these parameters into practical perspectives in order to check the actual quantities of packet size and achievable bit rate of CeilingTalk. Given the rear-facing camera of Nexus 6 as the CeilingTalk receiver, we have $R = 30$ fps and $F_r = 19$ kHz as we measured, $W_r = 3$ pixels (i.e., three columns are exposed at one time) under a preview resolution of 1920×1440, which allows us to derive $\phi = 2325$ pixels. For the front camera, the parameters are slightly different from the rear camera: $W_r = 4$ pixels and hence $\phi = 2007$ pixels under preview resolution of 1024×768. As the working frequency of LED can go up to a few GHz, the working frequency of CeilingTalk is restricted mainly by the capability of the receiver, namely the rolling-shutter frequency F_r of the camera.

Since we measured $F_r = 19$ kHz, we have to set $F \leq F_r/2 = 9.5$ kHz. We choose $F = 8$ kHz for reliability purpose, which results in a symbol width $W = 11$ pixels at preview resolution of the rear camera and $W = 9$ pixels at preview resolution of the front camera. Apparently, the working frequency is set to meet the decodability at the preview resolution, as we need some "guard pixels" to combat the blooming effect. In an indoor environment, the ceiling is around 3 m from a hand-held smartphone camera sitting right below it. Considering a 0 to 4 m horizontal distance, we have $d_{rc} = 5$ m as our maximum communication distance for the rear camera. As for the front camera,

normally we hold the phone in parallel with the floor, thus we regulate $d_{fc} = 3$ m as the maximum communication distance for the front camera.

Substituting $F = 8$ kHz and $d_{rc} = 5$ m and $d_{fc} = 3$ m into earlier formulas, we obtain suitable $N \leq 78$ for both rear and front cameras and thus maximum $P_{\text{size}} = 44$ bits.As we need a few guard bits to combat tilting of the phone or RoI extraction inaccuracy, we set the actual $P_{\text{size}} = 40$ bits. Therefore, CeilingTalk can offer a bit rate of 1200 bps with one transmitter at the maximum communication distance, given the frame rate $R = 30$ fps of the cameras, as summarized in TABLE 3.1 [1]. This bit rate can be further improved by combining more transmitters and using the full resolution of the camera. For example, if we have 6 transmitters within the communication range and we use either front camera or rear camera for decoding, the bit rate can be boosted to 7200 bps in theory.

For a single transmitter, there are other ways to improve the bit rate. According to Eq. (3.3), reducing the communication distance can increase the bit rate in proportion. Also, using a smartphone camera with a higher resolution and/or frame rate can also proportionally increase the bit rate. For example, if we use iPhone 5s with a frame rate 120 fps, the bit rate can be tripled.

Table 3.1: System setting and achievable capacity

	Rear-facing	Front-facing
Resolution	1920×1440	1024×768
F	8 kHz	8 kHz
W	11 pixels	9 pixels
d	5 m	3 m
N	78	84
P_{size}	40	40
C	1200 bps	1200 bps

[1] Although the current prototype of CeilingTalk is using Nexus 6 as the receiver, it can be readily extended to diversified smartphones and the parameters are set by the device with the lowest performance.

3.4.3 Practical Considerations

The above discussions assume rather ideal scenarios, but various interferences exist in a realistic deployment. One may expect the ambient lighting to be a major interference to CeilingTalk communications, but the fact is that ambient lighting only causes noticeable noise if a light sensor is used as the receiver [43] or if the rolling-shutter sensing is applied to some surface reflection [15, 16]. In our case, as CeilingTalk directly uses the LED luminaires as the signal source, the SNR is so high that we can run a receiver with an extremely short exposure time, suppressing the interference (ambient light "leaking into" the RoIs) to the largest extent. Therefore, the interference from ambient lighting can surely be neglected for CeilingTalk.

Although CeilingTalk regulates each packet to be transmitted within periodic 33.3 ms time frames (i.e. the video frame length captured by the camera), missing packets are inevitable due to varying inter-frame gaps and the gap jitter induced transmitter-receiver asynchrony. Raptor codes show its advantage again in combating the asynchrony: since the packet loss caused by inter-frame gaps (and their jitters) is about 5.6% as we measured, the overhead 25% that we use for Raptor encoding is sufficient to generate repair packets for compensating the packet loss caused by varying inter-frame gaps.

One major challenge CeilingTalk faces is user motion, in particular, hand micro-motion caused by user mobility during data reception. As we have cooperative transmissions to handle the user mobility during a reception, we shall only focus on the interference caused by hand micro-motion. Note that if a user totally moves out of a cooperative domain, the reception will fail but this is indeed the purpose of CeilingTalk's location-bound communication: the data service is location dependent.

For the hand micro-motion, we assume that its magnitude so minor that it does not cause mis-capturing of the transmitters, which is reasonable for users with normal physical conditions. Therefore, the major problem caused by hand micro-motion is twofold: on one hand, minor camera titling/rotating may distort the RoIs extracted from the first normal exposed frame, causing bit loss within an RoI. On the other hand, major camera tilting may cause certain RoIs un-decodable. While the minor changes can be compensated by gyroscope-assisted geometric transformations, we certainly need to constrain the major ones. Given a tilting angle α, we obtain the length of RoI $\frac{\phi L}{d} \times \cos(\alpha)$.

(a) An LED luminaire made of commercial LED strips

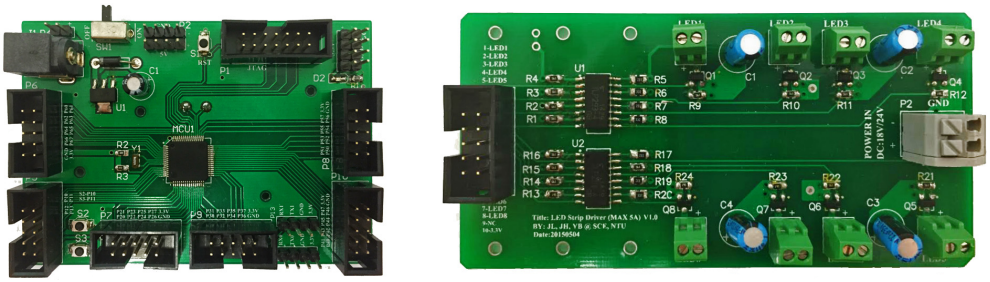

(b) The VLC control board and LED driver

Figure 3.11: A CeilingTalk transmitter.

Consequently, the bit rate in Eq. 3.3 is constrained by $C \leq \cos(\alpha) N_L R \left\lfloor \eta \times \frac{\phi LF - 7}{dW_r F_r} \right\rfloor$. In our current implementation, we choose $P_{\text{size}} = 40$bit that is 60 OOK bits subject to $N = 78$ OOK bits, so the rotation angle should be less than $\arccos(60/78) \approx 40°$ without incurring bit loss. Fortunately, we can let the application to alert a user for such packet loss and hence rely on user assistance to improve the performance.

3.5 Evaluation

We report the evaluation results on our CeilingTalk testbed in this section. We first explain the experiment settings, and then present the performance evaluations of CeilingTalk with respect to various parameters.

3.5.1 Experiment Settings

We build CeilingTalk transmitters with commercial LED strips [73] and self-developed LED driver. Fig. 3.11 shows one such transmitter; it includes an LED luminaire, a driver board, and a control unit. The LED luminaire is made of 16 LED strips each containing 36 LED chips, hence a dimension of 120 cm×8 cm similar to a common fluorescent luminaire. As this LED luminaire has a nominal drive current of 600 mA,

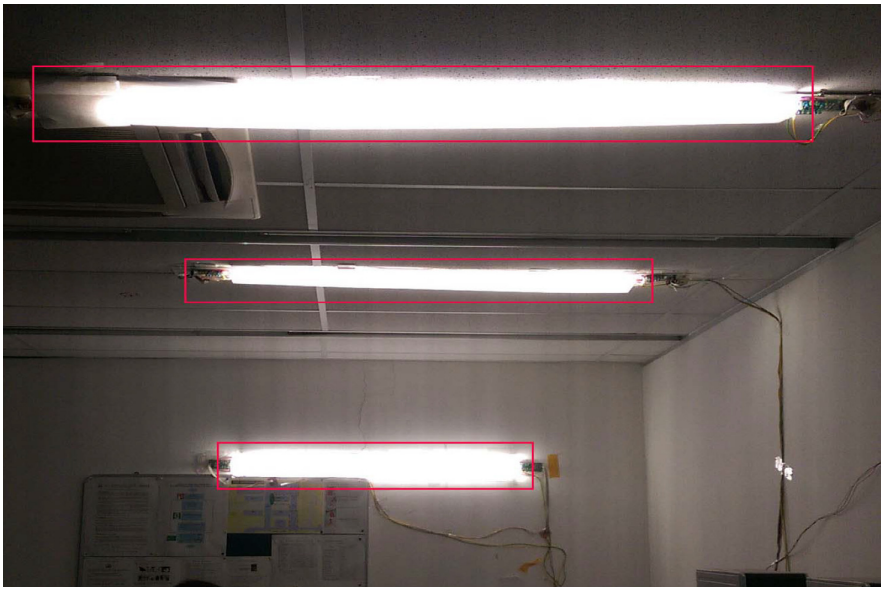

Figure 3.12: CeilingTalk testbed: three LED luminaires are mounted on wall and ceiling with an interval of 1.5 m, and the ceiling is 2.5 m above the floor.

we use low-cost transistors to build the driver circuit. To enhance the stability and readability of the transmitter, optocouplers are employed between the control unit and driver. In total, we deploy 3 such transmitters every 1.5 m in parallel in our lab, with one on the wall and the other two on the ceiling, as shown in Fig. 5.9. The one on the wall is deployed for performance evaluation at different transmission distances, while the other two are meant to emulate a realistic setting. We use a Nexus 6 smartphone as the receiver, with parameters specified in Sec. 3.4.2.

A message is divided into blocks, each contains k packets. Raptor code [70] encodes at the rate of $n = 1.25 \times k$. Given that the PSN field in a packet contains up to 8 bits, each block can have at most 256 coded packets. The decoding overhead is set $\epsilon = 0.15$. Each packet is transmitted repeatedly within a frame duration 33.3 ms.

For the dimming level setting, we vary the duty-cycle of PWM within its full range and ask 15 volunteers to observe the LED luminaires for dimming changes and flicker. We find that CeilingTalk's OOK-PWM modulation scheme can support a full range duty-cycle control, but when the duty-cycle is less than 3% , i.e. at very low dimming levels, the flicker becomes observable. Given that very low dimming levels are rare in the indoor environments, we fix the duty cycle of LED luminaires hereafter at 20% (roughly 250 lux at 1.5 m distance, a level with which all volunteers feel comfortable)

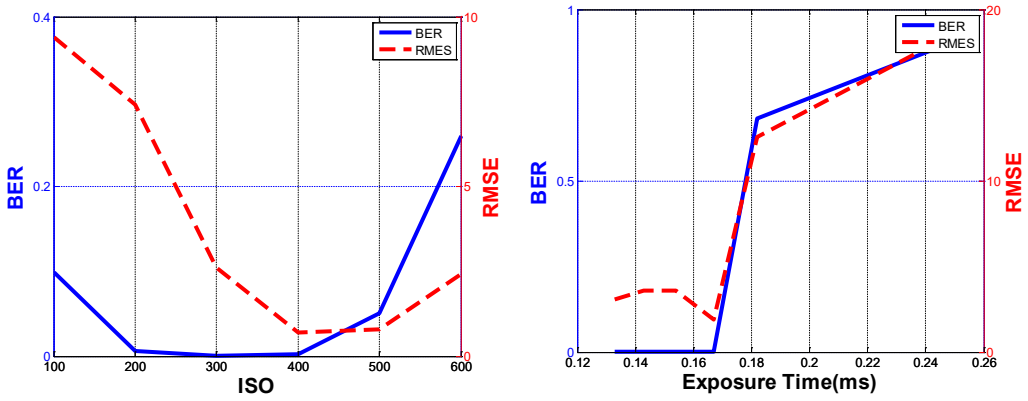

(a) BER vs. ISO

(b) BER vs. Exposure time

Figure 3.13: The impact of camera settings. (a) BER reaches the lowest at ISO from 200 to 400. (b) BER increases with the exposure time.

unless otherwise stated.

3.5.2 Camera Settings

In Sec. 3.4 we have analyzed how to choose the exposure time and ISO of the camera to strike a balance between high contrast and low blooming effect. Here we focus on the impact of camera setting on *Bit Error Rate* (BER) and *Packet Error Rate* (PER); both of them take the missing frames into account. In Fig. 3.13, we use *Root Mean Square Error* (RMSE) to measure the fluctuation in the widths of the bands. It indicates the difference between the widths of all detected bands and the widths of bands leading to accurate bit decision. RMSE has the direct impact on BER because the width of a band serves as the criterion for decoding. In Fig. 3.13(a), we fix the exposure time at 1/7000 s, the LED duty cycle at 20%, and communication distance at 3 m. With ISO varying from 100 to 600, RMSE and BER first decrease as the contrast is enhanced and then degrade as the blooming effect causes more irregular widths of bands. Fig. 3.13(b) illustrates how the exposure time affects the performance. We fix the ISO at 200 and other parameters as before. Due to the same reason of blooming effect, RMSE and BER remain stably low at short enough exposure time and then increase when the exposure time exceeds 1/6000 s. The result confirms to our analysis in Section 3.4. Therefore, CeilingTalk by default sets ISO at 200 and exposure time at 1/7000 s.

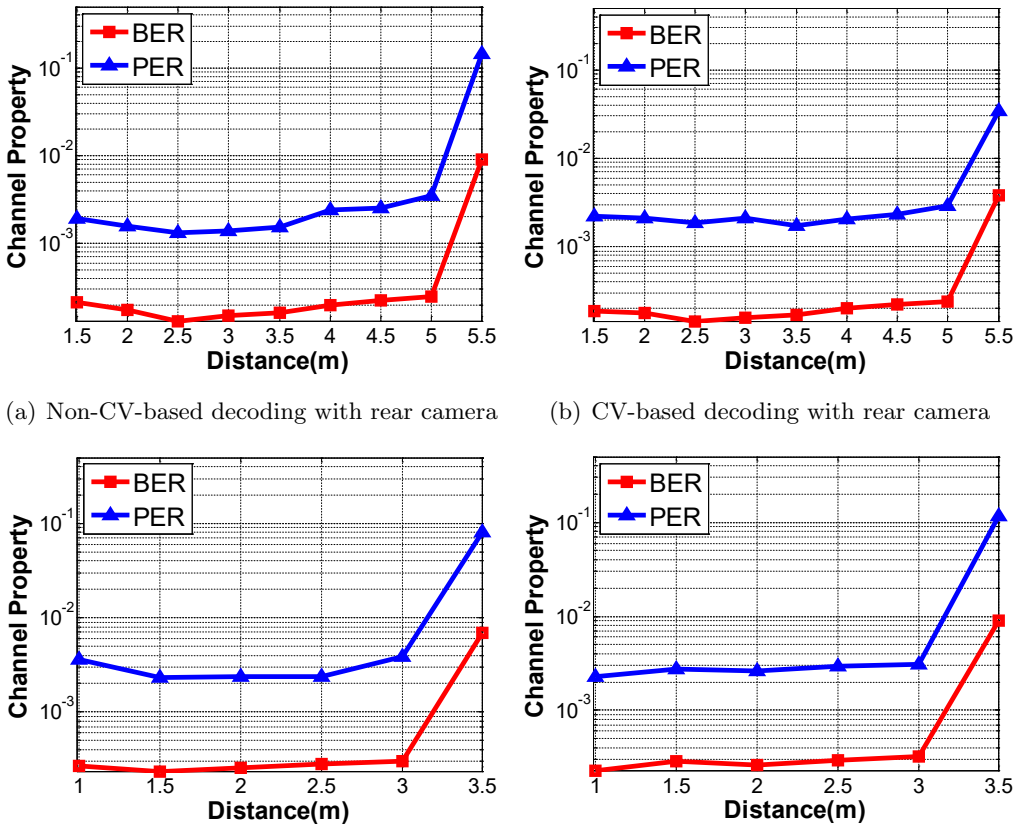

(a) Non-CV-based decoding with rear camera

(b) CV-based decoding with rear camera

(c) Non-CV-based decoding with front camera

(d) CV-based decoding with front camera

Figure 3.14: Channel properties under stationary scenarios. The channel is stable until the communication distance goes beyond 5 m and 3 m for rear and front cameras, respectively.

3.5.3 Channel Property

We first evaluate the channel properties with the camera fixed at a stationary position. In Fig. 3.14 we measure the channel properties in terms of BER and PER at different communication distances from 1.5 m to 5.5 m for the rear camera and from 1 m to 3.5 m for the front camera, and we also compare the performance of our Non-CV-based decoding method with the baseline CV-based decoding. We observe that both BER and PER stay at a low level regardless of the increasing communication distance until the $d > 5$ m for rear camera and $d > 3$ m for the front camera, respectively. At $d = 5.5$ m and $d = 3.5$ m, BER and PER of both rear and front cameras dramatically increase because the captured RoI becomes too small to cover P_{size}, thus causing non-negligible

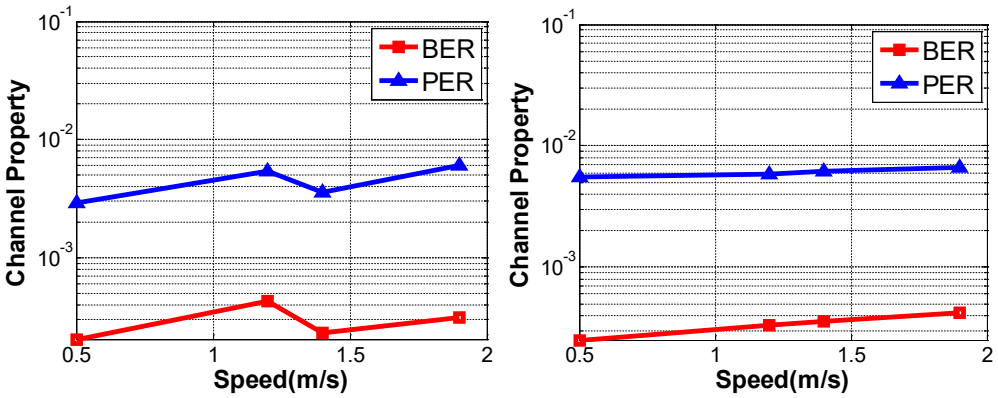

(a) CV-based decoding with rear camera (b) CV-based decoding with front camera

Figure 3.15: Channel properties under mobile scenarios. Both BER and PER stay at around 10^{-3} when users moving within a reasonable communication range.

decoding failures. Moreover, the performance in terms of BER and PER of the two decoding methods appear to be very similar, proving the superiority of our Non-CV-based method: the computation time is about 9 ms in our case, whereas the baseline CV-based method takes about 30 ms to complete.

We then evaluate the channel properties under mobile scenarios. We only use the CV-based decoding here due to drastic changes in the camera position. This experiment is conducted by two users. They hold the smartphone and walk arbitrarily within the communication range with different speed, while guaranteeing that the camera can always capture the targeted LED luminaire. During the experiment, the accelerometer on the phone is turned on to monitor the average walking speed. Fig. 3.15 shows that the BER and PER under mobile scenarios are comparable to (albeit slightly lower than) those of stationary scenarios, confirming the robustness of CeilingTalk against mobility. Both these two experiments allow us to conclude that CeilingTalk provides stable channels with very low BER/PER ($\sim 10^{-3}$) within a reasonable communication range for both rear and front cameras. Note that the non-monotonic trends of BER/PERs shown in both Fig. 3.14 and Fig 3.15 can be attributed to the non-uniformity in performing different sets of experiments. Therefore, we should interpret the results as roughly constant BER/PERs within a reasonable d.

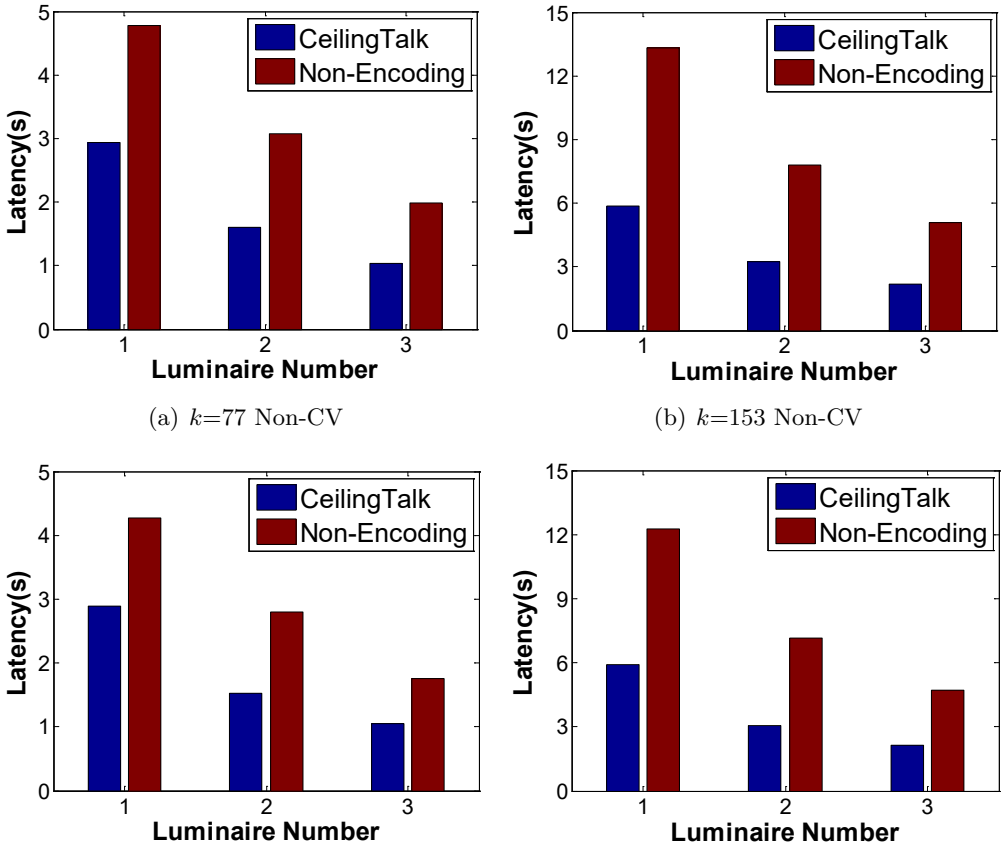

(a) k=77 Non-CV (b) k=153 Non-CV

(c) k=77 CV (d) k=153 CV

Figure 3.16: Latency vs. luminaire number with front camera. The improvement in terms of latency grows with the luminaire number.

3.5.4 Throughput and Latency

In this section, we evaluate the benefit of using Raptor codes in terms of throughput and latency, by comparing CeilingTalk with a baseline Non-Encoding mechanism that simply sends the set of k original packets assigned to individual luminaires in a circular shift manner. The latency is the elapsed time from when the camera starts to receive data to when it recovers (for CeilingTalk) or receives (for the baseline mechanism) all original packets. In an LED-camera communication session, the latency is determined by the frame rate of the camera since the frames are taken about every 33.3 ms that dominates other factors such as decoding computations. Therefore, the latency is approximately proportional to the numbers of camera frames needed for successful

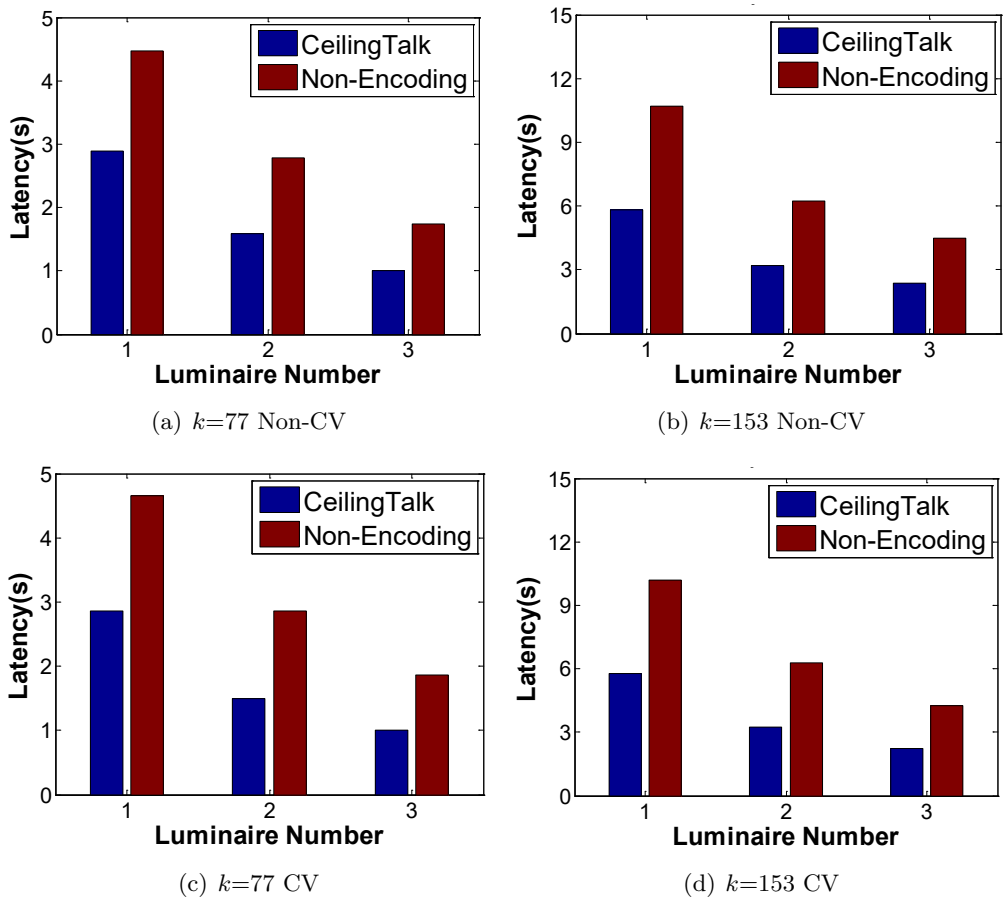

(a) k=77 Non-CV (b) k=153 Non-CV

(c) k=77 CV (d) k=153 CV

Figure 3.17: Latency vs. luminaire number with rear camera. The improvement in terms of latency grows with the luminaire number.

decoding. The throughput is computed as the total bits of the k packets divided by the latency. We conduct the experiments with $k = 77$ and $k = 153$ to evaluate how CeilingTalk performs under different k values.

We first evaluate the performance of CeilingTalk under stationary scenarios as explained in Sec. 3.5.3. The achieved latency by front and rear cameras is plotted in Fig. 3.16 and Fig. 3.17, respectively. The achieved throughput by front and rear cameras is plotted in Fig. 3.18 and Fig. 3.19. We can observe that both metrics get improved proportionally to the number of luminaires, and the throughput of both front and rear cameras can reach 3.0 kbps roughly with 3 luminaires. In fact, the rear camera of CeilingTalk has the potential to capture at most 6 luminaires in one frame, so it can

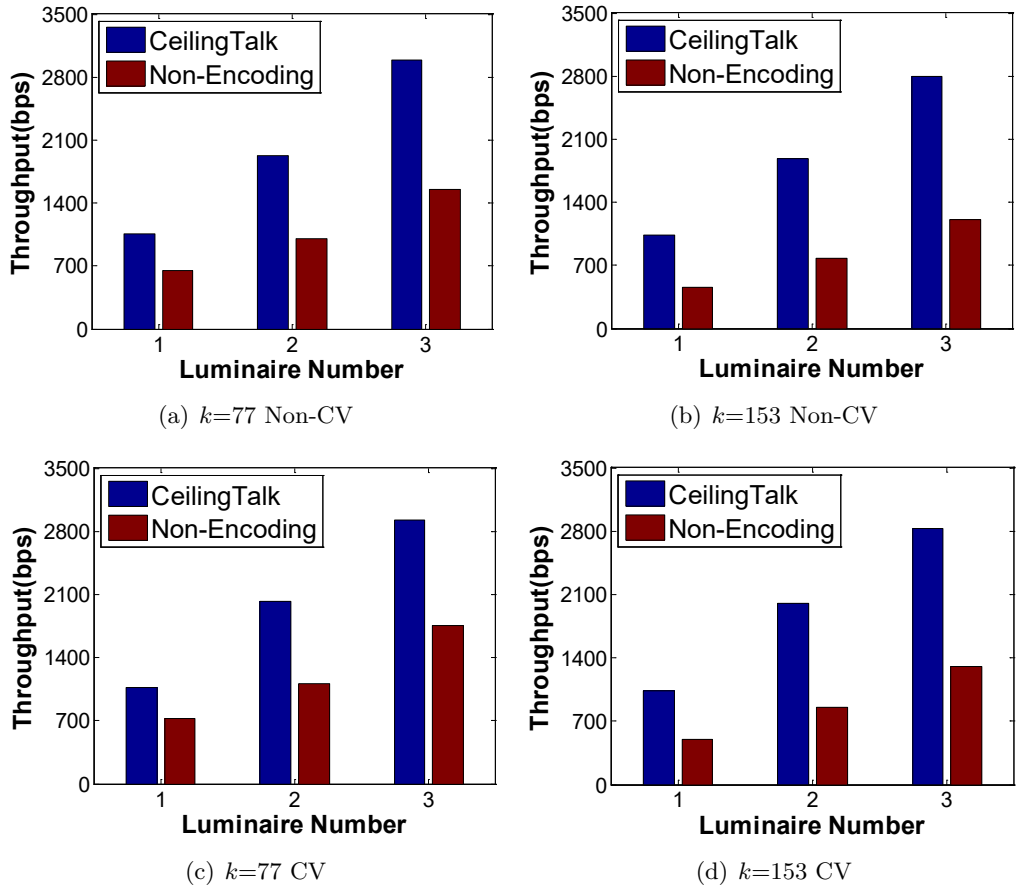

(a) k=77 Non-CV

(b) k=153 Non-CV

(c) k=77 CV

(d) k=153 CV

Figure 3.18: Throughput vs. luminaire number with front camera. The improvement in terms of throughput grows with the increasing luminaire number.

offer a throughput beyond 6.0 kbps.

We can also observe that, CeilingTalk brings more significant improvement when $k = 153$ than that when $k = 77$ compared with the baseline mechanism. As shown in Fig. 3.18 and Fig. 3.19, the gain of CeilingTalk over Non-Encoding mechanism rises from about 50% under $k = 77$ to about 80% under $k = 153$ with one luminaire and 50% to almost 100% with three luminaires. Therefore, the improvement also grows with k. This significant improvement stems from the increased packet loss rate under a larger k, for which the benefit of Raptor coding becomes more evident.

We also perform evaluations under mobile scenarios where we deliberately let the phone cameras of two users (A and B) mis-capture one or two luminaires from time to time, and the results are reported in Table 3.2 and Table 3.3. We have almost the

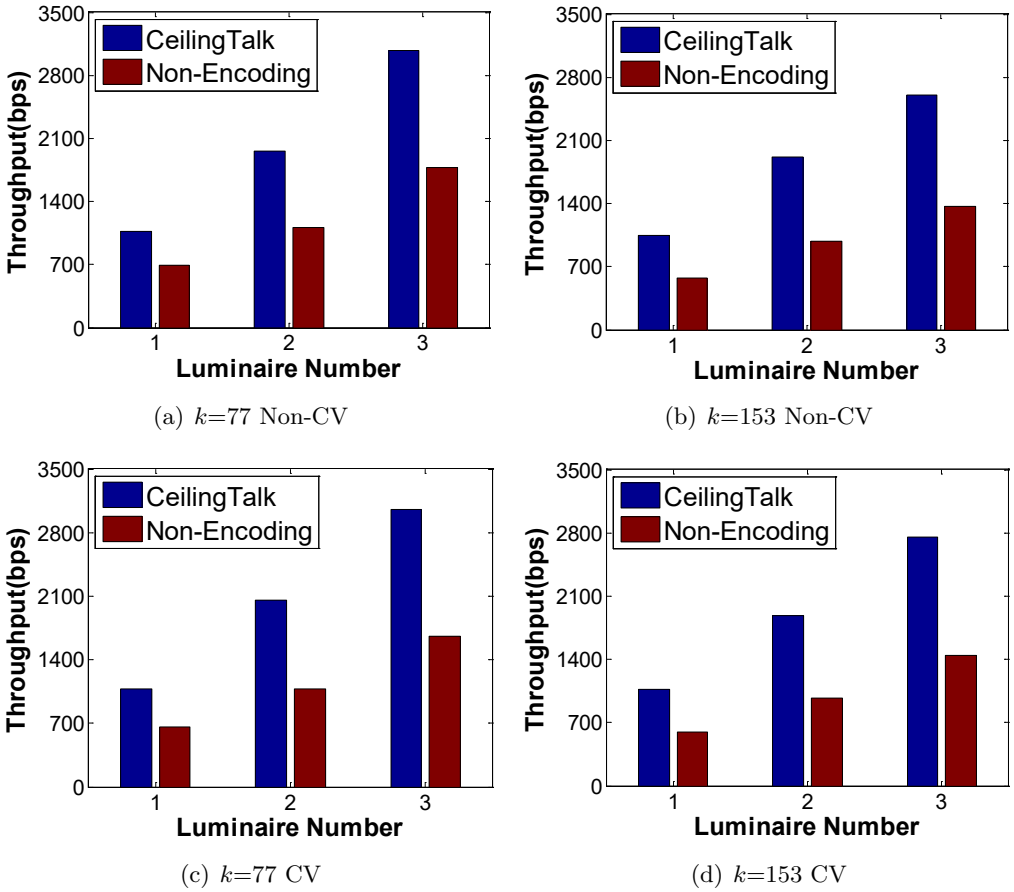

(a) k=77 Non-CV (b) k=153 Non-CV

(c) k=77 CV (d) k=153 CV

Figure 3.19: Throughput vs. luminaire number with rear camera. The improvement in terms of throughput grows with the increasing luminaire number.

same observations as those under stationary scenarios that CeilingTalk outperforms the baseline mechanism and the benefit grows with increasing k. In TABLE 3.3 user A with rear-facing camera and $k = 77$ obtains an average throughput 2.05 kbps with CeilingTalk but only 0.83 kbps otherwise, while user B obtains 1.96 kbps against 0.73 kbps otherwise. TABLE 3.2 shows the similar performance by using front camera. Therefore, these results again confirm the benefit of employing Raptor codes for enhancing reliability.

Table 3.2: Performance under mobile scenarios using front camera

	CeilingTalk		Non-Encoding	
k	Latency	Throughput	Latency	Throughput
77 (A)	1.68 s	1.84 kbps	4.67 s	0.66 kbps
77 (B)	1.77 s	1.75 kbps	5.21 s	0.59 kbps
153 (A)	3.89 s	1.57 kbps	17.74 s	0.35 kbps
153 (B)	4.13 s	1.48 kbps	15.88 s	0.39 kbps

Table 3.3: Performance under mobile scenarios using rear camera

	CeilingTalk		Non-Encoding	
k	Latency	Throughput	Latency	Throughput
77 (A)	1.50 s	2.05 kbps	3.73 s	0.83 kbps
77 (B)	1.58 s	1.96 kbps	4.21 s	0.73 kbps
153 (A)	3.43 s	1.78 kbps	13.38 s	0.46 kbps
153 (B)	3.34 s	1.83 kbps	12.37 s	0.49 kbps

3.5.5 Power Consumption

The power consumption of CeilingTalk has two parts: the consumption of LED control board and that of a camera for frame capture and decoding. Since CeilingTalk utilizes an existing lighting infrastructure as transmitters, the consumption of the communication front-end (the luminaires) is actually zero. The real consumption is caused by receiving data from Ethernet or PLC backbone, as well as the encoding computations. Our field experiments show that the driver of CeilingTalk has a power consumption of 40 mW, but this consumption appears to be constant regardless of encoding computations, suggesting that it is mainly the consumption of driving light emission (the default function of a luminaire). Therefore, we can conclude that the tx power consumption of CeilingTalk is negligible. As for Wi-Fi, existing Wi-Fi routers consume at least 800 mW according to [74, 75].

The receiver of CeilingTalk does lead to a rather high power consumption due to the use of image sensors. According to [76], the image sensor undergoes two states within a frame duration T_{frame}, i.e. active mode and idle mode. Given the duration and power for the two modes per frame, i.e. T_{active}, P_{active}, T_{idle} and P_{idle} respectively, the power of

Table 3.4: CeilingTalk vs. Wi-Fi: Comparison of Power Consumption.

	Transmitter (mW)	Receiver (mW)	Total (mW)
CeilingTalk	~ 0	<103 [76]	<103
Wi-Fi	>800 [75]	50 [77]	>850

CeilingTalk is formulated as $P = (P_{active}T_{active} + P_{idle}T_{idle})/T_{frame}$. In our case, based on our understanding of the information provided by Sony, we calculate $P_{active} \approx 183$ mW, $T_{active} = N/f$ where N is the resolution and $f > 338$ MHz is pixel rate, $P_{idle} \approx 77$ mW, $T_{idle} = T_{frame} - T_{active}$ and $T_{frame} = 33$ ms. With $N = 1024 \times 768$ used by CV-based RoI extraction and $N = 1920 \times 1440$ used by lightweight RoI extraction, we obtain the power $P < 84$ mW and $P < 103$ mW respectively. However, by using aggressive standby mechanism which lets the image sensor work in standby mode when no operation is performed [76], T_{idle} goes down to $T_{exposre} = 1/7000$ s so that P drops to $P \approx 20$ mW and 51 mW respectively. Moreover if optimal clock scaling is adopted, the power can be reduced further. Wi-Fi appears to be more efficient at the receiver side by consuming slightly more than 50 mW for data reception [77], so the receiver side energy consumption is a major limitation of CeilingTalk. We summarize these quantities in Table 3.4. In fact, as a data service, the transmitter side may constantly consume energy while the receiver side only causes consumption intermittently. Therefore, CeilingTalk is much more energy efficient than Wi-Fi in terms of the overall system consumption.

3.6 Summary

In this chapter, we have presented CeilingTalk as an LED-Camera VLC system. It innovates in both encoding and decoding schemes to improve link reliability and throughput, so that it allows us to have the first realistic LED-Camera VLC deployment, and it also provides us with practical insights on how such systems should be configured to reach its maximum capacity. Extensive field experiments have shown that our system can achieve a throughput much higher than a recent experimental prototype [27].

Chapter 4

CeilingSee: Device-Free Occupancy Inference through Lighting Infrastructure Based LED Sensing

In Chapter 3, we present CeilingTalk to verify the communication ability of LEDs as energy-efficient VLC transmitters. Its sensing ability has long been neglected albeit some researchers have used one single LED bead/chip as both transmitter and receiver in bidirectional VLC for short-distance communication. In this chapter, we intend to exploit the sensing ability of one practical LED luminaire with multiple LED chips to detect the presence of occupants, thus we build CeilingSee as a device-free occupancy inference system to detect the presence of occupants under LED luminaires and infer indoor occupancy. The contributions of CeilingSee are twofold: first it can work independently to monitor indoor occupancy as presented in this chapter. Second it can significantly extend a VLC system by offering perception ability of VLC transmitters to automatically associate users and relay a communication session, and it will be detailed in the following Chapter 5.

4.1 Introduction

The awareness of (indoor) occupancy is crucial to many aspects of smart building management; these include, among others, controlling the HVAC (Heating, Ventilation, and Air Conditioning) and lighting systems for the sake of energy conservation, choosing the right information service based on congestion level, as well as safely evacuating people under life-threatening circumstances. In the past two decades, various smart sensing technologies have been dedicated[1] to infer occupancy for indoor facilities, and most of them require deploying certain sensing infrastructure with mainly three typical sensors: passive infra-red (PIR) [81, 82, 83, 84], acoustic/ultrasonic [85, 86, 87], and camera [84, 88, 89, 90]. Other solutions attempt to infer occupancy indirectly by monitoring the usage of existing services (e.g., Wi-Fi [91] and power grid [92]). Whereas the former method requires installations of extra sensor infrastructure and hence incurs both high costs for building management and potential infringement of user privacy, the latter approach can hardly be accurate: what if some occupants simply do not use any services?

Our key observation is that, in any human occupied indoor spaces, lighting is a necessity while the resulting diffuse reflection can be "perturbed" by the presence of occupants. At the meantime, VLS, as a variance of heavily studied VLC [27, 93, 94, 95], has started to show its potential in many sensing-intensive applications [14, 47]. Therefore, a natural question is: *can we apply VLS to build an occupancy inference system that is free of reliance on both heavy infrastructures and user involvements?* In this chapter, we intend to provide readers with a positive answer through our CeilingSee.

The first idea of CeilingSee is very intuitive: from the ceiling point of view, the diffuse reflection (consisting of main reflections from the floor and variously fixed furniture on the floor) is bounded to be affected by the presence of occupants. Therefore, sensing such perturbations could allow us to infer occupancy. While simply installing an array of light sensors on the ceiling could be a solution, it would introduce yet another infrastructure. Fortunately, the increasing popularity of LED lighting systems and the readily verifiable photoelectric effect of LED [94, 96] have motivated our novel idea: re-designing the driver of a COTS LED could enable it to serve as both a light

[1]Though occupancy information can be derived from an indoor localization system (e.g., [14, 78, 79, 80]), few practical indoor localization systems have been widely adopted so far. Moreover, relying on user location tracking to "count" occupancy is highly inefficient and may infringe privacy.

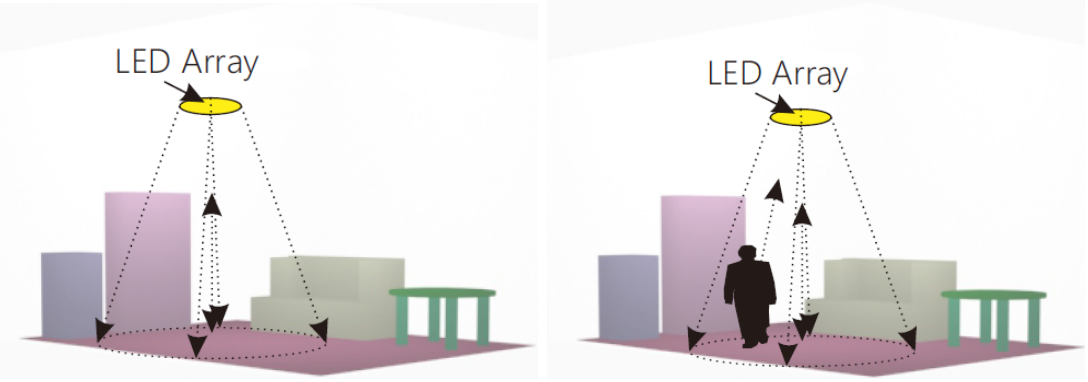

(a) Sensing coverage of LED array.

(b) Occupant under the coverage.

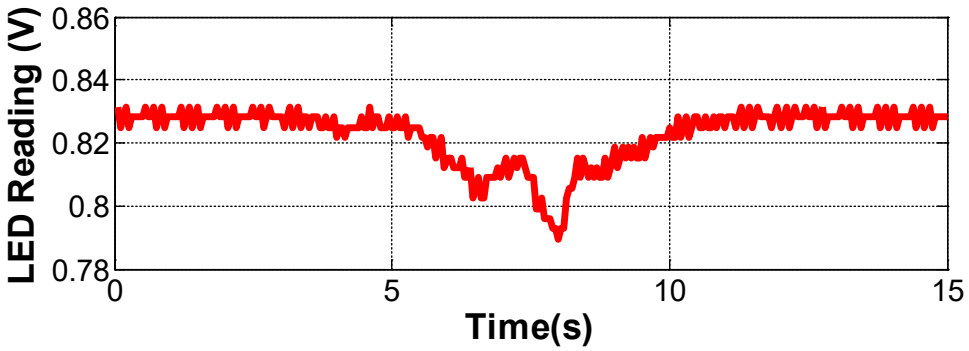

(c) Variances in LED readings due to absence/presence of occupant.

Figure 4.1: Inferring occupancy by LED sensing.

emitter and a light sensor. Consequently, CeilingSee simply leverages the existing LED lighting systems and borrows a fraction of LED chips to sense the variance in diffuse reflection. We illustrate these ideas in Fig. 5.1; it clearly demonstrates the potential and effectiveness of VLS-based occupancy inference.

The seemingly straightforward ideas of CelingSee impose on us two major challenges. Firstly, although conventional LED-to-LED communication [94] has already employed an LED as a receiver (a special form of the sensor), sensing the variance in diffuse reflection is much more challenging due to the very low SNR, hence it necessitates using the collective sensing ability of multiple LED chips. Existing LED receiver directly connects an LED chip to the I/O port of an MCU, thus relying on the controllable nature of the I/O port to toggle the states of the LED between *forward biased* (emitting or sending) and *reverse biased* (sensing or receiving). Unfortunately, this

would not work when multiple LED chips are used together, as the voltage/current would exceed what an I/O can take (normally no more than 3.3V/20mA). As a result, we design a novel circuit for accommodating the collective photoelectric effects of an LED array.

Secondly, as the sensing coverage (a.k.a., FoV)) of a single LED array (consisting of multiple "sensitized" LED chips) is limited, we have to use multiple arrays to cover a large indoor area, which happens to be in line with the lighting requirement. Moreover, CeilingSee needs to account for multiple occupants dispersed on the area, especially those not strictly under of an LED array. Therefore, it is necessary that efficient inference algorithms are in place to utilize the collective sensing outcomes of all LED arrays. CeilingSee responds to this challenge by engineering a machine learning algorithm that maps the multi-dimensional sensing data to the demanded occupancy count. To validate our design of CeilingSee, we build a testbed consisting of multiple LED arrays in order to cover a 30 m^2 office area. We implement the hardware part for controlling the LED arrays, as well as the software part for sensing data processing and hence occupancy inference. Our main contributions are as follows:

- We propose the novel idea of applying ceiling-mounted LED lighting systems for inferring occupancy, and we build CeilingSee to showcase the efficiency and effectiveness of this lightweight occupancy inference approach.
- We re-design the driver of a COTS LED so that CeilingSee can freely toggle an LED between light emitting and light sensing modes and a group of LEDs can be collectively used for sensing the variance in (indoor) diffuse reflection.
- We engineer data processing and machine learning algorithms to deduce the occupancy within the FoV of an LED array, and to infer full area occupancy by fusing the multi-dimensional sensing outcomes from all arrays.
- We conduct extensive field experiments in the past six months to validate the effectiveness of CeilingSee, and the results strongly demonstrate its high accuracy in occupancy inference.

We are not expecting CeilingSee to fully replace the existing occupancy inference solutions. Instead, we deem the technical implication of CeilingSee as twofold: i) it is an avatar of a VLS-based idea that minimizes the resource required for inferring occupancy

Table 4.1: Comparing CeilingSee with existing solutions for occupancy inference.

Sensor Type	Infrastructure reuse	Privacy Concern	Accuracy	Cost	Limitation
Ultrasonic [87]	No	No	$\geq 90\%$	Medium	Need prior maximum and distribution of occupants.
Thermal Sensor & PIR [83]	No	No	88.5%	Medium	Extra sensors.
Camera [89]	Possible	Yes	80%	High	Heavy computation, re-calibration based on dimming.
Camera & PIR [84]	Partial	Yes	94%	High	Heavy computation, re-calibration based on dimming.
Photosensors [55]	No	No	N/A	Low	Extra sensor, re-calibration based on dimming.
LED (CeilingSee)	Yes	No	$\geq 90\%$	Low	Re-calibration based on dimming.

and may thus inspire other applications of VLS, and ii) it serves as a complement to other solutions for improving the efficiency and scalability of occupancy inference systems. We comparing CeilingSee with typical existing solutions in Table 4.1. In the following, we first introduce the principle of LED sensing, along with the design and experience with a single sensing unit of CeilingSee in Sec. 4.2. Then we present our learning-based occupant inference algorithms in Sec. 4.3. We report the performance evaluation of CeilingSee in Sec. 4.4 and conclude this chapter in Sec. 4.5.

4.2 Sensing Reflection by LED

Lighting systems are pervasively deployed and used for indoor spaces due to the inadequate natural lighting from windows, especially when space has limited access to day light. Such lighting systems are normally ceiling-mounted and hence cause diffuse reflections from the floor (including various furniture on it), which is biased towards the

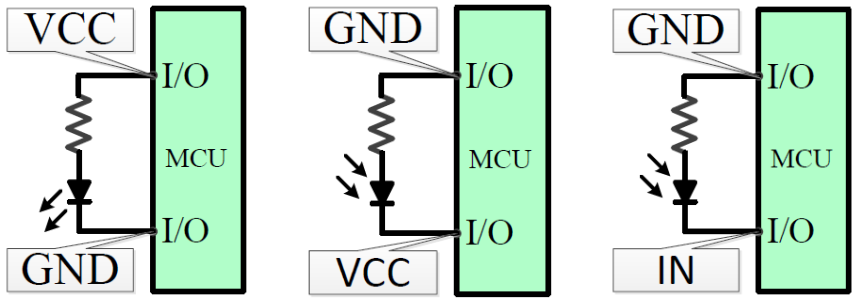

(a) (b) (c)

Figure 4.2: Conventional bidirectional interface between LED and MCU. (a) Normal I/O configuration for light emitting. (b) Reverse bias for light sensing. (c) I/O as input for reading sensed signal.

ceiling due to the blending with minor specular reflection. When occupants move into this "reflection field", they can cause perturbations readily sensible by certain ceiling-mounted light sensors. To avoid introducing an extra sensing infrastructure, our idea is to re-use part of the existing LED lighting system to serve the sensing function.

It is well known that LED has photoelectric effect, i.e., light shining upon an LED can cause it to emit electrons, which is a reverse effect of LED's default functionality [97]. This effect has motivated a few proposals to use an LED not only as a sender but also as a receiver in VLC [94, 96]. However, converting an LED receiver to an LED sensor is almost impossible as the light signal sent by an LED has a much higher SNR than the variance in reflection. Moreover, as we only "borrow" part of the LED lighting system for the sensing purpose, we want to toggle the LEDs between light emitting and light sensing modes when either is in need. Therefore, we present the details of CeilingSee's hardware implementation in this section, aiming to address the aforementioned issues.

4.2.1 From LED Receiving to LED Sensing

We briefly describe the conventional design of an LED receiver, and then we explain why and how the design of LED sensing for CeilingSee should be different.

4.2.1.1 Bidirectional Setting of LED Receiver

In a conventional design for light receiving in the LED-LED communication, a bidirectional interface to an LED is created by connecting the LED directly between the two I/O pins of a micro-controller (MCU) [96], as shown in Fig. 4.2. Fig. 4.2(a) shows that the LED emits lighting when its anode and cathode are connected to VCC and GND, respectively, via a simple I/O configuration. Reverting the I/O configuration sets the LED in reverse bias mode as in Fig. 4.2(b); it charges the inner stray capacitance of the LED and prepares the LED for light sensing. Fig. 4.2(c) further illustrates the actual measurement phase: MCU reads the voltage changes on LED's cathode and times how long it takes for the photocurrent to discharge the capacitance to the I/O pin's digital input threshold, as the discharging time is inversely proportional to the amount of incident light. The simplicity of this LED receiving circuit stems from the matching voltages between an MCU and an LED, which does not work if one wishes to drive more LEDs with one MCU.

4.2.1.2 Collective Sensing with Multiple LEDs

Compared with the LED-LED communication, the signal for our reflection sensing scenario is much weaker.[1] As a result, if we used the same circuit as described in Section 4.2.1.1, we would either fail to sense the signal due to the too weak photocurrent or experience a huge sensing delay thanks to the long discharging time. Whereas using multiple LEDs to collectively sense the weak signal appears to be a straightforward solution, the much higher voltage level caused by aggregating multiple LEDs renders the existing I/O-based circuit design invalid. Also, reverse biasing an array of LED is almost impossible for a normal MCU with limited absolute maximum voltage.[2]

Therefore, our intention is to use an LED array as one light sensing unit without the need for reverse biasing it. According to the LED's equivalent circuit model [96], an LED can be deemed as a current source with a shunt capacitor, while the current source is driven by incident light to generate tiny photocurrent. Whereas the current

[1]The signal could also be weaker in LED-LED communication if the transmission distance goes beyond the centimeter testing scenarios in [94, 96]. As a practical sensing system, CeilingSee has to work under a "transmission distance" (that from floor to ceiling) of several meters.

[2]Though this could be made possible by using special high-power components, e.g. high reverse voltage MOSFET, the high cost would compromise our purpose of building a lightweight occupancy inference system.

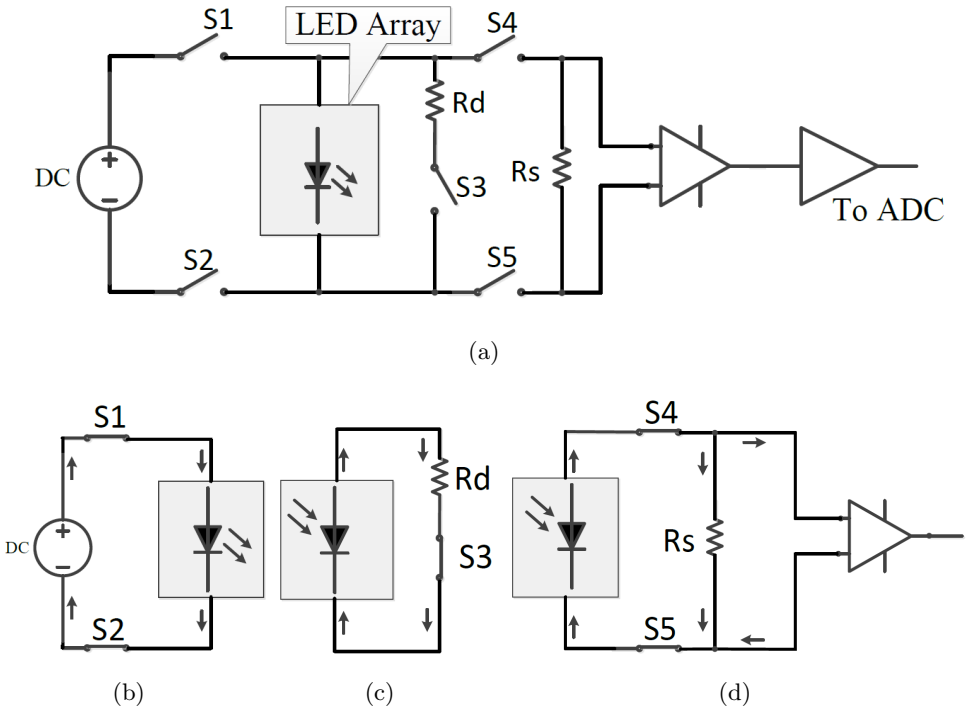

Figure 4.3: Architecture of the LED array driver. (a) Circuit schematic. (b) The equivalent circuit during light emitting. (c) The equivalent circuit for discharging. (d) The equivalent circuit during light sensing.

produced by one LED is too weak to be measurable (even through an amplifier), the aggregated current of the LED array (with a sufficient amount of LEDs) would suffice for the sensing purpose.

Based on the aforementioned ideas, we re-design the driver of COTS LED luminaires to control the LED state toggling, so that CeilingSee can duty-cycle part of the luminaire between light emitting (for normal lighting) and light sensing (for occupancy inference). Fig. 4.3 shows the architecture of this driver circuit and also its functionalities under different modes. The five switches in Fig. 4.3(a) are key components for the driver. The LED array emits light (lighting phase) if both S1 and S2 are ON and other switches are OFF, as shown by Fig. 4.3(b). Subsequently, Fig. 4.3(c) shows a short discharging window that allows residual charges on the array to be cleared for preparing sensing (discharging phase), by putting S3 ON while others OFF. Finally, switching S4 and S5 ON and others OFF enables the array to act as a light sensor (sensing phase): the resistor Rs ($> 10\text{M}\Omega$) converts weak photocurrents to voltage sig-

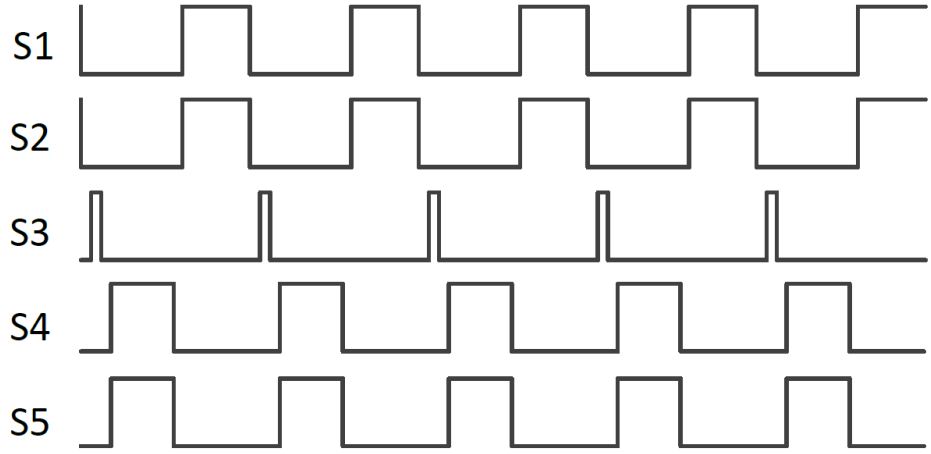

Figure 4.4: Duty-cycled control signal sequence for toggling between lighting and sensing.

nals that drive amplifiers to produce sensing outcome. We also show the duty-cycled control sequence of different switches in Fig. 4.4: to prevent short circuit, a dead-time should be inserted between two consecutive phases.

4.2.1.3 Design Details of the LED Driver

We elaborate on two key components of the driver here, namely discharging circuit and amplifier circuit.

Discharging Circuit. During the lighting phase, the inner capacitance of the LED array can be partially charged and the charging level cannot be controlled; this could interfere the sensing phase as the photocurrent produced by incident light is tiny. To this end, the discharging circuit is particularly designed for preparing the sensing phase without the need for reverse biasing the LEDs. It consists of a switch and a bleeder resistor shown in Figure 5.2(a). The discharging phase between the light and sensing phases can be very short (normally 100μs); it quickly clears the residual charges so as to get a clean start for the sensing phase. The switching from the lighting phase to discharging phase has to be strictly controlled by MCU with a dead-time in-between (another 100μs), otherwise the driver can be damaged due to short circuit.

Amplifier Circuit. During the sensing phase, the photocurrent excited by the incident light is converted to weak voltage signal by Rs, which needs to be amplified before being sampled by the ADC of MCU. Figure 4.5 shows the detailed schematic of the

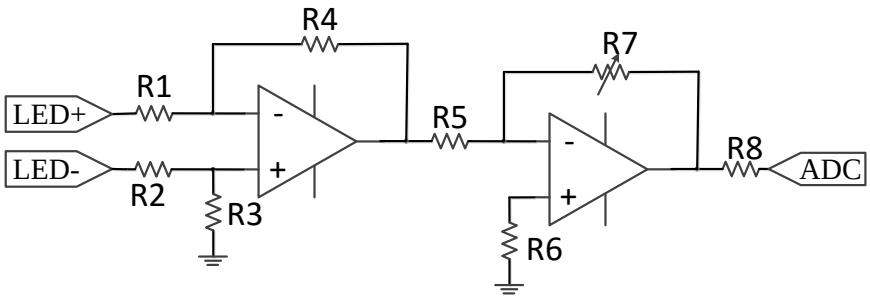

Figure 4.5: Amplifier circuits. The voltage difference between the cathode and anode of the LED array is firstly extracted by a differential amplifier. Then the differential signal is further amplified before sampled by ADC.

amplifier circuit; it consists of a differential amplifier with fixed-gain and an inverting amplifier with adjustable gain. The differential amplifier is used to amplify the voltage (difference) between the cathode and anode of the LED array; its output can be approximated as:

$$V_{\text{out1}} = -(V_{\text{LED+}} - V_{\text{LED-}}) \times \frac{\mathsf{R4}}{\mathsf{R1}}, \tag{4.1}$$

where $V_{\text{LED+}}$ and $V_{\text{LED-}}$ are the voltages of the LED array's cathode and anode, respectively, and V_{out1} is the output of differential amplifier.

The adjustable gain amplifier circuit includes a high gain inverting amplifier and an adjustable resistor R7. As a result, we have an adjustable output V_{ADC} expressed as (4.2), which is in turn related to the light excited voltage by (4.3).

$$V_{\text{ADC}} = -V_{\text{out1}} \times \frac{\mathsf{R7}}{\mathsf{R5}}. \tag{4.2}$$

$$V_{\text{ADC}} = (V_{\text{LED+}} - V_{\text{LED-}}) \times \frac{\mathsf{R4}}{\mathsf{R1}} \times \frac{\mathsf{R7}}{\mathsf{R5}}. \tag{4.3}$$

4.2.2 Experiencing Single Sensing Unit

Fig. 4.6 shows one *sensing unit* of CeilingSee; it consists of an 8×12 LED chip array [73] and a PCB carrying our re-designed driver. We separate the chips into two groups and duty-cycle them in a complementary manner to perform both lighting and sensing simultaneously while avoiding flickering. Currently, we toggle them at a long switching period (every 10 minutes) between lighting and sensing. Using this hardware platform, we first test the capability of single-unit occupancy inference, aiming to study the performance of such a unit under various parameter settings and situations. More hardware implementation details on the unit will be given in Section 4.4.1.

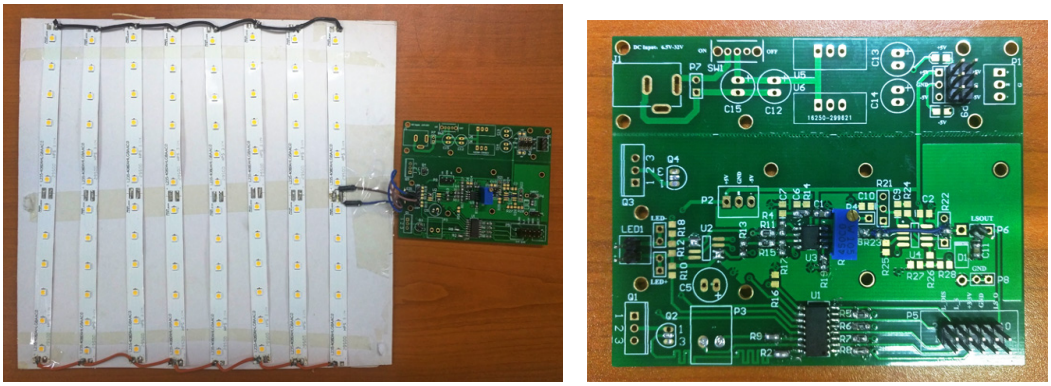

(a) Sensing/lighting uint (b) Re-designed driver

Figure 4.6: A sensing/lighting unit of CeilingSee, consisting of an LED array and a re-designed driver.

4.2.2.1 Raw Reading and Signal Smoothing

We first demonstrate the effectiveness of using LED sensing to indicate occupancy: we record V_{ADC} when one occupant walks into the sensing coverage and stay there, and the V_{ADC} in Fig. 4.7 clearly shows the variance in reflection incurred by an occupant. The rather unstable raw readings are mainly interfered by two sources: a minor random noise and a 50 Hz component.[1] Both interferences are very easy to be removed by applying a moving average with a window size of 100 ms. Therefore, we report only the smoothed readings hereafter. Also, we take the absolute difference between a V_{ADC} reading and the nominal reading (obtained in absence of any occupants, when we train or re-train CeilingSee) as the actual **sensing value**.

4.2.2.2 Impacts of Illuminance and Dimension

As a sensing unit is sensing the reflection, the outcome ought to be affected by the ambient illuminance. Also, according to Section 4.2.1.2, the sensitivity of the unit depends on the number of LED chips involved. We are here to quantitatively understand these impacts. Fig. 4.8(a) shows the sensing values are significantly affected by (average) illuminance, and an illuminance lower than 60 lux would affect the performance of

[1] As we deploy CeilingSee in a public research lab, the LED sensing units have to be co-located with existing fluorescent lights that cause the 50 Hz component. This happens to attest the compatibility of CeilingSee with legacy lighting systems.

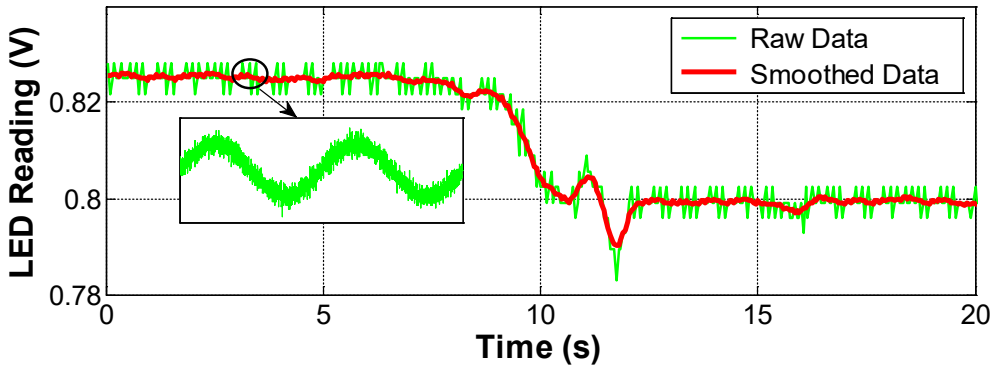

Figure 4.7: Raw and smoothed ADC readings (V_{ADC}) that indicate reflection variance due to occupancy.

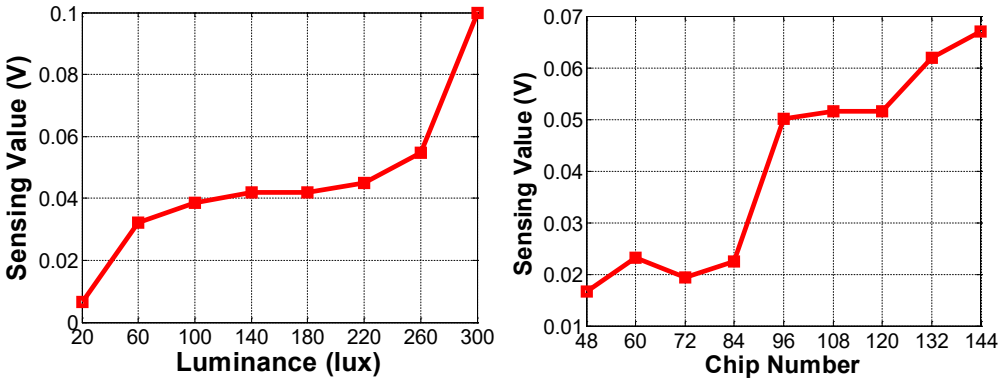

(a) Sensing value vs. illuminance

(b) Sensing vs. LED chips number.

Figure 4.8: Impact of ambient illuminance and chip number on sensitivity.

CeilingSee. Fortunately, normal office area has a light level of 200 lux and other public facilities such as supermarkets or theaters can reach 1000 lux [98]. In the following, we maintain the average illuminance to 150 lux: the one offered by the laboratory where CeilingSee is deployed. In Fig. 4.8(b), we vary the number of chips and check the resulting sensitivity. The results show that the unit with 96 chips appears to be the most cost-effective choice, hence leading to our design in Fig. 4.6.

4.2.2.3 Occupant Position and Number

In the previous experiments, we put an occupant right below a sensing unit. Now we let the occupant gradually move away from that center point, and record the corresponding sensing values in Fig. 4.9(a). Interestingly, whereas the values are generally decreasing

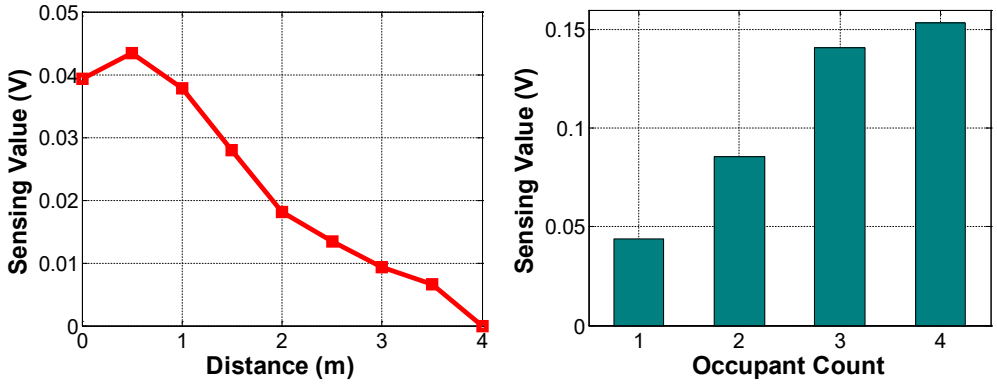

(a) Sensing values vs. distance

(b) Sensing values vs. occupancy

Figure 4.9: Changes in sensing value caused by the occupant position and number.

in distance, it has a peak at 0.5 m. This stems from the fact that the perturbation in reflection incurred by the occupant depends on not only the distance but also occupant's cross section with respect to the unit; the trade-off between these conflicting factors naturally leads to the peak. This is a nice property as it can effectively increase the FoV of one sensing unit.

We also vary the number of occupants that stand within a circle of radius 1 m around the unit. Fig. 4.9(b) shows an almost linear increase in sensing values with the occupant number, though with some saturation at 4 occupants. Normally, we do not expect to have so crowded situations where more than 4 people stand upon a roughly 3 m^2 area, so the results demonstrate the ability of a single unit to count the number of occupants within its FoV, and also explain the need for cooperative sensing with multiple units.

4.2.2.4 Postures and Gestures of an Occupant

An occupant may have different postures and we consider three typical ones: standing, seating, and squatting (rare). We study the impact of these postures on the sensing values when the occupant is at various distances from a sensing unit. Fig. 4.10(a) shows that, though squatting does lead to rather low sensing values, standing and sitting cause very close sensing values. This is explained by the fact that the sensing value incurred by the occupant depends on occupant's cross section. So certain occupants may "hide" from CeilingSee by squatting, but this is such a rare posture indoors that it

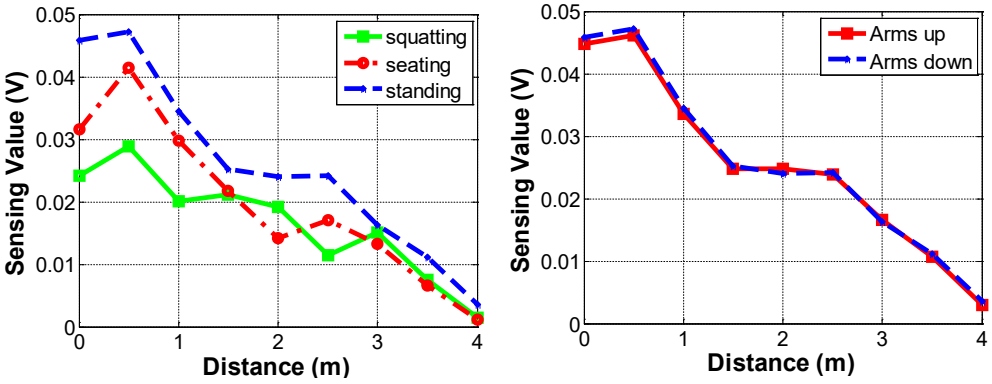

(a) Effect of occupants' postures (b) Effect of occupants' gesture

Figure 4.10: Changes in sensing value caused by different postures and gestures.

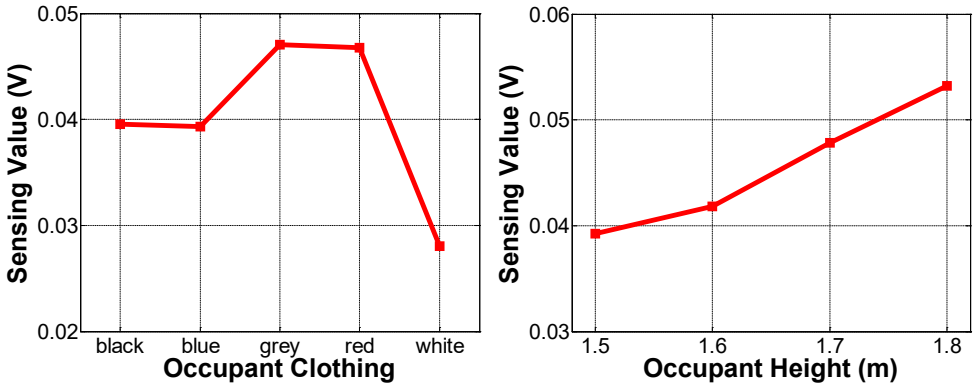

(a) Effect of dressing color (b) Effect of occupants height

Figure 4.11: Changes in sensing value caused by different dressing colors and occupant heights.

would not cause much trouble to the overall inference performance. An occupant may also change gestures without leaving the monitored area, and such interference should not be responded by CeilingSee. In Fig. 4.10(b), we show that CeilingSee is virtually insensitive to gesture changes (e.g., waving arms) of an occupant, implying that the occupancy inference function is robust against such an interference.

4.2.2.5 Color and Height of an Occupant

The dressing color and height of an occupant may also affect reflection, so we let one occupant dress in five different colors and also gather four occupants with heights varying

from 1.5 m to 1.8 m. According to Figure 4.11(a), CeilingSee is largely insensitive to dressing colors except for white. Fortunately, as far as we do not have majority of the occupants dressing in white, the bias caused by white dressing can be offset by other dressing colors. Figure 4.11(b) shows that CeilingSee is quite insensitive to occupant height, which has somewhat been inferred by the posture results.

4.2.2.6 Background Changes

We define sensing value (c.f. Section 4.2.2.1) with respect to the nominal readings of individual sensing units. Apparently, these nominal readings can be affected background changes, including furniture moving and natural light shedding in from windows. We study the impact of moving furniture by moving a chair away from the center of a unit, and we also choose two units very close to the window to check the variance of their nominal readings at different times of a day. According to Figure 4.12(a) and 4.12(b), the impact of both factors are minor compared with the variance caused by occupants presence. Therefore, we conclude that CeilingSee is immune to minor background changes. In cases that indoor space being totally refurbished (e.g., repainted or totally rearranged), we may re-train CeilingSee based on new nominal readings.

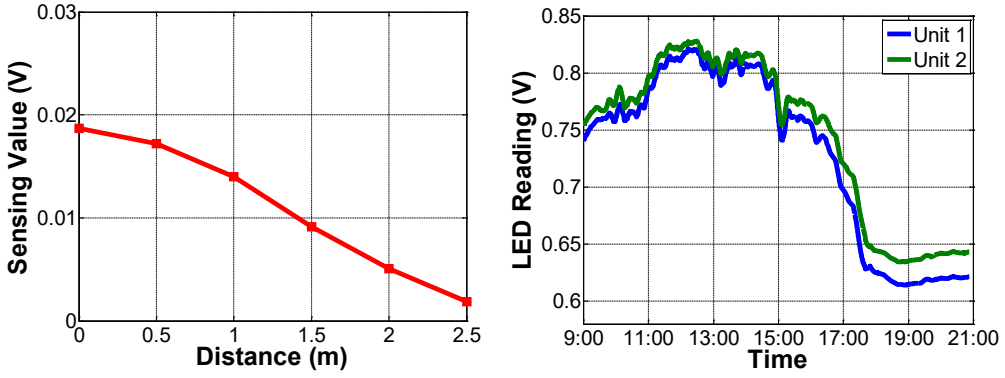

(a) Moving furniture

(b) Varying natural light.

Figure 4.12: Changes in sensing value caused by moving furniture and varying natural light.

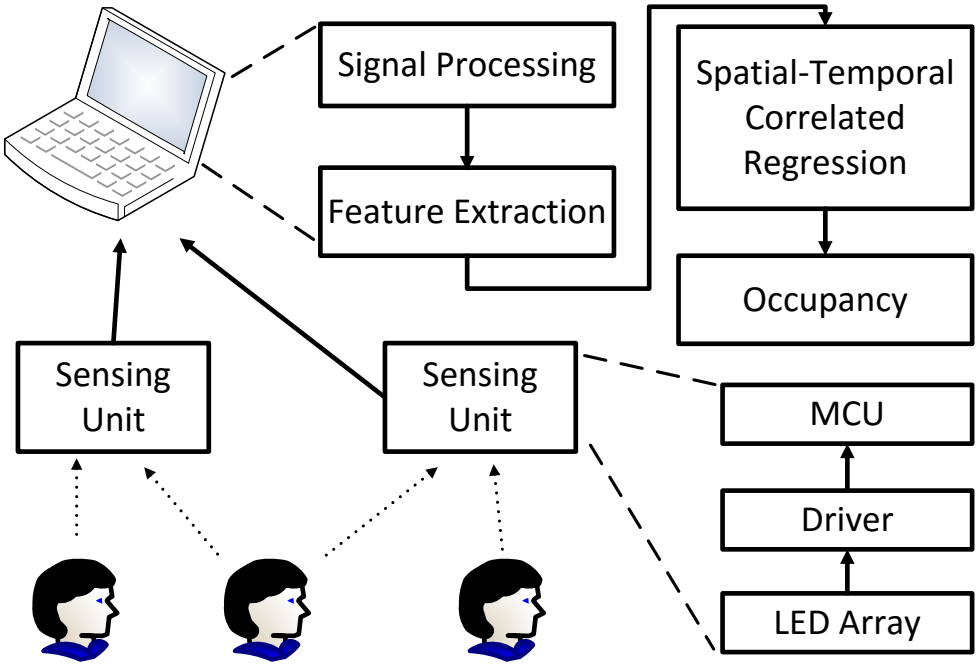

Figure 4.13: System architecture. CeilingSee gathers data from all sensing units, pre-processes them to remove noise, and then passes them to the regression module for inferring occupancy.

4.3 Occupancy Inference

As illustrated in Fig. 4.13, the LED sensing readings are first smoothed and sampled to obtain vectors of sensing values (termed *snapshots* hereafter) as described in Section 4.2.2. The snapshots are either directly taken or further differentiated to extract temporal features, and these inputs are fed to a fine-tuned regression module trained for occupancy inference.

4.3.1 Spatial Distribution of Sensing Values

When multiple occupants exist in an area monitored by CeilingSee, each sensing unit will produce a sensing value depending on the spatial distribution of the occupants around it (as studied in Section 4.2.2). We denote the sensing value of a unit by $x_\ell(t)$, where ℓ is the index of the unit and t is the time instant when the value is sampled. Combining all the values produced by the whole system, we end up with a time-varying vector $\mathbf{x}(t) = [x_1(t), x_2(t), \cdots, x_n(t)]$, where n is the number of sensing units. As we

always sample $\mathbf{x}(t)$ in a discrete manner, we actually use $\mathbf{x}_i$ to denote a *snapshot* at the i-th time slot, and the spatial distribution of the individual components of a $\mathbf{x}_i$ is correlated with that of the occupants during that time slot. We illustrate a few typical snapshots using our deployment in Fig. 4.15 of Section 4.4.1. In Fig. 4.14, we show 8 snapshots captured when there are 4, 8, 12 occupants and each with two spatial distribution patterns, namely all standing under the sensing units and away from them. A direct observation is that, in general, more occupants usually yield higher overall sensing values and a higher sensing value indicates more occupants around that unit. These observations agree with impact of distance/occupant number on sensing value shown in Fig. 4.9. More detailed inspections show that, with the same number of occupants at different positions, locating occupants right below the LED sensing units actually leads to lower overall sensing values than moving them away from the units. This stems from our finding in Fig. 4.9(a). Nevertheless, directly inferring occupancy from individual snapshots through linear regression may yield rather coarse-grained estimations with a low accuracy.

4.3.2 Regularized Regression

Given a training set $D = \{\mathbf{x}_i, y_i\}_{i=1,\cdots,m}$ where $\mathbf{x}_i \in \mathbb{R}^n$ denotes the input snapshots, $y_i \in \mathbb{R}$ is the corresponding label (i.e. the occupant count), and m is the cardinality of (sensory) data-label pairs, we need to find a function $f(\mathbf{x}) : \mathbb{R}^n \to \mathbb{R}$ in the form of $f(\mathbf{x}) = \langle \mathbf{w}, \mathbf{x} \rangle + b$ to fit the relationship between $\{\mathbf{x}_i\}$'s and $\{y_i\}$'s, where $\mathbf{w} \in \mathbb{R}^n$ is the vector of weight parameters and b is a bias factor (they are to be learned from the training set), and $\langle \cdot, \cdot \rangle$ is the inner product. To avoid the overfitting issue, we formulate the learning problem of $\mathbf{w}$ as a regularized regression problem by introducing a regularization term on $\mathbf{w}$ as follows,

$$\mathbf{w}^* = \arg\min_{\mathbf{w}} \left[\sum_{i=1}^{m} \mathcal{L}(f(\mathbf{x}_i), y_i) + \gamma \|\mathbf{w}\|_2^2 \right], \tag{4.4}$$

where $\mathcal{L}(\cdot)$ is a loss function and $\gamma \geq 0$ is a tradeoff parameter controlling the relative weight between the loss function and the regularization penalty $\|\mathbf{w}\|_2^2$. Different definitions of the loss function lead to specific regularized regression methods; here we adopt ε-insensitive loss that is described by

$$\mathcal{L}(f(\mathbf{x}), y) = \begin{cases} 0 & \text{if } |f(\mathbf{x}) - y| \leq \varepsilon, \\ |f(\mathbf{x}) - y| - \varepsilon, & \text{otherwise.} \end{cases}$$

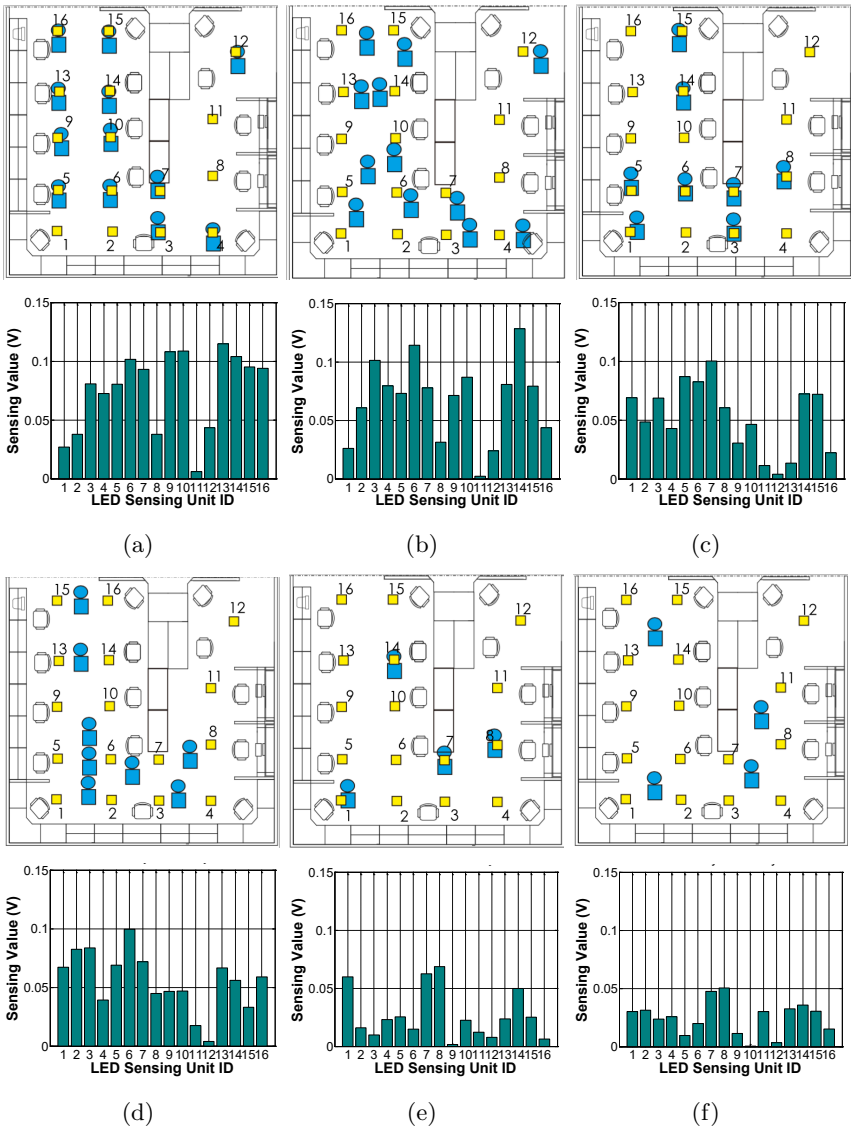

Figure 4.14: Snapshot examples: different occupancy patterns lead to different snapshots. Upper figures show the occupancy patterns, with yellow squares represent the sensing units and blue human-shaped marks indicate occupants. Lower figures show the corresponding snapshots. (a) 12 occupants are all under sensing units. (b) 12 occupants are all away from sensing units. (c) 8 occupants are all under sensing units. (d) 8 occupants are all away from sensing units. (e) 4 occupants are all under sensing units. (f) 4 occupants are all away from sensing units.

This leads to the well-known as Support Vector Regression (SVR) [99]. However, the function $f(\mathbf{x})$ learned by solving (4.4) can only capture the linear relationship

between $\{\mathbf{x}_i\}$'s and $\{y_i\}$'s, whereas the intrinsic relationship between snapshots and the corresponding occupancy counts can be highly nonlinear. To this end, we further formulate the learning problem of $\mathbf{w}$ as a nonlinear regularized regression problem by introducing a nonlinear feature map $\phi(\mathbf{x})$ that maps $\mathbf{x}$ to a Reproducing Kernel Hilbert Space (RKHS),

$$f^*(\mathbf{x}) = \arg\min_f \left[\sum_{i=1}^{m} \mathcal{L}(f(\mathbf{x}_i), y_i) + \gamma \|f\|_{\mathcal{H}}^2 \right], \tag{4.5}$$

where $\|\cdot\|_{\mathcal{H}}$ is the norm in the RKHS. By using the kernel trick, i.e., $\mathcal{K}(\mathbf{x}_i, \mathbf{x}_j) = \langle \phi(\mathbf{x}_i), \phi(\mathbf{x}_j) \rangle$, we can obtain the minimizer of the optimization (4.5):

$$f^*(\mathbf{x}) = \sum_{i=1}^{m} u_i \mathcal{K}(\mathbf{x}_i, \mathbf{x}) + b, \tag{4.6}$$

where u_i is obtained by solving the dual problem of (4.5) with the ε-insensitive loss [99]. Our design now focuses on choosing a proper kernel function $\mathcal{K}(\mathbf{x}_i, \mathbf{x}_j)$ and pre-processing $\{\mathbf{x}_i\}$'s so as to improve the inference performance.

4.3.3 Handling Spatial-Temporal Correlations

In order to achieve an accurate inference, we fine-tune the regression by taking into account three types of correlations among the training snapshots. As shown in Section 4.3.1, snapshots with similar labels are correlated, while the individual sensing values (collected by sensing units geographically distributed in a monitoring area) have spatial correlations. Moreover, the snapshots taken at consecutive time slots can be correlated depending on whether some occupants move or not.

The correlations among snapshots are handled by applying a Gaussian kernel $\mathcal{K}(\mathbf{x}_i, \mathbf{x}_j) = e^{-\nu \|\mathbf{x}_i - \mathbf{x}_j\|^2}$ with $\nu > 0$. Such a kernel aims to bring down the interferences between two rather "dissimilar" snapshots during the training process. The spatial correlation among sensing values can be handled by pre-processing the training data through the Geographically Weighted Regression (GWR), where each snapshot $\mathbf{x}$ is multiplied by a symmetric matrix W:

$$W(k, \ell) = \begin{cases} e^{-\mu(d_{k\ell}/h)^2} & \text{if} \quad d_{k\ell} < h \\ 0 & \text{otherwise} \end{cases}, \tag{4.7}$$

where $d_{k\ell}$ denotes the Euclidean distance between the k-th and ℓ-th sensing units and the "bandwidth" h is set according to the FoV of our sensing units.

The aforementioned approaches may work well when occupant are static. When occupants are moving, the individual snapshots can be rather unstable. Nevertheless, the occupant motion also provides more information, e.g., variance among two consecutive snapshots. Intuitively, minor temporal variances in the snapshots often indicate unchanged occupancy, while major ones may indicate otherwise. To take the advantage of this increased information dimension, we expand every snapshot $\mathbf{x}_i$ by further involving its variance with respect to the previous snapshot, so the new snapshot has the form of $[\mathbf{x}_i, \mathbf{x}_i - \mathbf{x}_{i-1}] \in \mathbb{R}^{2n}$.

4.3.4 Incremental Inference

Due to dynamics of a real-world environment, the learning-based system set up using training data pre-collected offline may be out-of-date, and thus perform poorly online. To adapt the system to environmental dynamics, a few training data need to be collected online periodically (normally every week). We also implement an incremental or online algorithm to update the trained SVR model whenever a new training sample is collected in real time [100], which entails a very efficient adaptation to a dynamic environment without the need for retraining from scratch.

4.4 System Evaluation

In this section, we evaluate the performance of CeilingSee in terms of inference accuracy, latency and power consumption through extensive field experiments.

4.4.1 Experimental Setup

We deploy a CeilingSee testbed in one of our university laboratories; it covers an area of 5m×6m. The testbed consists of 16 LED lighting/sensing units mounted on the ceiling with a height of 2.5 m above the floor as shown in Fig. 4.15(a). We try to deploy the units in 1.25 m × 1.25 m grid, but we have to slightly adjust the positions of some units adapting to the office layout. As briefly presented in Section 4.2.2, each sensing unit includes an 8×12 LED chips array and a re-designed driver. We connect all drivers to a Lenovo ThinkPad laptop computer via serial port, so the laptop acts as a lightweight server processing the sensing data to produce occupancy inferences.

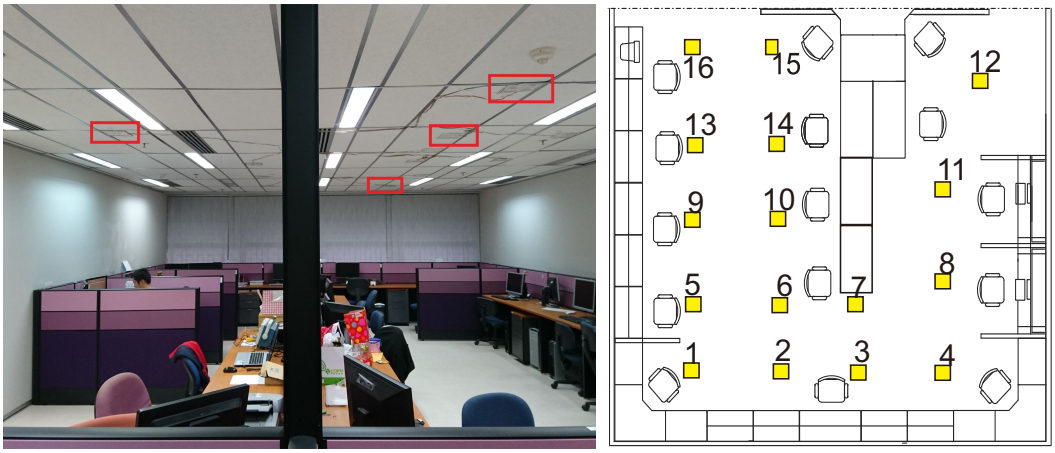

(a) Testbed in photo (b) Sensing units layout

Figure 4.15: CeilingSee testbed overview. Sixteen sensing units are deployed on the ceiling covering a 5 m × 6 m indoor area.

The MCU of our driver, CC2541, is a low-cost power-optimized system-on-chip module, running on up to 32 MHz and supporting 12-bit analog-to-digital conversions [101]. Most importantly, CC2541 is designed for Bluetooth Low Energy (BLE). Therefore, although we currently use a serial port to connect sensor units to the server, we plan to make CeilingSee a fully wireless system by using TI's BLE-STACK [102] to upload sensing data. In our testbed, we run the MCU at 16 MHz and let its ADC samples at 500 Hz, and the low-pass filter discussed in Section 4.2.2.1 is performed by the MCU so that the snapshots are uploaded to the server only at 10 Hz, given the low variation rate of the reflection.

This testbed has been running for about 6 months, during which we have kept monitoring the regular occupancy of the deployment site, and we have also invited groups with up to 20 volunteers to perform specific experiments on the system. All the experiments are performed based on two occupancy patterns: i) *static pattern* where occupants stand or sit at arbitrary locations, and 2) *dynamic pattern* where all occupants walk or even run freely in the lab. For each pattern, the number of occupants varies from 1 to 20, and we encourage the occupants to change their postures between standing and sitting, as well as to perform other daily activities during the tests. We gather more than 10,000 snapshots for each pattern; they are all labeled manually.

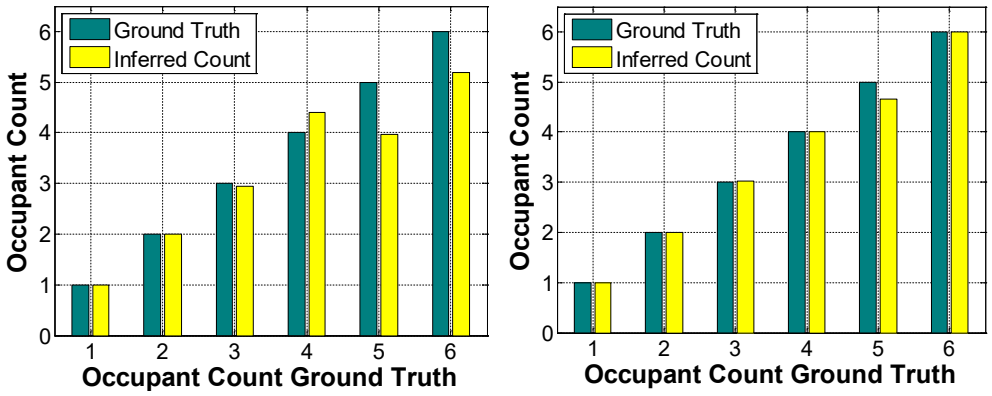

(a) Single sensing unit.

(b) Multiple sensing units.

Figure 4.16: Comparing the accuracy of occupancy inference between (a) single sensing unit and (b) multiple sensing units.

4.4.2 Single Sensing vs. Multiple Sensing

We first evaluate the detection capacity of one sensing unit in CeilingSee. We randomly select one of 16 sensing units (Unit 6 in Figure. 4.15(b)) to detect nearby occupants within its sensing range. We choose the radius of FoV as 1.5 m since it corresponds to a relatively robust sensing value as shown in Figure 4.9(a). We assume the maximum occupants within a circle of radius 1.5 m is 6 as otherwise it would be too crowded. We collect the data when 0 to 6 occupants standing or sitting within the FoV of Unit 6. Applying the regularized regression on the sensing values obtained by Unit 6, Figure 4.16(a) shows the estimated occupancy counts with corresponding ground truth values. An estimated occupancy count is calculated as the average of over 1000 inferences for true occupancy count, so the values are not integers anymore. We observe that the inference for fewer occupants are more accurate and the accuracy decreases slightly with an increasing occupancy count.

This can be explained by the fact that the occupants' cross sections overlap with each other when the density increases. The overall accuracy of Unit 6 is only 77.9%, with the accuracy metric defined as the ratio between the number of correct inferences and that of all tests.

$$\frac{\sum_{i=1}^{c} \mathbb{J}_{f^*(\mathbf{x}_i)=y_i}}{c}, \tag{4.8}$$

where $\mathbb{J}$ is the indicator function and c is the cardinality.

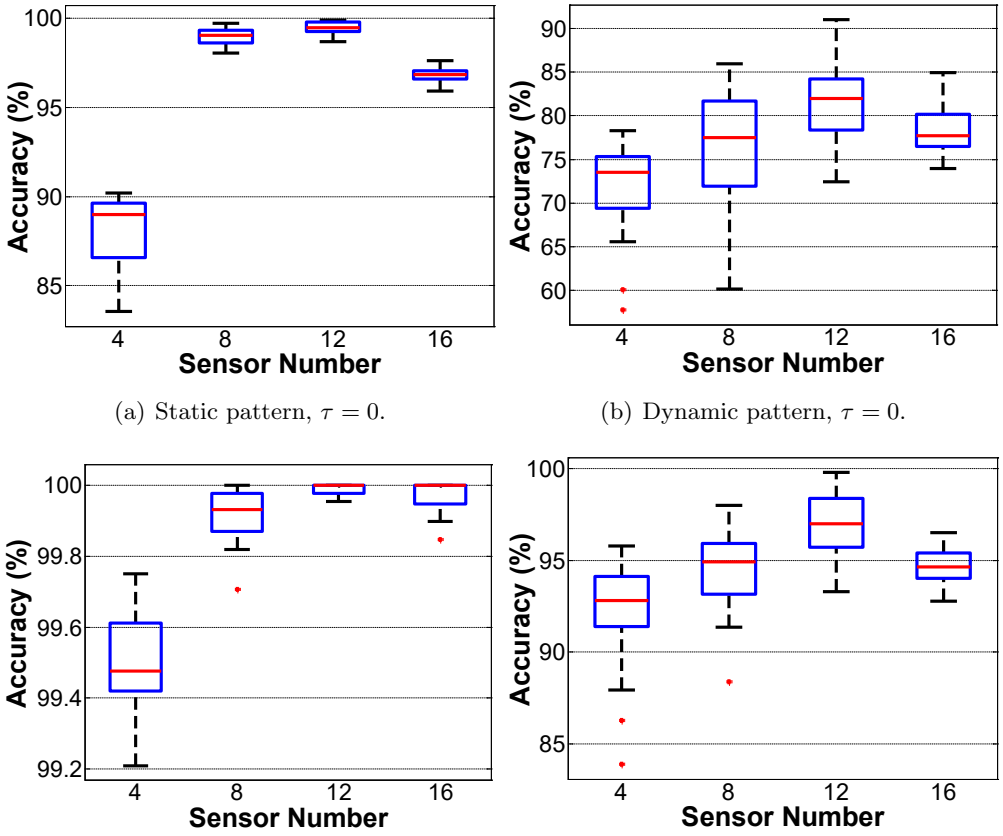

(a) Static pattern, $\tau = 0$.

(b) Dynamic pattern, $\tau = 0$.

(c) Static pattern, $\tau = 1$.

(d) Dynamic pattern, $\tau = 1$.

Figure 4.17: Accuracy vs. varying number of sensing units.

Intuitively, applying multiple sensing units would improve the inference accuracy as it yields a high dimension in sensing data. Now we intend to study to what extend the inference accuracy is improved when multiple sensing units are used collectively. Given the same occupant settings, we gather the sensing values from Units 1, 2, 3, 5, 6, 7, 9, 10 as the inputs for regression, which lead to the results shown in Figure 4.16(b). It boosts the overall inference accuracy up to 96.8%, 19% higher than that of the single sensing unit.

4.4.3 Impact of Sensor Density and Training Intensity

Before evaluating the performance of CeilingSee, we firstly experimentally study the two design parameters of CeilingSee, namely how dense the sensing units should be deployed and how much training is needed. For the first aspect, we select 4 (i.e. unit

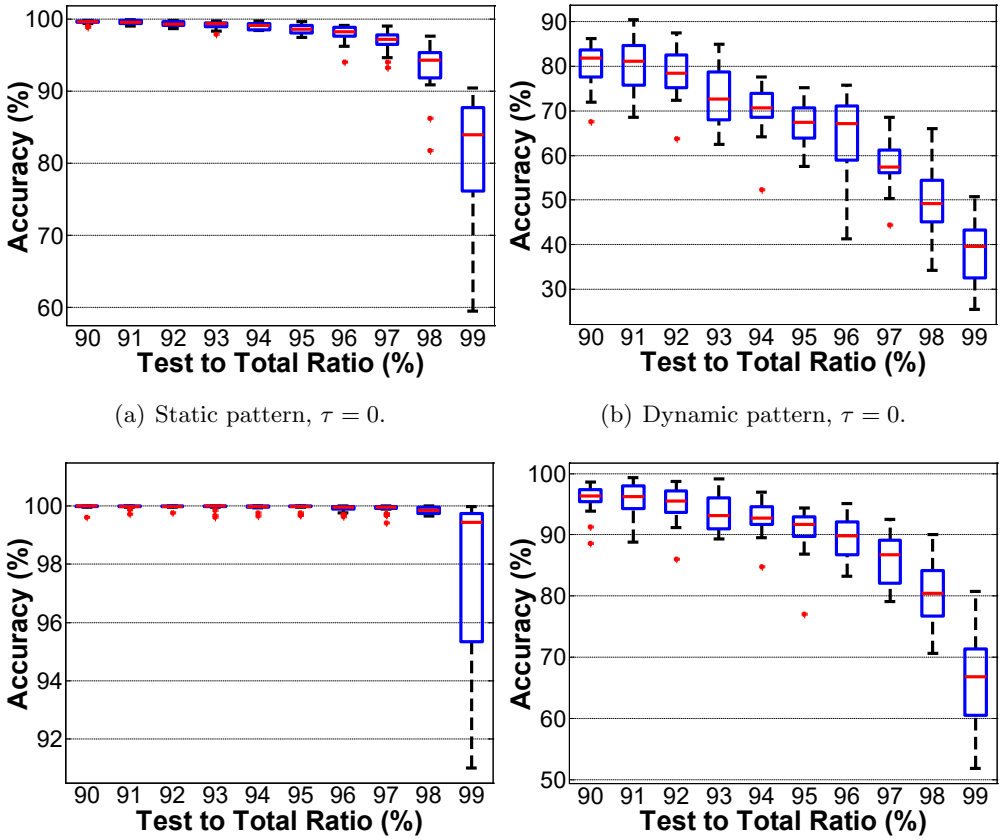

(a) Static pattern, $\tau = 0$.

(b) Dynamic pattern, $\tau = 0$.

(c) Static pattern, $\tau = 1$.

(d) Dynamic pattern, $\tau = 1$.

Figure 4.18: Accuracy with varying TTR given $\tau = 0$ and $\tau = 1$.

6, 8, 14 and 12), 8 (i.e. unit 3, 6, 8, 9, 11, 12, 14 and 16), and 12 (i.e. unit 2, 4, 5, 8, 9, 10, 11, 12, 13, 14, 15 and 16) readings out of each snapshot to derive new snapshots, so that we can evaluate the impact of sensor density. For the second aspect, we take a substantial fraction of the labeled data as testing data while using the remaining fraction for the training purpose. We vary the Test to Total Ratio (TTR) from 90% to 99%, where TTR indicates the fraction of data chosen for testing the regression model. To better understand the accuracy performance, we introduce a new accuracy metric that allows for a certain number of miscounts indicated by a non-negative integer τ. In particular, we define *accuracy with miscount tolerance* as $\left(\sum_{i=1}^{c} \mathcal{I}_{|f^*(\mathbf{x}_i)-y_i|\leq\tau}\right)/c$, where $\mathcal{I}$ is the indicator function and c is the cardinality..

Fig. 4.17 shows the impact of the number of sensing units. While 8 units appear to already offer very good accuracy for a static pattern, 12 units perform the best in both

cases and they would be necessary to cope with dynamic situations. Denser deployments beyond 12 units are clearly not beneficial, because it yields a higher dimension of sensed data and complicates the training procedure of the inference model. Fig. 4.17 further shows the statistics given $\tau = 1$. The relatively low accuracy for a dynamic pattern with $\tau = 0$ is mostly due to a single miscount, as raising τ to 1 would allow even 4 units to almost always achieve an accuracy beyond 90% under both patterns, although the better performance of static pattern and the superiority of 12 units still remain. We will continue observing the performance difference between these two patterns, which shall be further explained in Section 4.4.5. To get the highest accuracy, we will keep using 12 units for the remaining experiments.

Fig. 4.18 evaluates the impact of training intensity by varying TTR from 90% to 99%. As expected, the higher the TTR (hence less training), the worse the performance (in terms of the mean and variance) is, but the performance degrades in a rather graceful manner. In fact, if one miscount can be tolerated, only 2% training data would be needed for the static pattern and 5% for dynamic one. Given our abundant training data, we stick to 90% TTR for the remaining experiments to obtain the best performance.

4.4.4 Breakdown of Inference Accuracy

We now study the occupancy inference accuracy with respect to varying occupancy counts; the statistics are reported for both static and dynamic patterns in Fig. 4.19. We observe that the accuracy based on static pattern is always higher than 97% for all occupancy counts, and tolerating one miscount brings almost all of them to 100%. Though the accuracy for dynamic pattern appears to be rather disappointing, the majority of the miscounting cases involve only one miscount, because setting $\tau = 1$ causes drastic improvements to all occupancy counts.

Under static pattern, the inference accuracy is relatively stable with various occupancy counts, while it is generally degrading as the occupancy count increases for both $\tau = 0$ and $\tau = 1$ under dynamic pattern. This can be largely attributed to the drastic increase in transient states when more occupants are constantly moving, as we shall elaborate in Section 4.4.5. All in all, if we simply allow one miscount, the inference accuracy based on both static and dynamic pattern can be maintained above 90% for all tested occupancy counts. Therefore, CeilingSee achieves a very promising inference

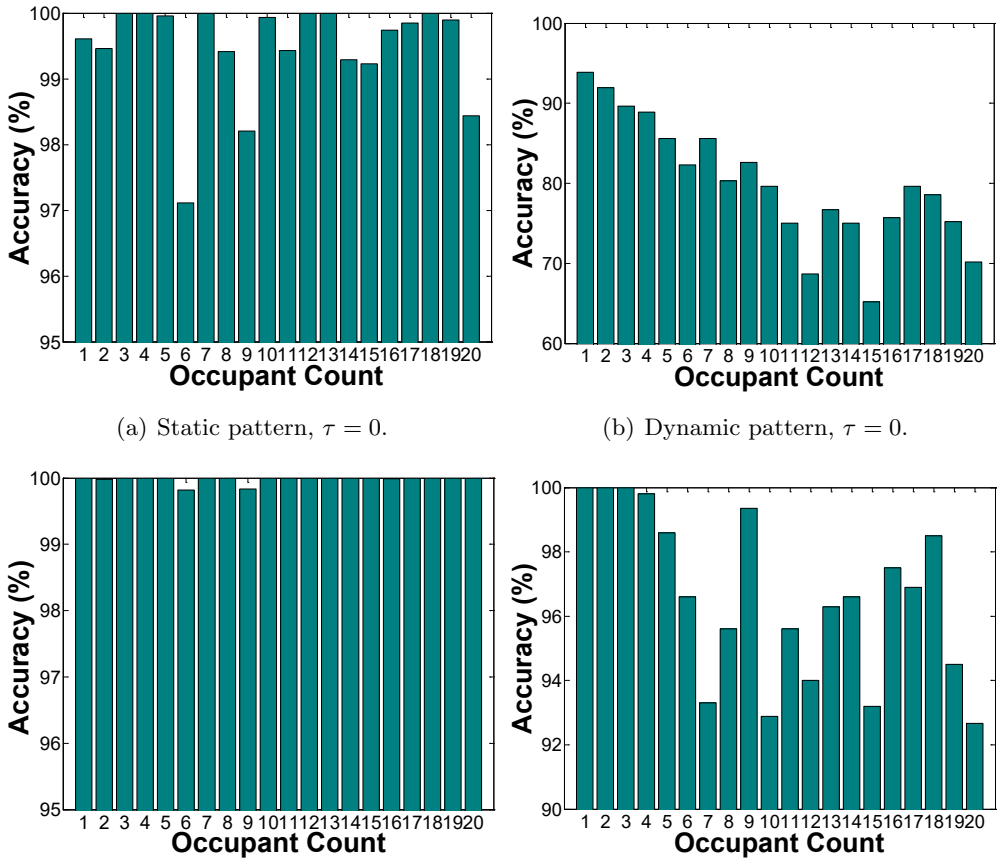

(a) Static pattern, $\tau = 0$.

(b) Dynamic pattern, $\tau = 0$.

(c) Static pattern, $\tau = 1$.

(d) Dynamic pattern, $\tau = 1$.

Figure 4.19: Accuracy with varying number of occupants.

accuracy by using only existing lighting infrastructure. We refrain from comparing CeilingSee with existing proposals at the system level, because, on one hand, it is unfair as they are based on very different technologies, and on the other hand, CeilingSee is not meant to replace other systems, but rather acts as a lightweight complementary solution.

4.4.5 Responsiveness and Real Life Scenarios

As CeilingSee may serve as input to indoor energy management systems (e.g., for HVAC), its responsiveness is a concern and hence entails the need for evaluating how quickly CeilingSee can respond to changes in occupancy count. CeilingSee's sensing units configure their sample rates of ADC as 500 Hz. A moving average filter in the

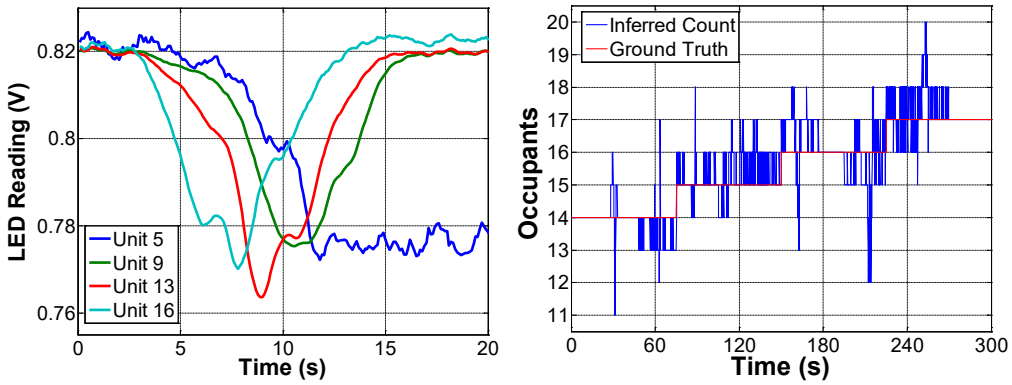

(a) Variations in LED readings

(b) Oscillations under dynamics

Figure 4.20: Dynamic response of CeilingSee.

MCU processes the output of ADC and produces snapshots at 10 Hz, which causes a 100 ms delay. The transmissions of snapshots to the CeilingSee's server via serial port are done at a baud rate of 115,200 bps, consuming less than 1 ms. The server takes less than 1 ms on average to figure out the occupancy counts by operating our regression algorithm. Therefore, inference latency is about 100 ms in total which is mainly consumed by sampling and preliminary data processing on MCU. We could further reduce this delay by running the filter with a smaller window size, but it does not appear to be necessary, because the variations in LED readings take a much slower pace (in seconds), as shown by Fig. 4.20(a) when an occupant passes by 4 units and stops at the last. In fact, the current high level of responsiveness is one of the main reasons that cause miscounts under dynamic pattern. As shown in Fig. 4.20(b), the occupancy counts reported by CeilingSee may oscillate between two actual count changes if occupants keep moving. This causes miscounts as shown earlier, but it is the price the system has to pay for instantaneously detecting count changes.

In order to put the performance of CeilingSee into a practical perspective, we choose to report a whole day monitoring data (for 18 February, 2016) among several-month operation of the system. In Fig. 4.21(a), we plot the inferred occupancy count (without ground truth) from 9 a.m. to 22 p.m. The reported data exhibit a rather plausible pattern: occupants start to arrive in the early morning, they leave for lunch during the noon but come back after lunch; more occupants show up in the afternoon, but most of them leave around 6pm, leaving only a few working till late evening. Between two

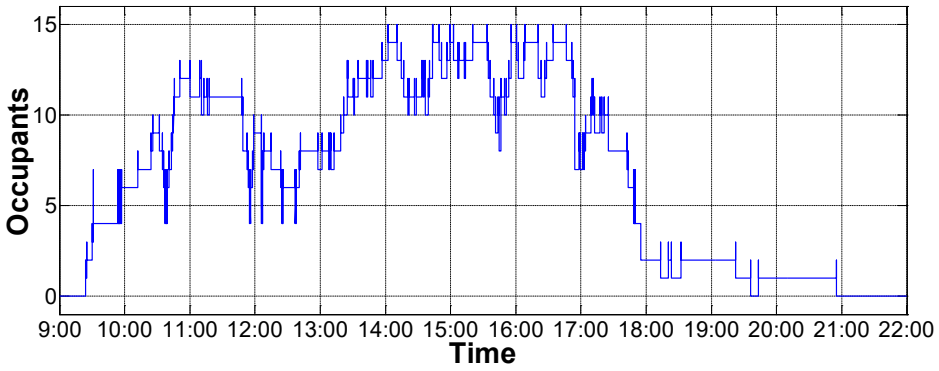

(a) Occupancy count monitored through a day.

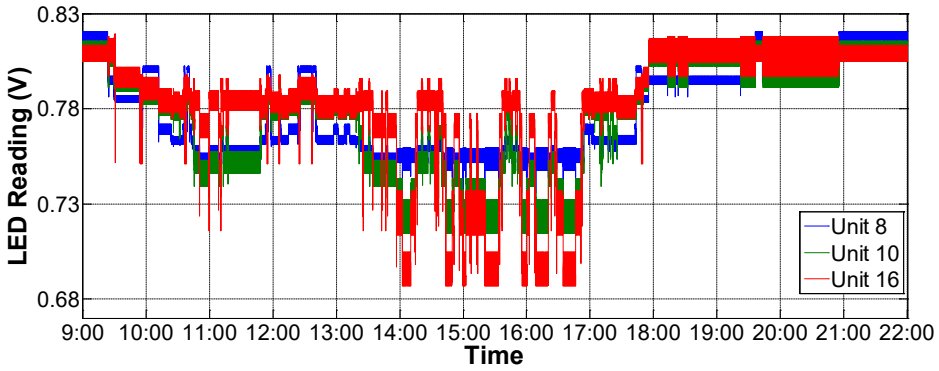

(b) Selected LED readings during the same period.

Figure 4.21: A real life monitoring scenario for one day.

occupancy count changes, the actual daily activity pattern is a mixture of both static and dynamic patterns: it can be rather stable while most of the occupants are sitting (presumably working), while it fluctuates from time to time due to the activities such as taking a short break, mingling with other colleagues, and so on.

We also arbitrarily choose three sensing units, unit 8, 10, 16, to plot their readings in Fig. 4.21(b). The trends of these readings are consistent with that of occupancy count. In particular, sensor readings vary only slightly when there are fewer occupants in the morning, lunch time and off work time, whereas it changes more actively when there are relatively more occupants in the afternoon (as the chance of they being moving becomes higher). If we further look into these readings, for example, those around 14:00 and 15:00, fluctuations are so intense that the sampled snapshots can vary rapidly. The resulting large variations in snapshots reduce the effectiveness of regression and hence the inference accuracy. This explains why CeilingSee performs less accurately under

dynamic pattern as reported in Section 4.4.3 and 4.4.4. Fortunately, as we have shown, the miscounts caused by such fluctuations are largely negligible. We could apply Hidden Markov Models (HMMs) [103] to maintain the temporal consistency of occupancy count so as to improve the inference accuracy under dynamic pattern. Nevertheless, it would certainly retard the response of CeilingSee to count actual changes.

4.4.6 Energy Consumption

Since CeilingSee utilizes existing lighting infrastructure as light sources, we do not count in the energy consumption for illumination. Consequently, the energy consumption of CeilingSee mainly involves the energy consumed by the driver circuits and microcontrollers of the LED sensing units. The driver circuit of one sensing unit works at a DC voltage of $\pm$ 5 V. It consumes 10.1 mW when it works in the sensing state, and at most 50 mW when working in the illuminating state. The energy consumption of the MCU is 24 mW. Therefore, the total energy consumption is 34.1 mW for a typical CeilingSee sensing unit under its sensing state. As MCUs and drivers are default components, in general, LED illumination devices, the extra power consumption of our CeilingSee sensing unit is only 10.1 mW. This extra power consumption is incurred by the amplifier circuits on the re-designed driver. Moreover, since data transmission of sensed data can also be integrated into VLC or Power Line Communication (PLC) [71], the power consumption for data transmission can be neglected. The energy consumption caused by computations on the laptop can also be ignored given that the laptop is working on many other tasks at the same time. All in all, we can conclude our CeilingSee is a truly low-cost energy-efficient system for occupancy inference. We illustrate the power consumption in Table 4.2.

Table 4.2: Energy consumption of one sensing unit.

	Sensing	Sensing & illuminating
Driver	10.1 mW	50.0 mW
MCU	24.0 mW	24.1 mW
Total	34.1 mW	74.1 mW

4.5 Summary

In this chapter, to efficiently estimate indoor occupancy leveraging the sensing ability of LEDs, we have developed a device-free system, CeilingSee, that piggybacks on existing LED lighting infrastructure. The system consists of two main components: 1) a re-designed LED driver, which leverages LED's photoelectric effect to transform a light emitter to a light sensor, so as to obtain variances in ambient reflection in the form of snapshots at any time, and 2) a machine-learning-based algorithm to infer indoor occupancy using the snapshots as input in real time. To verify the efficiency and effectiveness of the developed system, we have conducted extensive experiments in a testbed covering a 30 m^2 laboratory area. The experimental results have shown a very promising performance of CeilingSee and hence demonstrated its great potentials to be applied to many smart building applications.

Chapter 5

Roaming in Connecting Light: Practical Visible Light Communication Leveraging LED Sensing

Similar to the cellular network, VLC systems should offer roaming service for mobile users. However, traditional VLC transmitters built upon LED luminaires cannot automatically associate the user and transmit information to the targeted user due to lack of user detection in a conventional LED-Camera VLC system. In aforementioned Chapter 3 and 4, we investigate VLC system and VLS system respectively. In this chapter, we first combine those two systems to confront the roaming issue in VLC system, i.e. providing seamless connectivity to mobile users. In particular, we present RoCLight as the first attempt to provide roaming support to an LED-Camera VLC system by leveraging LED sensing, and build a real tested demonstrating the effectiveness of RoCLight.

5.1 Introduction

While traditional VLC research is still pursuing a high data rate using specialized high speed photodiode receivers [11, 20, 104, 105, 106, 107, 108], there is a recent trend in exploiting COTS devices (in particularly smartphones) to implement readily deployable VLC systems that offer only a moderate level of data rate [15, 16, 27, 30, 31, 34,

35, 36, 95, 109, 110]. This new trend actually involves two main directions, namely Screen-Camera Communication [30, 31, 34, 35, 36, 109] and LED-Camera Communication [15, 16, 27, 95, 110]. Whereas the former focuses on short-distance (sub-meter) communications, the latter has the potential to cover almost all indoor areas given the pervasive installation of LED enabled lighting systems. Nevertheless, this latter potential has still been hampered by the lack of roaming support.

Similar to the cellular network scenario where each cellular tower has a limited coverage, the individual LED luminaire in an LED-Camera VLC system also have their own effective transmission range. Therefore, roaming support is necessary to maintain wireless connectivity upon user mobility. As the location-bound communication ability of VLC is commonly believed to be geared towards location-based services such as coupons or advertisements deliveries [95], a practical VLC system does not need to support a full range roaming, yet it at least has to guarantee the continuity in receiving messages when a user is moving in a room-level area. For example, as shown in Fig. 5.1(a), after a broadcasting is triggered for LED1 due to a user's attention on a commodity (e.g., a painting on the wall), the user moves out of the range of LED1 before completing the transmission. A range-limited roaming support would be helpful in this case, as it can trigger LED2 and LED3 to relay the unfinished transmission.

Unfortunately, all the existing VLC systems relying on COTS devices only offer a single-direction communication; this has made it extremely difficult to support roaming as a feedback channel is necessary for the handoff between neighboring luminaires [9]. Combining the existing RF communication techniques, heterogeneous VLC-RF networks could rely on RF to offer a feedback channel for supporting seamless roaming connectivity in a VLC system [18], which in turn enables further energy-efficient optimization to be performed on the user-to-network association structure [20]. Nonetheless, a HetNet infrastructure incurs extra management and operation overhead, so it may substantially limit the applicability of COTS-enabled VLC systems that are meant to operate in a plug-and-play mode at places where RF may not be available.

In this chapter, we aim to confront the aforementioned challenge. As it appears to be almost impossible to initiate a feedback channel from the receiver of an LED-Camera VLC system (i.e., a smartphone camera), innovation can only be made on the sender side. To this end, we propose RoCLight (**Ro**aming in **C**onnecting **Light**) as the first attempt to offer roaming support to LED-Camera VLC systems. Essentially, our design

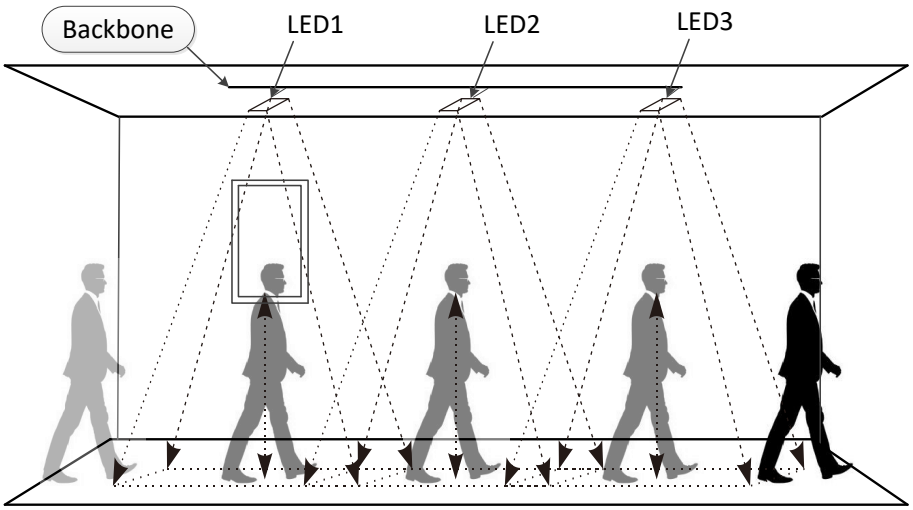

(a) A user moves across three LED luminaires.

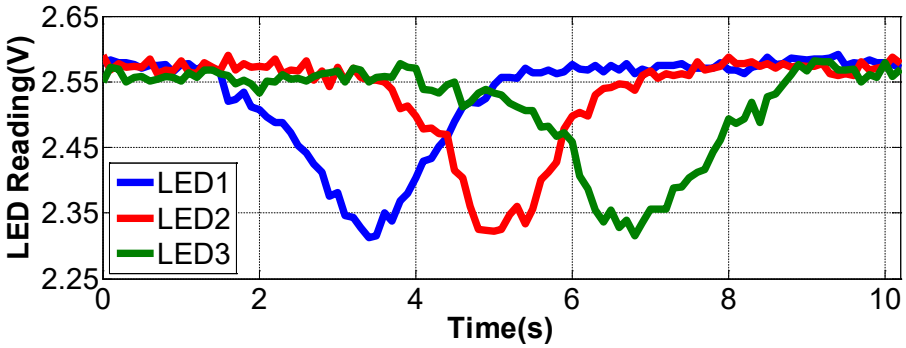

(b) The variance in LED readings due to user mobility.

Figure 5.1: Tracking user mobility by LED sensing. The diffuse reflection change caused by user moving can be sensed by LED luminaires.

exploits the photoelectric effect of LEDs so that an LED luminaire can be converted into both a light emitter and a light sensor. In addition, it leverages the disturbance to the indoor (light) diffuse reflection caused by user mobility. Consequently, RoCLight, while continuing using the light emitter side to act as a VLC transmitter, employs the light sensor side to keep track of user mobility: it senses the disturbance to reflection, as illustrated by Fig. 5.1(b), and hence adjusts the coding/transmission to maintain the connectivity to a given user. Our major contributions are:

- We propose an innovative idea of applying ceiling-mounted LED lighting system to track user mobility in a limited scale.

- We re-engineer the driver of COTS LED luminaire so that the LED chips can be toggled between light emitting and light sensing modes.
- We employ rateless codes to VLC transmissions so that a communication session can be relayed to another LED luminaire once a user moves towards it.
- We build RoCLight as a practical VLC system with roaming support, using the mobility tracking function as the feedback channel to properly relay a communication session between neighboring LED luminaires.
- We conduct field experiments to validate the effectiveness of RoCLight using a small scale deployment.

The rest of this chapter is organized as follows. First we present the design of the LED sensing component in Sec. 5.2, before introducing the system architecture of RoClight in Sec. 5.3. We report the system evaluations in Sec. 5.4, and summarize this chapter in Sec. 5.5

5.2 Tracking User Mobility with LED Sensing

In this section, we first introduce how to detect the user by using ceiling-mounted LED luminaires. Then we present the circuit design that allows us to convert an LED luminaire into a light sensor. Finally, we briefly discuss the properties of this sensor, as well as the user tracking algorithm designed for making use of it.

5.2.1 Sensing Disturbance to Reflection

Since lighting systems are normally ceiling mounted, the induced diffuse reflections from the floor (including various furniture on it) are biased towards the ceiling due to the blending with minor specular reflection. When (human) occupants move in this reflection field, they cause disturbance readily sensible by certain ceiling-mounted light sensors. As it may not be cost-effective to introduce an extra sensing infrastructure, we aim to re-use part of the existing LED lighting system to serve as the sensors.

It is well known that LED has photoelectric effect, i.e., light shining upon an LED can cause it to emit electrons, and has motivated a few proposals to use an LED not only as a sender but also as a receiver in VLC [94]. However, converting an LED

receiver to an LED sensor is almost impossible as the light signal sent by an LED has a much higher SNR than the variance in reflection. Moreover, as our LED lighting system needs to serve both transmission and sensing purposes, we need the LEDs to be toggled between light emitting and light sensing modes when either is in need. These are what our design in RoCLight should handle.

5.2.2 Converting Luminaire into Sensor

In a conventional design for light receiving in the LED-LED communication, a bidirectional interface to an LED is created by connecting the LED directly between the two I/O pins of a micro-controller (MCU) [94]. As a result, the LED emits light when its anode and cathode are connected to VCC and GND, respectively, by an I/O configuration. Reverting the I/O configuration sets the LED in reverse bias mode in order to charge the inner stray capacitance of the LED so as to prepare the LED for light sensing. The actual measurement is done by MCU reading the voltage changes on LED's cathode and timing how long it takes for the photocurrent to discharge the capacitance to the I/O pin's digital input threshold. Obviously, the discharging time is inversely proportional to the amount of incident light. The simplicity of this LED receiving circuit stems from the matching voltages between an MCU and an LED. Apparently, it does not work if several LEDs are to sense together unless the same number of MCUs are used.

Compared with receiving signals sent by another LED a few centimeters away [94], sensing the disturbance in reflection is much more challenging. This is not only because the signal is much weaker, but also because the effective "transmission distance" (from floor to ceiling) is much longer. Consequently, we need a new circuit design to boost the sensitivity, and this is done by involving multiple LED chips belonging to one LED luminaire to collectively sense the weak signal. Note that we cannot rely on reverse bias in our circuit either, as the much higher voltage level caused by aggregating multiple LEDs renders the reverse extremely hard (if not impossible) to achieve using commonly available electronic components.

Therefore, we aim to construct a light sensing unit using an array of LED chips without the need for reverse biasing the whole unit. Each LED chip, according to its equivalent circuit model, can be considered as a current source with a shunt capacitor, with the current source driven by the incident light to generate tiny photocurrent.

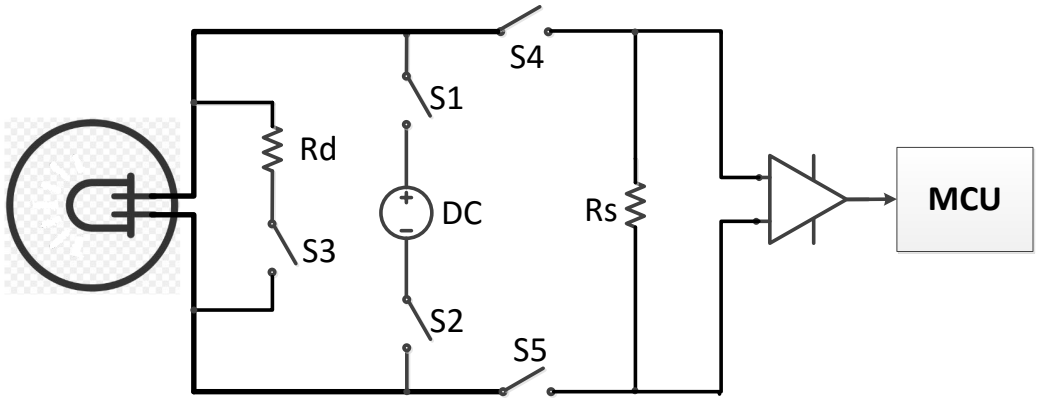

(a) Circuit schematic of the driver.

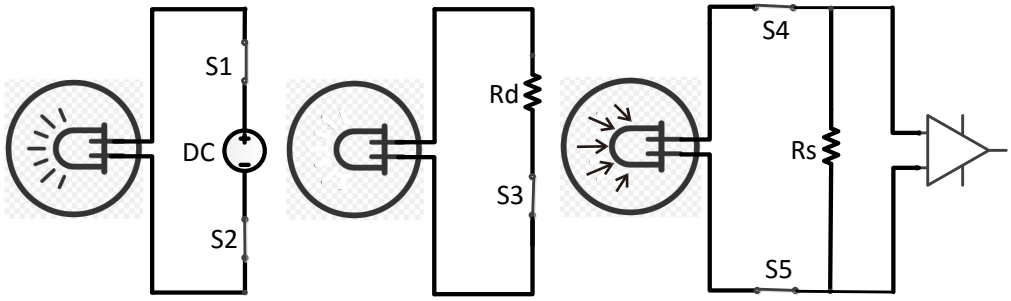

(b) Emitting. (c) Discharging. (d) Sensing.

Figure 5.2: The re-engineered LED array driver. (a) Circuit schematic of the driver. (b) The equivalent circuit during light emitting. (c) The equivalent circuit for discharging. (d) The equivalent circuit during light sensing.

Although the current produced by one chip is too weak to be measurable, the aggregated current of the LED array (with a sufficient amount of LEDs) would be adequate for the purse of sensing weak signals. To this end, we re-engineer the driver of COTS LED luminaires so as to toggle the LED state between light emitting (for normal lighting and data transmission) and light sensing (for tracking user mobility).

The basic schematic of our design is shown in Fig. 5.2, along with the equivalent circuits corresponding to different modes. The five switches in Figure 5.2(a) are key components for the driver. The LED array emits light (lighting phase) if both S1 and S2 are ON and other switches are OFF, as shown by Figure 5.2(b). Subsequently, Figure 5.2(c) shows a short discharging window that allows residual charges on the array to be cleared for preparing sensing (discharging phase), by putting S3 ON while others

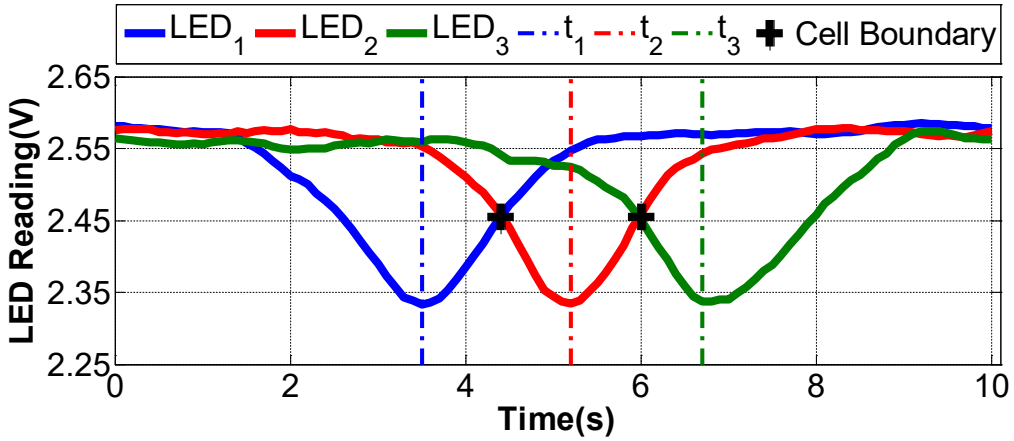

Figure 5.3: Tracking user mobility by filtered sensing values.

OFF. Finally, switching S4 and S5 ON and others OFF enables the array to act as a light sensor (sensing phase): the resistor Rs (> 10 MΩ) converts weak photocurrents to voltage signals that drive amplifiers to produce sensing outcome.

5.2.3 From Reflection Sensing to Mobility Tracking

As illustrated by Fig. 5.1, user mobility does cause changes in reflection and they can be sensed by the sensing module of RoCLight. Due to the page limit, we omit more detailed elaborations on reflection sensing but directly proceed to the discussions on mobility tracking. We denote the sensing value of an LED luminaire by $x_i(t)$, where i is the index of that LED and t is the time instant when the value is sampled. Suppose that we have N LEDs in a RoCLight system and a user is walking under the coverage of this system from time 0 to t, we have, for the i-th LED luminaire, the sensing sequence $\mathbf{x}_i = \{x_i(0), x_i(1), \cdots, x_i(t)\}$. As RoCLight is also used for VLC that transmits data to users by emitting modulated pulses, this leads to a switching "noise" persisting in the sensing value. To combat this inevitable noise, we apply a moving average filter with a window size of 90ms before extracting features concerning user mobility. Fig. 5.3 shows the results of the filtered sensing values of three LED luminaires.

For each sequence $\mathbf{x}_i$, we can find out the minimum value indicating that a user is right below the i-th luminaire, as well as the corresponding timestamp $t_i = \arg\min \mathbf{x}_i$. Consequently, we obtain a vector of timestamp $\mathbf{t} = [t_1, t_2, \cdots, t_N]$, by finding out the timestamps of all minimum sensing values for N LED luminaires. This vector

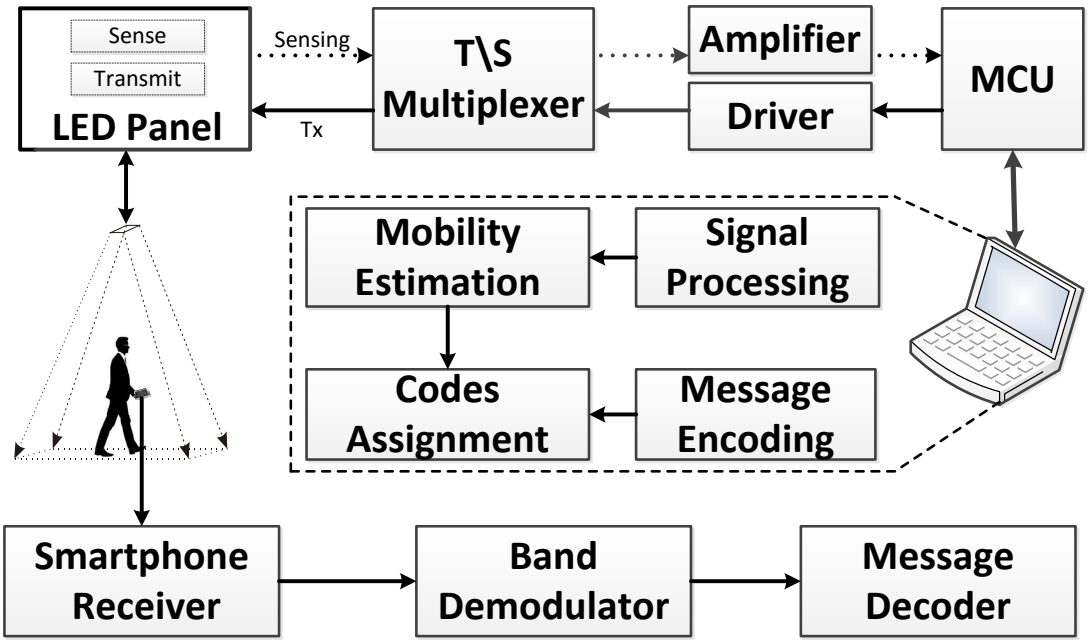

Figure 5.4: System architecture of RoCLight

allows us to further infer the speed and direction (thus the velocity) of a user. For example, the time interval of a user passing two neighbor luminaires $i-1$ and i can be easily computed as $t_i - t_{i-1}$. Combining the known mounting distance d between luminaires, user's walking speed is derived as $s = d/(t_i - t_{i-1})$. The moving direction can be readily observed from the ascending order of elements in $\mathbf{t}$. The crossing points (assuming overlapping cells as indicated in Fig. 5.3) are used as the cell boundaries [9] of individual luminaires where handoffs should take place, and they also indicate instant moving directions. In fact, RoCLight can even figure out the location of a user at a certain instant by processing the sequences of the sensor readings as shown in Fig. 5.3. Note that, although our examples always involve a single user to ease the exposition, tracking multiple users is possible as demonstrated in Sec. 5.4.2.

5.3 RoCLight: Supporting Roaming in VLC

As a practical LED-Camera VLC system, RoCLight consists of three basic components: COTS LED luminaires as stationary transmitters, smartphones as receivers, and in particular, an LED sensing module to support roaming.

The system overview of RoCLight is shown in Fig. 5.4. On the transmitter side, the photoelectric effect of LED chips is exploited to track user mobility Once users are sensed by a transmitter of RoCLight, the transmitter automatically associates itself with the users and starts sending follow-up messages (with the knowledge of the previous transmitter) to the users. On the receiver side, RoCLight leverages the rolling-shutter effect of CMOS camera to decode the modulated signals emitted by LED luminaires. Therefore, a user holding a smartphone can seamlessly receive messages from all passed luminaire cells of RoCLight. In this section, we concentrate on elaborating our ideas in designing coding/decoding mechanisms for the roaming support.

5.3.1 Basic Modulation

In order to embed the information on the visible light, RoCLight employs a hybrid modulation of On-Off Keying (OOK) and high frequency Pulse-Width Modulation (PWM) proposed in [95]. This combination enables the simple OOK to fully support dimming control of LED lumination and alleviates potential flicker. The packet structure of RoCLight is set as shown in Fig. 5.5. Each packet has an OOK based preamble "011110" and Manchester coding [15] based significant bits. In this way, the preamble leads to a widest bright band indicating the start of a packet. For reliability improvement and seamless communication, Hamming correction coding [111] is utilized in RoCLight. Thus after the preamble, it is actually followed by a 21-16 Hamming format in Manchester coding carrying up to 8-bit Packet Sequence Number (PSN) and 8-bit data payload.

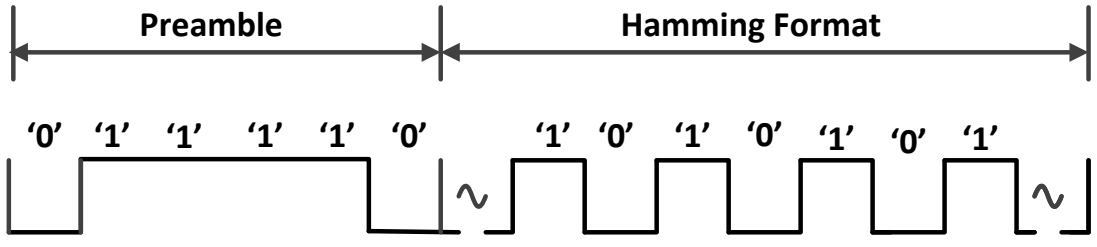

Figure 5.5: The packet structure of RoCLight: a packet consists of a preamble of "011110" and two significant bytes of data (8-bits PSN and 8-bit payload), along with 5 error correcting bits in a 21-16 Hamming format.

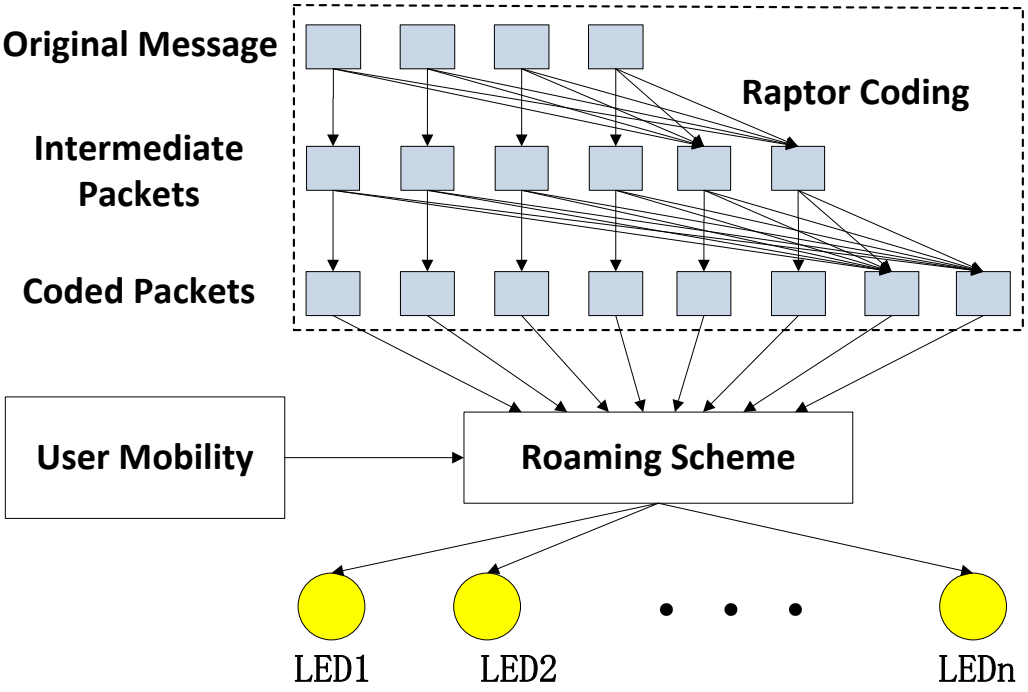

Figure 5.6: Raptor coding and roaming scheme in RoCLight.

5.3.2 Applying Rateless Code

Though RoCLight has a feedback channel to track the user mobility, the channel is not actually established from the receiver to the transmitter and hence the LED-Camera VLC is still unidirectional. This means that a transmitter has no knowledge about the reception status of a receiver. Therefore, an FEC scheme has to be taken to combat the packet loss, especially for the mobile scenarios considered by RoCLight. Furthermore, reception from different LED luminaires also calls for an encoding mechanism to realize coordinated transmission and thus seamless roaming service. Rateless codes appear to be a promising choice to tackle these issues; it encodes k original packets into a potentially infinite number of packets so that the receiver can successfully recover the original message by receiving any m encoded packets, where $m > k$.

Among all rateless codes, Raptor code [69] is chosen for its linear time encoding/decoding, low computation complexity, as well as low decoding overhead. The top part of Fig. 5.6 shows the typical raptor coding mechanism. A set of intermediate packets are first generated from the original message so that reception of the intermediate

packets is sufficient to reconstruct the original ones. Additional repair packets are then produced by applying LT encoding, each of which is calculated by XORing a number of intermediate packets. The output encoded packets are a sequential combination of the original and repair ones. Due to the lack of feedback to stop coding and sending on transmitter side, fixed overhead is configured in RoCLight. That means the transmitter will send out $n = \gamma \times k$ encoded packets for every k original packets where $\gamma > 1$. In our current small scale implementation of RoCLight, we choose a fixed $\gamma = 1.25$. Nevertheless, we are on the way to investigate the benefit of making γ an increasing function of s. This makes sense as a higher speed suggests a possibly higher packet loss, which may need a more aggressive FEC to cope with. Now we have both a cell boundary crossing detection (see 5.2.1) and a convenient FEC at hand, so we shall explain how RoCLight combines them to realize roaming support.

5.3.3 Roaming under User Mobility

Consider a simple scenario shown in Fig. 5.7 that a user passes through two adjacent luminaires LED_i and LED_{i+1}. Suppose we configure the luminaires to work independently as the existing VLC systems, then the user may either suffer a higher packet loss when leaving the cell of LED_i due to non-overlapping cells, or otherwise receive duplicate packets from both LEDs at the boundary of two cells, as shown in Fig. 5.7(b) and 5.7(c). Although the Raptor codes adopted by RoCLight automatically handle the packet loss, it comes at the cost of increased latency especially when transmitted packets get lost. The duplicated receptions also require a particular solution, as it could reduce the throughput to the point that no user can receive a full message within a limited number of cells.

To tackle the mentioned problem, RoCLight enables its luminaires to transmit encoded packets adaptively according to the user's current position and velocity. We take Fig. 5.7 as an example to illustrate the how we address the roaming issue. Suppose a message contains k original packets and $n = \gamma \times k$ encoded packets after Raptor coding as detailed in Sec. 5.3.2. Assume that LED_i has completed sending the first j packets, where j is less than the number of packets needed for successful decoding, when a user moves across the cell boundary as shown in Fig. 5.7(c). RoCLight detects the boundary crossing event and the next cell to be entered with its sensing ability explained in Sec. 5.2.3. Subsequently, the user would expect new packets from LED_{i+1} starting from

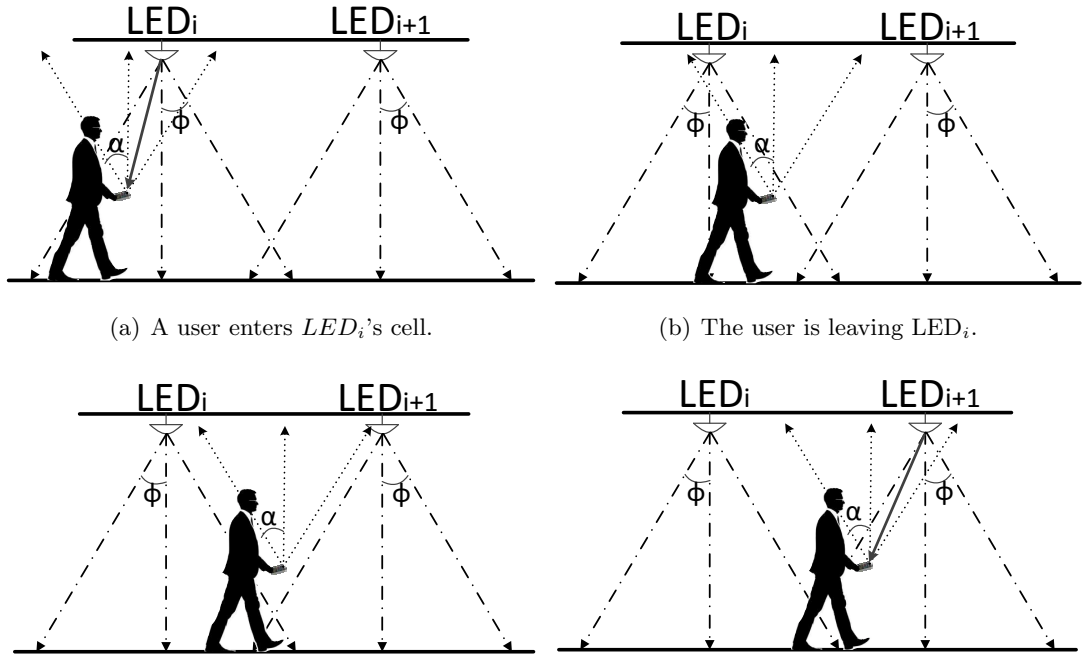

(a) A user enters LED_i's cell.

(b) The user is leaving LED_i.

(c) The user is crossing cell boundary.

(d) The user enters LED_{i+1}'s cell.

Figure 5.7: Roaming under RoCLight's transmissions. (a) A user is associated with LED_i and receiving message from it. (b) The user is leaving LED_i and may start to get a higher packet loss. (c) The user is under the gap between LED_i and LED_{i+1} and hence receiving from both. (d) The user fully enters the cell of LED_{i+1}.

$j+1$ when entering the cell of LED_{i+1} as shown in Fig. 5.7(d) if the previous packets were perfectly received. In our implementation, we introduce a small overlapping offset o_i for each transmitter, i.e. the sequence numbers of the packets assigned to LED_{i+1} is actually from $j+1-o_{i+1}$: while $o_{i+1} > 0$ may combat potential packet losses taking place between cell boundaries, $o_{i+1} < 0$ handles the duplicated receptions. Therefore, RoCLight first tracks the user's localization and velocity, and then assigns the codes to the luminaire whose cell the user has just moved into. Apparently, this roaming scheme may potentially improve both throughput and reliability by adaptively sending necessary packets to the user.

5.3.4 Throughput when Roaming

Assuming the offset o_i can perfectly compensate either the loss or the duplication, the throughput should be the same as static case when the user is under the coverage of

RoCLight, i.e., RP_{size} as derived in [95] where R is the camera frame rate and P_{size} is the packet size decided by camera specifications. Therefore, the throughput under mobility depends on the fraction of time under coverage and is hence decided by the inter-luminaire distance d and the cell radius r_c. According to Fig. 5.7, a cell boundary should be determined by the minimum among three quantities, namely the angle of view (AoV) of the camera, the transmission range of the LED luminaire, and the field of view (FoV) of the LED sensor. According to our experience, the latter two often lead to a wider boundary than the first one, so we only consider AoV (defined by α) hereafter, i.e., we assume $\phi = \alpha$ in Fig. 5.7.

Given the ceiling height h, the cell radius on the ground becomes $r = h \times \tan\alpha$, given our assumption that $\phi = \alpha$. Since α is defined by the image sensor dimension d_s and effective focal length f, we have $\alpha = \arctan\frac{d_c}{2f}$ [112]. Therefore, we obtain the cell radius as $r = \frac{hd_c}{2f}$. In reality, the smartphone receiver is held by a user, so the effective communication cell is actually a disk with radius:

$$r_c = \frac{(h - h_c)d_s}{2f}. \tag{5.1}$$

where h_c is height of the smartphone receiver held by a user. Now with a given inter-luminaire distance d, we can derive the fraction of time under coverage and hence the maximum bit rate achievable by RoCLight as:

$$C \leqslant \begin{cases} RP_{\text{size}} & \text{if} \quad d \leqslant 2r_c \\ RP_{\text{size}} \times \frac{2r_c}{d} & \text{otherwise} \end{cases}. \tag{5.2}$$

Here $d \leq 2r_c$ implies a rather dense deployment leading to full throughput, otherwise throughput is lower due to the lack of full coverage. In our RoCLight testbed, the typical parameters are $r_c = 1.0$ m and $d = 1.5$ m. Therefore, RoCLight can achieve a full throughput in theory, and we refer readers to [95] for more detailed analysis on static throughput.

5.3.5 Demodulation and Decoding on Smartphone

For LED-Camera VLC, a rolling-shutter camera shoots VLC transmitters at very short exposure time (e.g. 1/7500 s) to obtain the banded images (frames) carrying modulated information. Before demodulating the banded frame, the smartphone applies specific image processing procedures to denoise the received frame and extract the contour of

(a) Original image. (b) Detected contour.

Figure 5.8: Image processing for extracting VLC transmitter's contour.

the target VLC transmitter. In particular, we employ the noise subtraction method proposed in [27] to denoise the image and subsequently computer vision techniques [14] to extract the contour of target VLC transmitter. Fig. 5.8 briefly illustrates the image processing for detecting such a contour.

After extracting the contour of VLC transmitter, RoCLight chooses a threshold to distinguish bright and dark strips after scanning the whole packet within the detected contour. Then the demodulation starts from the widest bright strips, i.e. the preambles presented in Sec. 5.3.1, to obtain Manchester OOK bits. RoCLight will recover the original packet or discard the error one after Hamming decoding, and it stores the correct packet for contributing to Raptor decoding. Upon receiving $m = k(1 + \epsilon)$ encoded packets, where $\epsilon = 0.1$ is chosen to be the overhead of Raptor codes for RoCLight, Gaussian elimination is employed for LT decoding in RoCLight. The whole procedure is sufficiently lightweight for Android smartphones.

5.4 System Evaluation

In this section, we evaluate the performance of RoCLight in terms of user mobility detection accuracy, channel property, throughput, latency, as well as power consumption. We first explain the experiment settings, and then discuss the experimental results of RoCLight with respect to various metrics.

5.4.1 Experiment Settings

We deploy a RoCLight testbed with 5 LED luminaires spanning a length of 7.5 meters in one university laboratory as shown in Fig. 5.9. Each LED luminaire is made by 8 commercial LED strips [73] and it contains in total 288 LED chips. We separate the

Figure 5.9: RoCLight testbed: five LED luminaires are mounted on the ceiling with an interval of 1.5 m, and the ceiling is 2.5 m above the floor.

chips into two groups with a dimension of 60 cm $\times$ 4 cm (36×4 LED chips) similar to a common fluorescent luminaire and duty cycle them in a complementary manner so that one group performs lighting (transmitting) and the other one performs sensing at the same time.

For lighting(transmitting), we use Darlington transistors as the driver to drive LED luminaire lighting while transmitting. The luminaire may run at maximum drive current of 2.4 A for each LED strip has a maximum drive current of 600 mA. We connect all the five luminaires to an ASUS laptop computer via Zigbee, so that the laptop works as a lightweight server to process the sensing data and dispatch encoded packets according to user's location and speed. Fig. 5.10 shows the PCB board of RoCLight driver and the employed Zigbee module.

RoCLight employs the low-cost system-on-chip wireless micro-controller, CC2530, as the MCU of the re-designed driver. CC2530 runs on up to 32 Mhz and supports 12-bit ADC (analog-to-digital conversions) [113] along with a full Zigbee networking stack [114]. Most importantly, CC2530 offers sufficient timers, i.e., one 16-bit timer and two 8-bit timers, for our RoCLight to generate hybrid modulated signal and the sample clock of ADC. We run the MCU at 32 MHz and configure its ADC sampling rate at 500 Hz to collect the user mobility information, and we use two timers to generate the OOK-

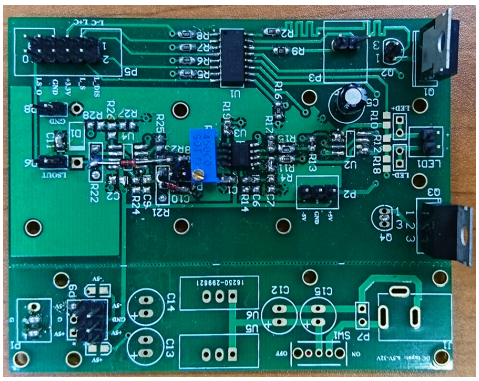

(a) LED driver consisting of amplifier circuits and transistors.

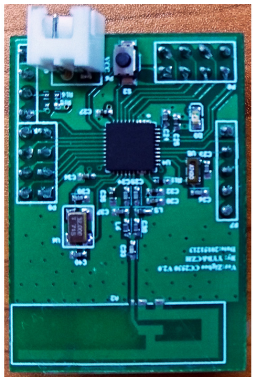

(b) Zigbee module with TI's CC2530.

Figure 5.10: Re-engineered driver and Zigbee module used in RoCLight.

PWM modulation signal. To suppress excessive data transmission on Zigbee network, the low-pass filter mentioned in Sec. 5.2.3 is built on MCU to preprocess and compress data so that RoCLight's server receives data every 90 ms. Meanwhile, the laptop server encodes a message by Raptor coding and dispatches encoded packets every 33 ms to the target luminaire where the user is. We implement our demodulation/decoding scheme on a Nexus 6 smartphone using its front camera. RoCLight by default sets the frame rate at 30 fps, ISO at 200, exposure time at $1/7500\ s$, preview resolution of 1024×768 pixels unless otherwise specified. To demonstrate the advantages of RoCLight, we have also implemented a (baseline) Non-Roaming mechanism that sends identical Raptor encoded packets synchronously in a circulating manner for all luminaires [95].

5.4.2 Sensing Multiple Users

We first evaluate the capability RoCLight in detecting multiple users. We select LED3 shown in Fig. 5.9 to detect nearby users in its FoV (a disk with a radius of 1.2 m). We assume the maximum occupants within this FoV is 6 as otherwise it would be too crowded. We collect the data when 0 to 6 occupants appearing within the FoV of LED3. Applying the regularized regression on the sensing values obtained by LED3, Fig. 5.11(a) shows the estimated occupancy counts with corresponding ground truth values. An estimated occupancy count is calculated as the average of over 1,000 inferences for true user count, so the values are not integers anymore. We observe that the

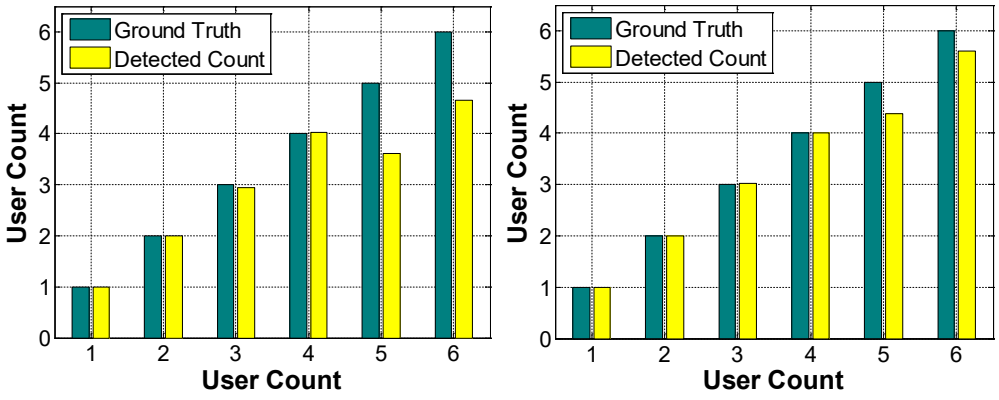

(a) Single LED. (b) Multiple LEDs.

Figure 5.11: Comparing the accuracy of user presence between single LED and multiple LEDs.

inference accuracy decreases slightly with an increasing occupancy count. This can be explained by the fact that the occupants' cross sections overlap with each other when the density increases. The overall accuracy of LED3 is 73.9%, with the accuracy metric defined as the ratio between the number of correct inferences and that of all tests.

Intuitively, applying multiple LEDs would improve the inference accuracy as it yields a high dimension in sensing data. Now we intend to study to what extend the inference accuracy is improved when multiple LEDs are used collectively. Given the same occupant settings, we gather the sensing values from LED2, LED3, and LED4 as the inputs for regression, which leads to the results shown in Fig. 5.11(b). It boosts the overall inference accuracy up to 87.9%, 14% higher than that of single LED. Although RoCLight cannot tell one certain user from others, this does not matter due to the broadcasting nature of the VLC system, i.e. all users under the same LED should receive identical messages.

5.4.3 Performance of Mobility Tracking

We evaluate the performance of mobility tracking of RoCLight as explained in 5.2.3. A user with a upward-facing smartphone passes through the lane covered by our testbed at different speeds repeatedly, during which the accelerometer on the phone is turned on to monitor the average walking speed as the ground truth. The accuracy of tracking

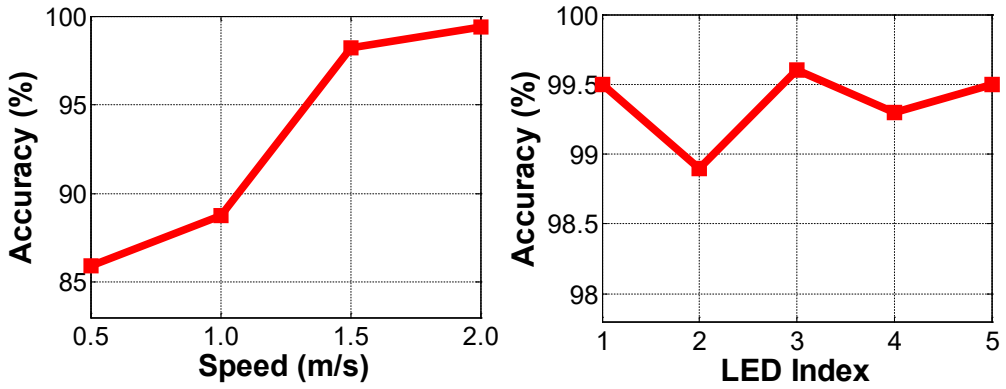

(a) Speed detection accuracy.

(b) Presence detection accuracy.

Figure 5.12: RoCLight's performance on user tracking. Detection accuracy in terms of both speed and user's presence are high by RoCLight.

is defined as

$$\frac{s_g - |s - s_g|}{s_g} \times 100\%. \tag{5.3}$$

where s is the estimated speed by RoCLight, s_g is the ground truth obtained by a phone app.

Fig. 5.12(a) reports the average accuracy for four typical user speeds indoors. We observe that accuracy is beyond 85% for all speeds that verify the mobility detection ability of RoCLight. Moreover, the accuracy grows higher as the speed increases. This improvement benefits from more sharp disturbance of the sensed signal caused by fast motion. We choose the radius of FoV as 1.0 m according to our measurement, i.e. within such FoV area the camera held by a user can capture the light. Fig. 5.12(b) shows the presence detection accuracy by RoCLight when a user is in the FoV of a luminaire. All luminaires have an accuracy around 99%, which is definitely enough to support our roaming scheme.

5.4.4 Packet Reception Ratio under User Mobility

As analyzed in Sec. 5.3.3, packet loss is inevitable under user mobility because many factors, such as hand micro-motion (shaking and tilting) and larger distortions in images captures at the cell boundaries, can cause failure in decoding a packet. Therefore, we evaluate the packet reception ratio (PRR) when user walks at three different speeds: slow (around 0.5 m/s), medium (around 0.8 m/s) and fast (around 1.2 m/s) under

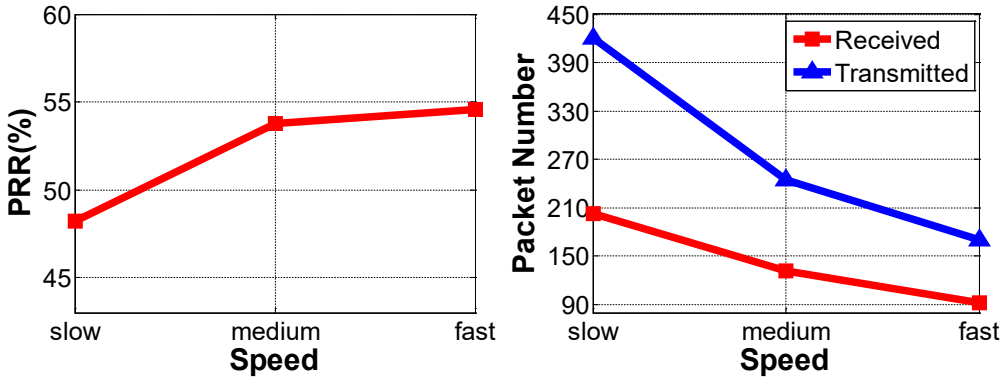

(a) PRR vs. speed.

(b) Total received and transmitted packets vs. speed.

Figure 5.13: Reception ability under user moving. A rather stable throughput under various speeds is implied by RoCLight.

RoCLight. We let all luminaires start transmitting continuously an identical packet when a user enters the testing area and stop transmitting once the user leaves. We thus calculate PRR as

$$\frac{n_r}{t \times R} \times 100\%. \tag{5.4}$$

where n_r is the number of correctly received packets , t is the elapsed time of a user passing through our testing area, and R is the frame rate of the smartphone camera.

While the relatively low PRR shown in Fig. 5.13(a) is normal for LED-Camera VLC [27], mobility does exacerbate the situation in our case. Fortunately, RoCLight's FEC can well handle this low PRR, as shown later. The slightly higher PRR under higher speed is probably due to the higher (user's hand) stability when moving faster. As illustrated in Fig. 5.13(b), the total number of received packets is roughly proportional to the time spent under the testbed, suggesting a stable throughput under various speeds.

5.4.5 Adaptive Transmission under User Mobility

We further evaluate the benefits of RoCLight in terms of transmission efficiency given its mobility adaptive ability. We let a user walk through RoCLight's testbed with three different speeds same as those used in Sec. 5.4.4, while the luminaires cooperatively transmitting a message of $k = 26$. We evaluate the total transmitted packets number

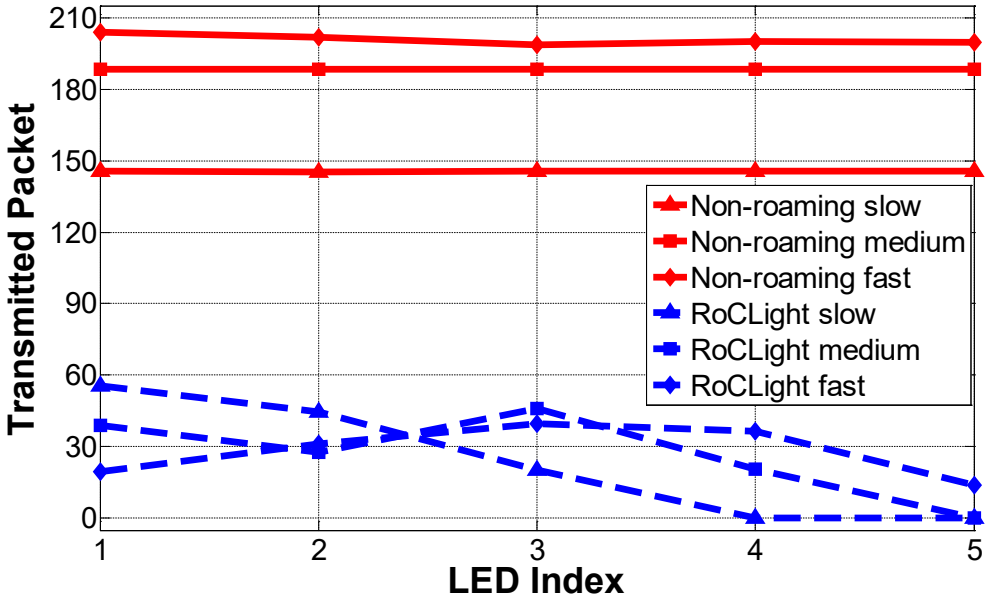

Figure 5.14: Transmitting benefit offered by RoCLight's roaming scheme.

until the receiver fully decodes the sent messages, and we compare RoCLight with the Non-Roaming mechanism.

We conduct 30 trials and plot the average number of transmitted packets in Fig. 5.14. As expected, the amount of transmitted packets by all luminaires or transmitted packets by each luminaire in RoCLight are both far less than those of the baseline mechanism. Each luminaire transmits the same amount of packets without mobility adaptation, but RoCLight dispatches specific codes to individual luminaires adaptively so as to achieve a higher efficiency. We take the number of transmitted packets of individual LEDs as examples to highlight this efficiency improvement. Under the slow mobility case, LED1 sends 59 packets by RoCLight while transmitting 146 packets by the baseline. Also, LED4 and LED5 do not transmit any packets by RoCLight, as opposed to 146 each by the baseline regardless of user presence. In total, the transmitted packets by RoCLight are only 14% of that by the baseline. This higher efficiency implies either a higher energy efficiency or a higher serviceability for other users.

5.4.6 Throughput and Latency

We evaluate the improvement of our roaming scheme in terms of throughput and latency in this section, by comparing RoCLight with a baseline non-roaming mechanism that

all luminaires send identical Raptor encoded packets synchronously in a circulating manner. The latency in our evaluation is the elapsed time from when the camera starts to receive data to when it recovers the original messages. The throughput is computed as the number of bits of the k packets of the original message divided by the latency.

We first conduct the experiment with three different user speeds same as those in Sec. 5.4.4. The achieved throughput and latency are plotted in Fig. 5.15. We can observe that both metrics are significantly improved as compared with the non-roaming scheme. As shown in Fig 5.15(a), the gain of RoCLight over non-roaming mechanism rises about 27% under fast speed to 35% under slow speed. As shown in Fig. 5.15(b), the gain in terms of latency is beyond 20% for all cases. The significant improvement stems from the relay ability of RoCLight, i.e. RoCLight can track the user to accurately assign encoded packets to be relayed, whereas the baseline only repeatedly broadcasts the identical message in a circular manner so that a user may need to wait for the whole round to receive a sufficient number of encoded packets.

Subsequently, we verify the benefits with larger k under the user speed of 0.5m/s. We conduct 10 trials for each of the three k values: $k = 26$, $k = 50$, and $k = 76$, and we calculate the respective average elapsed times for message recovery as the latency. Fig. 5.16 shows the performance of RoCLight and the baseline scheme with varying k. We can observe that both metrics get significantly improved by RoCLight. The throughput of RoCLight can reach up to 140 bps, whereas the throughput of non-

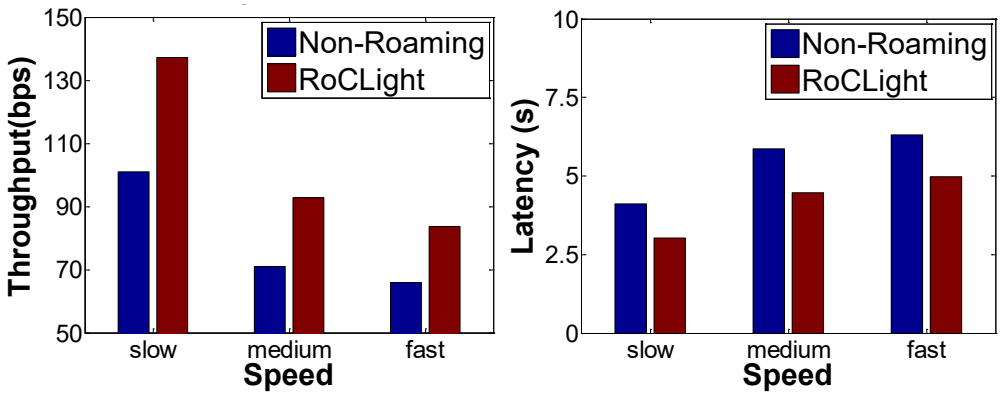

(a) Throughput vs. speed.

(b) Latency vs. speed.

Figure 5.15: Throughput and latency of RoCLight under different user speed. The improvements in terms of throughput and latency are over 20%.

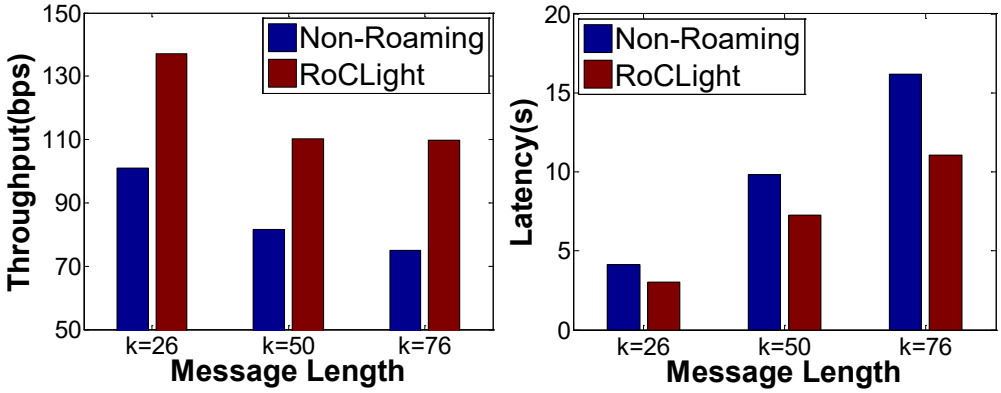

(a) Throughput vs. message length.

(b) Latency vs. message length.

Figure 5.16: Throughput and latency of RoCLight under different length of the original message. The throughput and latency are both improved.

roaming is maximum 100 bps and suffers a drastic decrease with an increasing k. We can also observe the improvement brought by RoCLight is more significant for larger k, as the baseline circular transmission cannot quickly compensate the loss. We believe that these improvements could become more evident if we apply RoCLight to larger scale deployments, simply because roaming would take place more frequently in such scenarios.

5.4.7 Power Consumption

The energy consumption of RoCLight is incurred by two parts: the consumption of re-designed driver caused by driving luminaires and sensing, and that of smartphone for frame capture and decoding. Since RoCLight utilizes the existing lighting infrastructure as transmitters, we do not count the energy consumption for illumination (thus light pulse emitting). Consequently, the transmission consumption introduced by RoCLight mainly involves the power consumed by the driver circuit, amplifier circuit and microcontroller of the re-devised driver, as well as wireless transmission from/to the lightweight server. Our field experimental results show that the driver and amplifier circuits of RoCLight have a power consumption of 20.2 mW, very close to that of a normal LED driver. The power consumed by the microcontroller for generating OOK-PWM signal, ADC sampling and wireless communication with a server is dominant at

Table 5.1: Power of RoCLight.

	Transmitter (mW)	Receiver (mW)	Total (mW)
RoCLight	< 110	< 76.5	< 186.5
Wi-Fi	>800 [75]	50 [77]	>850

around 89.8 mW, since we currently configure CC2530 at router mode in Zigbee network for simplifying profile development. We leave it as our future work to set CC2530 at end-device mode in Zigbee network that can save over 60% of energy. Moreover, we can employ Power Line Communication (PLC) [71] for data exchange since all luminaires are connected to the same power grid. Therefore, the power consumption by current MCU and Zigbee communication can be reduced significantly. According to the data sheet of a WiFi router, existing commercial WiFi routers consume at least 800mW [74, 75].

The smartphone receiver of RoCLight does consume slightly more energy, since image sensor is a well-known power hungry sensor. The image sensor of camera has two states within a frame duration T_f, i.e. active mode and idle mode [76]. Thus we have the power for two modes per frame $P = (P_a T_a + P_i T_i)/T_f$, where P_a, T_a, P_i and T_i are the power and duration for active mode as well as idle mode respectively. In RoCLight, we implement receiver program on Nexus 6 with front camera. Based on our understanding, the front camera of Nexus 6 is equipped a generic image sensor with maximum resolution of 2 Megapixel [115]. We take an universal COTS image sensor AS0260 as example, typically we have $P_a = 272$ mW and $P_i = 12$ mW [116]. From [76], we derive $T_a \approx 8.19$ ms and $T_i \approx 24.81$ ms, respectively. Therefore, the power consumption is only around 76.5 mW under the resolution of 1024×768. In fact, by using aggressive standby mechanism and optimal clock scaling proposed in [76], the power can be reduced further. WiFi seems to consume slightly more than 50mW at the receiver side for data reception [77]. Table 5.1 summarizes the power consumptions of RoCLight, as opposed to those of WiFi. Note that this comparison is only for putting the numbers into perspective, as WiFi roaming is significantly different from the roaming support offered by RoCLight.

5.5 Summary

This chapter has presented RoCLight, a practical LED-Camera VLC system with roaming support enabled by LED sensing. RoCLight relies on existing lighting infrastructure for both user mobility tracking and VLC transmitting simultaneously. It innovates in both VLS and VLC: on one hand, it leverages LED sensing to track user mobility, so as to obtain information concerning user motion. On the other hand, it adapts Raptor code to the user mobility information for improving both throughput and efficiency. Our prototype and extensive field experiments based on it have demonstrated that RoCLight can achieve a throughput of more than 110 bps in a normal indoor area for a mobile user. We believe that the first attempt of RoCLight in combining VLS and VLC for roaming support will push the COTS-enabled VLC towards practical deployments in realistic application scenarios.

Chapter 6

Conclusion

Favored as green technologies of communication and sensing piggybacking on lighting infrastructure, VLC and VLS have become very hot research topics in both academic and industrial communities. Various approaches have been proposed to improve VLC/VLS systems in terms of feasibility and practicability to apply them into our daily lives. To accelerate this progress, in this thesis, we deeply exploit sensing and networking abilities of visible light so as to realize practical VLC and VLS systems with handy COTS devices and solely LED lighting systems detailed in Chapter 3 and Chapter 4, respectively. Furthermore, we make an attempt to address the tough issue of user mobility in VLC systems to offer seamless connectivity for mobile users in Chapter 5. We conclude this thesis by summarizing our contributions and discussing some future directions in following section 6.1 and 6.2, respectively.

6.1 Research Contributions

In Chapter 3, we have proposed CeilingTalk, an LED-Camera VLC system with collaborative transmissions, to field study the realistic deployment of an indoor VLC-based broadcast system. In CeilingTalk, we employ common LEDs as transmitters and COTS smartphones as receivers, without relying on media other than the light itself. In order to improve the network throughput and link reliability, rateless codes and a novel codes assignment scheme are involved among several neighbor LED luminaires due to an indoor lighting system is normally under dense deployment. Besides, we also invent a lightweight decoding method to lower computational complexity on receiver side for

tackling both spatial and temporal asynchrony in transmissions, making it adaptable to a full smartphone-based implementation. Based on our experience of implementing CeilingTalk, we build a communication model to characterize this LED-Camera VLC by extracting parameters to provide guidelines on practical deployments. Finally, extensive experimental results show the effectiveness of the proposed LED-Camera VLC model and the promising performance of CeilingTalk.

Inspired by the finding when we deploy CeilingTalk, we devise and build CeilingSee in Chapter 4. Our key observation is that in a normal VLC system, LED transmitters are mounted on the ceiling for lighting and transmitting, while the resulted diffuse reflection can be changed by the presence of users. On the other hand, the LED's photoelectric effect which is unexploited in VLC can sense the change of reflected light. Therefore, we propose the novel idea of only using ceiling-mounted LED luminaires to infer occupancy by re-designing the LED driver so that it can convert an LED into a light sensor. We also design data processing and machine learning algorithms to infer whole room occupancy by fusing outcomes of the multiple sensing units deployed in the room. We conduct extensive field experiments to validate the effectiveness of CeilingSee, and the results strongly demonstrate LED luminaires can accurately detect and even track users who are moving under them.

In Chapter 5, we present an innovative idea of tracking user mobility with LED transmitters in VLC, based on our previous observations in CeilingSee. Buying the similar idea of employing rateless codes for collaborative transmissions in building CeilingTalk, we implement RoCLight as a practical VLC system with elaborate handover scheme to provide seamless connectivity for mobile users. LED transmitters in RoCLight can detect users who are within their FoV, and automatically associate the mobile devices held by the users so as to maintain seamless transmissions in scalable indoor VLC. We deploy a RoCLight testbed with 5 LED luminaires in one university laboratory. Our prototype and extensive experimental results have demonstrated the availability of RoCLight, and it can achieve a throughput of greater than 110bps under our current testbed for a mobile user. The benefits of RoCLight will be more evident if under a larger testbed where roaming would take place more frequently.

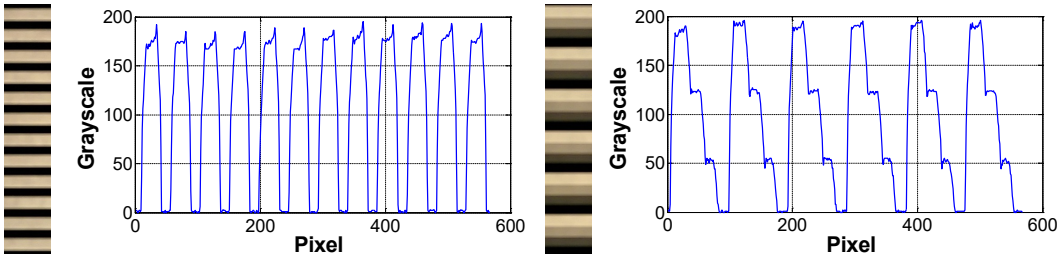

(a) 2-ASK (OOK).

(b) 4-ASK (Four distinguishable grayscale value of bands).

Figure 6.1: ASK symbols based on grayscale value.

6.2 Future Directions

While some novel techniques have been proposed and realized to substantially improve both VLC and VLS systems in this thesis, there are still some limitations which can be overcome in future research. For example, in CeilingTalk we may further exploit the grayscale value of banded images to realize high-order modulation for improving symbol rate so as to boost the network throughput. As shown in Fig. 6.1, the camera receiver can clearly capture the grayscale of bands. Correspondingly, some more effective coding/decoding schemes could be designed to further improve CeilingTalk in terms of throughput and energy efficiency.

In Chapter 4, the newly proposed LED sensing system needs to be extended to adapt various dimming levels under different application scenarios due to it senses light level of ambient light in essence. Moreover, the re-designed driver could be improved to shorten switching time between sensing and lighting so as to perform detecting and illuminating in a manner without human perceived flicker. CeilingSee could also be devised to track and recognize individual occupant with advanced learning methodology, since each occupant has different body parameters resulting in different reflection change under the same environment[1]. Therefore, we are on the way to extend our CeilingSee for more potential applications.

As for RoCLight in Chapter 5, handling the user mobility is a real problem which seriously confines VLC's practical application. However, current RoCLight can only

[1]As shown in Fig. 4.11 users with different hights intuitively cause different reflection, though it does not impact on occupancy inference, we may still use this difference to distinguish users.

support roaming for one user, albeit it is possible to broadcast messages for multiple users who are moving on an identical trajectory. Providing customized services for mobile users is necessary for a practical wireless access technique. Again let us look into the different changes in sensing value caused by different users shown in Fig. 4.11, as aforementioned we may distinguish user's identity by further exploiting sensing data and locate a certain user exactly, thus we could use some directional transmission techniques similar in RF communication. In a VLC system, the LED tranmitters normally consist of multiple LED chips, so it is possible to group partial LED chips to serve the user at certain location. Therefore, it may be feasible to provide customized services for multiple users with the help of the LED sensing apporac. We are also on the way to enlarge the scale of RoCLight's testbed for conducting more comprehensive research to better understand its limitations and how to improve RoCLight.

References

[1] T. Nguyen, A. Islam, T. Hossan, and Y. M. Jang. **Current Status and Performance Analysis of Optical Camera Communication Technologies for 5G Networks**. *IEEE Access*, **5**:4574–4594, 2017. 1

[2] X. Ge, H. Cheng, M. Guizani, and T. Han. **5G Wireless Backhaul Networks: Challenges and Research Advances**. *IEEE Network*, **28**(6):6–11, 2014. 1

[3] R. Q. Hu and Y. Qian. **An Energy Efficient and Spectrum Efficient Wireless Heterogeneous Network Framework for 5G Systems**. *IEEE Communications Magazine*, **52**(5):94–101, 2014. 1

[4] S. Wu, H. Wang, and C. H. Youn. **Visible Light Communications for 5G Wireless Networking Systems: From Fixed to Mobile Communications**. *IEEE Network*, **28**(6):41–45, 2014. 1

[5] G. Pang, K. L. Ho, T. Kwan, and E. Yang. **Visible Light Communication for Audio Systems**. *IEEE Transactions on Consumer Electronics*, **45**(4):1112–1118, 1999. 2

[6] Y. Tanaka, S. Haruyama, and M. Nakagawa. **Wireless Optical Transmissions With White Colored LED for Wireless Home Links**. In *Personal, Indoor and Mobile Radio Communications, 2000. PIMRC 2000. The 11th IEEE International Symposium on*, **2**, pages 1325–1329, 2000. 2

[7] Y. Tanaka, T. Komine, S. Haruyama, and M. Nakagawa. **Indoor Visible Communication Utilizing Plural White LEDs as Lighting**. In *Personal,*

Indoor and Mobile Radio Communications, 2001 12th IEEE International Symposium on, **2**, pages F–F, 2001. 2

[8] S. Rajagopal, R.D. Roberts, and S. Lim. **IEEE 802.15.7 Visible Light Communication: Modulation Schemes and Dimming Support**. *IEEE Communications Magazine*, **50**(3):72–82, 2012. 2, 13, 18

[9] Institute of Electrical and Electronics Engineers (IEEE). **IEEE Standard for Local and Metropolitan Area Networks–Part 15.7: Short-Range Wireless Optical Communication Using Visible Light**. *IEEE Std 802.15.7-2011*, pages 1–309, 2011. 2, 73, 79

[10] R.J. Drost and B.M. Sadler. **Constellation Design for Channel Precompensation in Multi-Wavelength Visible Light Communications**. *IEEE Trans. on Antennas and Propagation*, **62**(6):1995–2005, 2014. 2, 14

[11] H. Burchardt, N. Serafimovski, D. Tsonev, S. Videv, and H. Hass. **VLC: Beyond Point-to-Point Communication**. *IEEE Communications Magazine*, **52**(7):98–105, 2014. 2, 14, 72

[12] A. Ganick and D. Ryan. **ByteLight Scalable Indoor Location**. http://www.bytelight.com. 2, 14

[13] N. Rajagopal, P. Lazik, and A. Rowe. **Visual Light Landmarks for Mobile Devices**. In *Proc. of the 13th ACM IPSN*, pages 249–260, 2014. 2, 7, 8, 14

[14] Y. Kuo, P. Pannuto, K. Hsiao, and P. Dutta. **Luxapose: Indoor Positioning with Mobile Phones and Visible Light**. In *Proc. of the 20th ACM MobiCom*, pages 447–458, 2014. 2, 6, 7, 8, 9, 14, 21, 43, 85

[15] C. Danakis, M. Afgani, G. Povey, I. Underwood, and H. Haas. **Using a CMOS Camera Sensor for Visible Light Communication**. In *Proc. of 31th IEEE GLOBECOM*, pages 1244–1248, 2012. 2, 6, 7, 8, 14, 22, 30, 72, 73, 80

[16] N. Rajagopal, P. Lazik, and A. Rowe. **Hybrid Visible Light Communication for Cameras and Low-Power Embedded Devices**. In *Proc. of 1st ACM VLCS*, pages 33–38, 2014. 2, 7, 8, 14, 30, 72, 73

[17] X. Zhou and A.T. Campbell. **Visible Light Networking And Sensing**. In *Proc. of the 1st ACM workshop on Hot topics in wireless*, pages 55–60, 2014. ix, 2, 9, 10

[18] R. Zhang, J. Wang, Z. Wang, Z. Xu, C. Zhao, and L. Hanzo. **Visible Light Communications in Heterogeneous Networks: Paving The Way for User-Centric Design**. *IEEE Wireless Communications*, **22**(2):8–16, 2015. 3, 11, 73

[19] P. Hu, P. H. Pathak, A. K. Das, Z. Yang, and P. Mohapatra. **PLiFi: Hybrid WiFi-VLC Networking Using Power Lines**. In *Proc. of the 3rd ACM VLCS*, pages 31–36, 2016. 3, 11

[20] R. Zhang, H. Claussen, H. Haas, and L. Hanzo. **Energy Efficient Visible Light Communications Relying on Amorphous Cells**. *IEEE Journal on Selected Areas in Communications*, **34**(4):894–906, 2016. 3, 72, 73

[21] R.J. Xie, N. Hirosaki, K. Sakuma, Y. Yamamoto, and M. Mitomo. **Eu2+-doped Ca-a-SiAlON: a Yellow Phosphor for White Light-Emitting Diodes**. *Applied Physics Letters*, **84**(26):5404–5406, 2004. 5

[22] S. Muthu and J. Gaines. **Red, Green And Blue LED-based White Light Source: Implementation Challenges And Control Design**. In *Industry Applications Conference, 2003. 38th IAS Annual Meeting. Conference Record of the*, **1**, pages 515–522, 2003. 6

[23] Y. Wang, M. Zhang, Y. Wang, W. Fang, L.Tao, and N. Chi. **Experimental Demonstration of Visible Light Communication Based on Subcarrier Multiplexing of Multiple-Input-Single-Output OFDM**. In *Opto-Electronics and Communications Conference (OECC), 2012 17th*, pages 745–746, 2012. 6

[24] M. Ijaz, D. Tsonev, J. J.D. McKendry, E. Xie, S. Rajbhandari, H. Chun, G. Faulkner, E. Gu, M. D. Dawson, D. O'Brien, et al. **Experimental Proof-of-Concept of Optical Spatial Modulation OFDM Using Micro LEDs**. In *Communication Workshop (ICCW), 2015 IEEE International Conference on*, pages 1338–1343, 2015. 6

[25] T. Saito, S. Haruyama, and M. Nakagawa. **A New Tracking Method Using Image Sensor and Photo Diode for Visible Light Road-to-Vehicle Communication**. In *Advanced Communication Technology, 2008. ICACT 2008. 10th International Conference on*, **1**, pages 673–678, 2008. 6

[26] H. C.N. Premachandra, T. Yendo, M. P. Tehrani, T. Yamazato, H. Okada, T. Fujii, and M. Tanimoto. **High-Speed-Camera Image Processing Based LED Traffic Light Detection for Road-to-Vehicle Visible Light Communication**. In *Intelligent Vehicles Symposium (IV), 2010 IEEE*, pages 793–798, 2010. 6

[27] H.Y. Lee, H.M. Lin, Y.L. Wei, H. Wu, H.M. Tsai, and K.C.J. Lin. **RollingLight: Enabling Line-of-Sight Light-to-Camera Communications**. In *Proc. of the 13th ACM MobiSys*, pages 167–180, 2015. 6, 7, 8, 21, 41, 43, 72, 73, 85, 90

[28] M. Valisakis. **Dynalight: A Dynamic Visible Light Communication Link for Smartphones**. Masters Thesis. Embedded Systems, Delft University of Technology; Delft, The Netherlands: 2015. 6, 7, 8

[29] B. Zhang, K. Ren, G. Xing, X. Fu, and C. Wang. **SBVLC: Secure Barcode-Based Visible Light Communication for Smartphones**. *IEEE Trans. on Mobile Computing*, **15**(2):432–446, 2016. 6, 7

[30] T. Hao, R. Zhou, and G. Xing. **COBRA: Color Barcode Streaming for Smartphone Systems**. In *Proc. of the 10th ACM MobiSys*, pages 85–98, 2012. 6, 7, 72, 73

[31] S.D. Perli, N. Ahmed, and D. Katabi. **PixNet: Interference-Free Wireless Links using LCD-Camera Pairs**. In *Proc. of the 16th ACM MobiCom*, pages 137–148, 2010. 6, 7, 72, 73

[32] W. Du, J.C. Liando, and M. Li. **SoftLight: Adaptive Visible Light Communication over Screen-Camera Links**. In *Proc. of the 35th IEEE INFOCOM*, pages 1620–1628, 2016. 6, 7

[33] T. Fujihashi, T. Koike-Akino, P. V. Orlik, and T. Watanabe. **Experimental Throughput Analysis in Screen-Camera Visual MIMO Communications**. In *Global Communications Conference (GLOBECOM), 2016 IEEE*, pages 1–6, 2016. 6

[34] A. Wang, S. Ma, C. Hu, J. Huai, C. Peng, and G. Shen. **Enhancing Reliability to Boost the Throughput over Screen-Camera Links**. In *Proc. of the 20th ACM MobiCom*, pages 41–52, 2014. 6, 72, 73

[35] W. Hu, J. Mao, Z. Huang, Y. Xue, J. She, K. Bian, and G. Shen. **Strata: Layered Coding for Scalable Visual Communication**. In *Proc. of the 20th ACM MobiCom*, pages 79–90, 2014. 6, 73

[36] W. Hu, H. Gu, and Q. Pu. **LightSync: Unsynchronized Visual Communication Over Screen-Camera Links**. In *Proc. of the 19th ACM MobiCom*, pages 15–26, 2013. 6, 73

[37] W. Huang and W. Mow. **PiCode: 2D Barcode with Embedded Picture and ViCode**. In *Proc. of the 19th ACM MobiCom*, pages 139–242, 2013. 6

[38] T. Li, C. An, X. Xiao, A.T. Campbell, and X. Zhou. **Real-Time Screen-Camera Communication Behind Any Scene**. In *Proc. of the 13th ACM MobiSys*, pages 197–211, 2015. 6, 7

[39] J. Wang, W. Huang, and Z. Xu. **Demonstration of A Covert Camera-Screen Communication System**. In *13th International Wireless Communications and Mobile Computing Conference (IWCMC)*, pages 910–915, 2017. 7

[40] P. Luo, Z. Ghassemlooy, H. L. Minh, X. Tang, and H. M. Tsai. **Undersampled Phase Shift ON-OFF Keying for Camera Communication**. In *Wireless Communications and Signal Processing (WCSP), 2014 Sixth International Conference on*, pages 1–6, 2014. 7, 8

[41] P. Hu, P. H. Pathak, X. Feng, H. Fu, and P. Mohapatra. **Colorbars: Increasing Data Rate of Led-to-Camera Communication Using Color Shift Keying**. In *Proceedings of the 11th ACM Conference on Emerging Networking Experiments and Technologies*, page 12, 2015. 7, 8

[42] C. Chan, H. Tsai, and K. C. Lin. **POLI: Long-Range Visible Light Communications Using Polarized Light Intensity Modulation**. In *Proceedings of the 15th Annual International Conference on Mobile Systems, Applications, and Services*, pages 109–120, 2017. 7, 8

[43] L. Li, P. Hu, C. Peng, G. Shen, and F. Zhao. **Epsilon: A Visible Light Based Positioning System**. In *Proc. of the 11th ACM NSDI*, pages 331–343, 2014. 8, 14, 30

[44] Z. Yang, Z. Wang, J. Zhang, C. Huang, and Q. Zhang. **Wearables Can Afford: Light-weight Indoor Positioning with Visible Light**. In *Proc. of the 13th ACM MobiSys*, pages 317–330, 2015. 9

[45] S.H. Yang, H.S. Kim, and Y.H. Sonand S.K. Han. **Three-Dimensional Visible Light Indoor Localization Using AOA and RSS With Multiple Optical Receivers**. *Journal of Lightwave Technology*, **32**(14):2480–2485, 2014. 9

[46] G.B Prince and T.D. Little. **A Two Phase Hybrid RSS/AoA Algorithm for Indoor Device Localization Using Visible Light**. In *Global Communications Conference (GLOBECOM), 2012 IEEE*, pages 3347–3352, 2012. 9

[47] T. Li, C. An, Z. Tian, A. T. Campbell, and X. Zhou. **Human Sensing Using Visible Light Communication**. In *Proc. of the 21st ACM MobiCom*, pages 331–344, 2015. 9, 43

[48] C. An, T. Li, Z. Tian, A.T. Campbell, and X. Zhou. **Visible Light Knows Who You Are**. In *Proc. of the 2nd ACM VLCS Workshop*, pages 39–44, 2015. 9

[49] T. Li, Q. Liu, and X. Zhou. **Practical Human Sensing in The Light**. pages 71–84, 2016. 9

[50] C. Zhang, J. Tabor, J. Zhang, and X. Zhang. **Extending Mobile Interaction Through Near-Field Visible Light Sensing**. In *Proceedings of the 21st Annual International Conference on Mobile Computing and Networking*, pages 345–357, 2015. 9

[51] Q. Wang and M. Zuniga. **Passive Sensing and Communication Using Visible Light: Taxonomy, Challenges and Opportunities**. *arXiv preprint arXiv:1704.01331*, 2017. 10

[52] X. Guo, M. Mohammad, S. Saha, M.C. Chan, S. Gilbert, and D. Leong. **PSync: Visible Light-based Time Synchronization for Internet of Things (IoT)**. In *Computer Communications, IEEE INFOCOM 2016-The 35th Annual IEEE International Conference on*, pages 1–9, 2016. 10

[53] Z. Li, W. Chen, C. Li, M. Li, X. Li, and Y. Liu. **Flight: Clock Calibration Using Fluorescent Lighting**. In *Proceedings of the 18th annual international conference on Mobile computing and networking*, pages 329–340, 2012. 10

[54] E. D. Lascio, A. Varshney, T. Voigt, and C. Perez-Penichet. **Poster Abstract: LocaLight - A Battery-Free Passive Localization System Using Visible Light**. In *2016 15th ACM/IEEE International Conference on Information Processing in Sensor Networks (IPSN)*, pages 1–2, 2016. 10

[55] I. Mohamed, N. Viet, R. Siddharth, J. Minitha, G. Marco, and H. Richard. **Visible Light Based Activity Sensing Using Ceiling Photosensors**. In *Proc. of the 3rd ACM VLCS Workshop*, pages 43–48, 2016. 10, 46

[56] M. A. Kaholokula. **Reusing Ambient Light to Recognize Hand Gestures**. Technical Report TR2016-797, Dartmouth College, Computer Science, 2016. 10

[57] Q. Wang, M. Zuniga, and D. Giustiniano. **Passive Communication With Ambient Light**. In *Proceedings of the 12th International on Conference on Emerging Networking EXperiments and Technologies, CoNEXT '16*, pages 97–104, 2016. 10

[58] J. Zhang, Q. Wang, and M. Zuniga. **Leveraging Smart Lights for Passive Localization**. `http://goo.gl/u2PHb7`, 2017. Delft University of Technology, The Netherlands. 10

[59] J. Hou and D. C. O'Brien. **Polling Scheme for Indoor LOS Optical Wireless LAN**. *Electronics Letters*, **39**(10):794–795, 2003. 11

[60] A. Ashok, M. Gruteser, N. Mandayam, J. Silva, M. Varga, and K. Dana. **Challenge: Mobile Optical Networks Through Visual MIMO**. In *Proceedings of the sixteenth annual international conference on Mobile computing and networking*, pages 105–112, 2010. 11

[61] T. Borogovac, M. Rahaim, and J. B. Carruthers. **Spotlighting for Visible Light Communications and Illumination**. In *2010 IEEE GLOBECOM Workshops (GC Wkshps)*, pages 1077–1081, 2010. 11

[62] A. M. Vegni and T. D.C. Little. **Handover in VLC Systems With Cooperating Mobile Devices**. In *2012 International Conference on Computing, Networking and Communications (ICNC)*, pages 126–130, 2012. 11

[63] J. Hou and D. C. O'Brien. **Vertical Handover-Decision-Making Algorithm Using Fuzzy Logic for The Integrated Radio-and-OW System**. *IEEE Transactions on Wireless Communications*, **5**(1):176–185, 2006. 11

[64] M. B. Rahaim, A. M. Vegni, and T. D.C. Little. **A Hybrid Radio Frequency And Broadcast Visible Light Communication System**. In *2011 IEEE GLOBECOM Workshops (GC Wkshps)*, pages 792–796, 2011. 11

[65] H. Ma, L. Lampe, and S. Hranilovic. **Coordinated Broadcasting for Multiuser Indoor Visible Light Communication Systems**. *IEEE Trans. on Communications*, **63**(9):3313–3324, 2015. 11

[66] S. Schmid, T. Richner, S. Mangold, and T. R. Gross. **EnLighting: An Indoor Visible Light Communication System Based on Networked Light Bulbs**. In *Proc. of the 13th IEEE SECON*, pages 1–9, 2016. 11

[67] M. Rahaim, G. B. Prince, and T. D.C. Little. **State Estimation And Motion Tracking for Spatially Diverse VLC Networks**. In *2012 IEEE Globecom Workshops*, pages 1249–1253, 2012. 11

[68] A. V. Oppenheim, R. W. Schafer, J. R .Buck, et al. *Discrete-Time Signal Processing*, **2**. Prentice hall Englewood Cliffs, NJ, 1989. 16

[69] A. Shokrollahi. **Raptor Codes**. *IEEE Trans. on Information Theory*, **52**(6):2551–2567, 2006. 19, 81

[70] M. Luby, A. Shokrollahi, and T. Stockhammer. **The Open Source Implementation of Raptor Code RFC5053**. https://code.google.com/p/raptor-code-rfc/. 19, 32

[71] H. Ma, L. Lampe, and S. Hranilovic. **Integration of Indoor Visible Light and Power Line Communication Systems**. In *Proc. of the 17th IEEE ISPLC*, pages 291–296, 2013. 20, 70, 94

[72] G. Corbellini, K. Aksit, S. Schmid, S. Mangold, and T. Gross. **Connecting Networks of Toys and Smartphones with Visible Light Communication**. *IEEE Communications Magazine*, **52**(7):72–78, 2014. 21

[73] **LUXEON XF-3535L**. http://www.lumileds.com/products/matrix-platform/luxeon-xf-3535l. 31, 51, 85

[74] **WiFi Router Power Consumption Database**. http://www.tpcdb.com/list.php?type=11. 40, 94

[75] G. Palem and S. Tozlu. **On Energy Consumption of Wi-Fi Access Points**. In *Proc. of the 7th IEEE CCNC*, pages 434–438, 2012. 40, 41, 94

[76] R. LiKamWa, B. Priyantha, M. Philipose, L. Zhong, and P. Bahl. **Energy Characterization and Optimization of Image Sensing toward Continuous Mobile Vision**. In *Proc. of the 11th ACM MobiSys*, pages 62–82, 2013. 40, 41, 94

[77] A. Carroll and C. Heiser. **An Analysis of Power Consumption in a Smartphone.** In *USENIX annual technical conference*, **14**, 2010. 41, 94

[78] P. Bahl and V.N. Padmanabhan. **RADAR: an In-building RF-based User Location and Tracking System**. In *Proc. of 19th IEEE INFOCOM*, pages 775–784, 2000. 43

[79] C. Zhang, F. Li, J. Luo, and Y. He. **iLocScan: Harnessing Multipath for Simultaneous Indoor Source Localization and Space Scanning**. In *Proc. of the 12th ACM SenSys*, pages 91–104, 2014. 43

[80] C. Zhang, K.P. Subbu, J. Luo, and J. Wu. **GROPING: Geomagnetism and cROwdsensing Powered Indoor NaviGation**. *IEEE Trans. on Mobile Computing*, **14**(2):387–400, 2015. 43

[81] L. Audin. *Occupancy Sensors: Promise and Pitfalls.* Tech Update, Tu-93-8. E Source, Inc., Boulder, CO, 1999. 43

[82] R.H. Dodier, G.P. Henze, D.K. Tiller, and X. Guo. **Building Occupancy Detection Through Sensor Belief Networks**. *Elsevier Energy and Building*, **38**(9):1033–1043, 2006. 43

[83] A. Beltran, V. L. Erickson, and A. E. Cerpa. **ThermoSense: Occupancy Thermal Based Sensing for HVAC Control**. In *Proc. of the 5th ACM BuildSys*, pages 11:1–11:8, 2013. 43, 46

[84] V. L. Ericksonand S. Achleitner and A. E. Cerpa. **POEM: Power-Efficient Occupancy-based Energy Management System**. In *Proc. of the 12th ACM/IEEE IPSN*, pages 203–216, 2013. 43, 46

[85] S. P. Tarzia, R. P. Dick, P. A. Dinda, and G. Memik. **Sonar-based Measurement of User Presence and Attention**. In *Proc. of the 11th ACM UbiComp 2009*, pages 89–92, 2009. 43

[86] T. W. Hnat, E. Griffiths, R. Dawson, and K. Whitehouse. **Doorjamb: Unobtrusive Room-level Tracking of People in Homes Using Doorway Sensors**. In *Proc. of the 10th ACM SenSys*, pages 309–322, 2012. 43

[87] O. Shih and A. Rowe. **Occupancy Estimation Using Ultrasonic Chirps**. In *Proc. of the 6th ACM/IEEE ICCPS*, pages 149–158, 2015. 43, 46

[88] D.B. Yang, H.H. Gonzalez-Banos, and L.J. Guibas. **Counting People in Crowds with a Real-Time Network of Simple Image Sensors**. In *Proc. of the 9th IEEE ICCV*, pages 122–129, 2003. 43

[89] V.L. Erickson, M.A. Carreira-Perpinan, and A.E. Cerpa. **OBSERVE: Occupancy-Based System for Efficient Reduction of HVAC Energy**. In *Proc. of the 10th ACM/IEEE IPSN*, pages 258–269, 2011. 43, 46

[90] C. L. Chen, S. Gong, and T. Xiang. **From Semi-Supervised to Transfer Counting of Crowds**. In *Proc. of the 14th IEEE ICCV*, pages 2256–2263, 2013. 43

[91] B. Balaji, J. Xu, A. Nwokafor, R. Gupta, and Y. Agarwal. **Sentinel: Occupancy Based HVAC Actuation Using Existing WiFi Infrastructure Within Commercial Buildings**. In *Proc. of the 11th ACM SenSys*, pages 17:1–17:14, 2013. 43

[92] L. Yang, K. Ting, and M. B. Srivastava. **Inferring Occupancy from Opportunistically Available Sensor Data**. In *Proc. of the 12th IEEE PerCom*, pages 60–68, 2014. 43

[93] T. Komine and M. Nakagawa. **Fundamental Analysis for Visible-Light Communication System using LED Lights**. *IEEE Trans. on Consumer Electronics*, **50**(1):100–107, 2004. 43

[94] S. Schmid, G. Corbellini, S. Mangold, and T.R. Gross. **LED-to-LED Visible Light Communication Networks**. In *Proc. of the 14th ACM MobiHoc*, pages 1–10, 2013. 43, 44, 47, 48, 75, 76

[95] J. Hao, Y. Yang, and J. Luo. **CeilingCast: Energy Efficient and Location-Bound Broadcast Through LED-Camera Communication**. In *Proc. of the 35th IEEE INFOCOM*, pages 1629–1637, 2016. 43, 73, 80, 84, 87

[96] D. Paul, Y. William, and L. Darren. **Very Low-Cost Sensing and Communication Using Bidirectional LEDs**. In *Proc. of the 5th ACM UbiComp 2003*, pages 175–191, 2003. 43, 47, 48

[97] F. M. Mims. *Siliconnections: Coming of Age in the Electronic Era*. McGraw-Hill, New York, 1986. 47

[98] Illuminance. **http://www.engineeringtoolbox.com/light-level-rooms-d_708.html**. 53

[99] A. J. Smola and B.Schölkopf. **A Tutorial on Support Vector Regression**. *Statistics and Computing*, **14**(3):199–222, 2004. 59, 60

[100] J.Ma, J. Theiler, and S. Perkins. **Accurate On-line Support Vector Regression**. *Neural Computation*, **15**(11):2683–2703, 2003. 61

[101] CC2541. **http://www.ti.com/lit/ds/symlink/cc2541.pdf**. 62

[102] BLE-STACK. **http://www.ti.com/product/CC2541/toolssoftware**. 62

[103] L. R. Rabiner. **A tutorial on Hidden Markov Models and Selected Applications in Speech Recognition**. *Proceedings of the IEEE*, **77**(2):257–286, 1989. 70

[104] S. Pergoloni, M. Biagi, S. Rinauro, S. Colonnese, R. Cusani, and G. Scarano. **Merging Color Shift Keying and Complementary Pulse Position Modulation for Visible Light Illumination and Communication**. *IEEE/OSA Journal of Lightwave Technology*, **33**(1):192–200, 2015. 72

[105] S. Rajbhandari, H. Chun, G. Faulkner, K. Cameron, A. V.N. Jalajakumari, R. Henderson, D. Tsonev, M. Ijaz, Z. Chen, H. Haas, et al. **High-Speed Integrated Visible Light Communication System: Device Constraints and Design Considerations**. *IEEE Journal on Selected Areas in Communications*, **33**(9):1750–1757, 2015. 72

[106] C. Gong, S. Li, Q. Gao, and Z. Xu. **Power and Rate Optimization for Visible Light Communication System with Lighting Constraints**. *IEEE Trans. on Signal Processing*, **63**(16):4245–4256, 2015. 72

[107] M. S.A. Mossaad, S. Hranilovic, and L. Lampe. **Visible Light Communications using OFDM and Multiple LEDs**. *IEEE Trans. on Communications*, **63**(11):4304–4313, 2015. 72

[108] J. C. Chau, C. Morales, and T. D.C. Little. **Using Spatial Light Modulators in MIMO Visible Light Communication Receivers to Dynamically Control the Optical Channel**. In *Proc. of the 13th EWSN*, pages 347–352, 2016. 72

[109] B. Zhang, K. Ren, G. Xing, X. Fu, and C. Wang. **SBVLC: Secure Barcode-Based Visible Light Communication for Smartphones**. In *Proc. of the 33rd IEEE INFOCOM*, pages 2661–2669, 2014. 73

[110] G. Corbellini, K. Aksit, S. Schmid, S. Mangold, and T. Gross. **Connecting Networks of Toys and Smartphones with Visible Light Communication**. *IEEE Communications Magazine*, **52**(7):72–78, 2014. 73

[111] S.B. Wicker. *Error Control Systems for Digital Communication and Storage*, **1**. Prentice hall Englewood Cliffs, 1995. 80

[112] E. McCollough. **Photographic Topography**. *Industry: A Monthly Magazine Devoted to Science, Engineering and Mechanic Arts*, (54):65, 1893. 84

[113] **CC2530, Second Generation System-on-Chip Solution for 2.4 GHz IEEE 802.15.4 / RF4CE / ZigBee**. `http://www.ti.com/product/CC2530`. 86

[114] **Z-Stack**. `http://www.ti.com/tool/z-stack`. 86

[115] **Nexus 6**. `https://www.support.google.com/nexus/answer/6102470`. 94

[116] **AS0260: 2 MP 1/6" CMOS Image Sensor System-on-Chip**. `http://www.onsemi.com/PowerSolutions/product.do?id=AS0260`. 94

Publications

Journal Articles

1. **Yanbing Yang***, Jie Hao*, and Jun Luo. CeilingTalk: Lightweight Indoor Broadcast Through LED-Camera Communication. IEEE Transactions on Mobile Computing. Vol. 16, no. 12, pp. 3308-3319, 2017. (*Equal contributing authors.)

2. **Yanbing Yang**, Jie Hao, Jun Luo, and Sinno Jialin Pan. CeilingSee: Device-Free Occupancy Inference through Lighting Infrastructure Based LED Sensing. (Extended from conference version) Pervasive and Mobile Computing. (Invited and accepted.)

3. **Yanbing Yang**, Shuya Ding, Jun Luo, and Jie Hao. RoCLight: Supporting Roaming for Visible Light Communication via LED Sensing. IEEE Transactions on Mobile Computing. (Submitted.)

Conference Papers

4. **Yanbing Yang**, and Jun Luo. Boosting the Throughput of LED-Camera VLC via Composite Light Emission. In Proceedings of the 37th IEEE Conference on Computer Communications (INFOCOM'18). (To appear.)

5. **Yanbing Yang**, Shuya Ding, Jie Hao, and Jun Luo. Roaming in Connecting Light: Practical Visible Light Communication Leveraging LED Sensing. 4th ACM Workshop on Visible Light Communication Systems, ACM VLCS'17, pp 9-14, Snowbird, Utah, USA, October 2017.

6. **Yanbing Yang**, Jiangtian Nie, and Jun Luo. ReflexCode: Coding with Superposed Reflection Light for LED-Camera Communication. In Proceedings of the 23rd Annual International Conference on Mobile Computing and Networking, ACM MobiCom'17, pp 193-205, Snowbird, Utah, USA, October 2017. [acceptance ratio = 35/186 (19%)]

7. **Yanbing Yang**, Jie Hao, Jun Luo, and Sinno Jialin Pan. CeilingSee: Device-Free Occupancy Inference through Lighting Infrastructure Based LED Sensing. In Proceedings of the 15th IEEE Conference on Pervasive Computing and Communications (PerCom'17), pp 247-256, Kona, Big Island, Hawaii, USA, March 2017. [acceptance ratio = 28/192 (15%)]

8. Jie Hao*, **Yanbing Yang***, and Jun Luo. CeilingCast: Energy Efficient and Location-Bound Broadcast Through LED-Camera Communication. In Proceedings of the 35th IEEE Conference on Computer Communications (INFOCOM'16), pp 1-9, San Francisco, CA, USA, April 2016. [acceptance ratio = 300/1644 (18%)].(* Equal contributing authors.)

OTHERS

9. **Yanbing Yang**. Practical Visible Light Communication System Utilizing LED Sensing. PhD Forum on Pervasive Computing and Communications (PerCom'17), pp 109-110, Kona, Big Island, Hawaii, USA, March 2017.

10. **Yanbing Yang**, Jiangtian Nie, and Jun Luo. Demo: Coding with Superposed Reflection Light for LED-Camera Communication. In Proceedings of the 23rd Annual International Conference on Mobile Computing and Networking, ACM MobiCom'17, pp 513-515, Snowbird, Utah, USA, October 2017.